TECHNISCHE UNIVERSITÄT MÜNCHEN
TUM School of Medicine and Health

ENDOSOMAL TRAFFICKING COMPLEXES IN THE REGULATION OF LIVER METABOLISM

Karsten Falk Motzler

Vollständiger Abdruck der von der TUM School of Medicine and Health der Technischen Universität München zur Erlangung eines Doktors der Naturwissenschaften (Dr. rer. nat.) genehmigten Dissertation.

Vorsitz: Prof. Dr. Roland M. Schmid

Prüfer*innen der Dissertation:

1. Prof. Dr. Stephan Herzig
2. Prof. Dr. Nina H. Uhlenhaut
3. Prof. Dr. Bart Staels

Die Dissertation wurde am 30.03.2023 bei der Technischen Universität München eingereicht und durch die Fakultät für Medizin am 30.09.2023 angenommen.

ABSTRACT

The endosomal trafficking system as regulator of metabolism has been increasingly acknowledged in recent years. Metabolically active organs like the liver, require proper spatial and temporal distribution of proteins such as hormone receptors and transporters upon changes in nutrient availability. These quick adaptations are in part facilitated by the endosomal system. Particularly hepatocytes depend on a tight regulation of this system in order to maintain the polar distribution of basolateral membrane components, facing the blood stream, and apical membranes, facing the bile. Here, three components of the endosomal trafficking system are examined for their function within hepatic and whole-body metabolism. Using adeno-associated viruses or lipid nanoparticles, adaptor protein subunit Ap4e1, membrane tether Vps33b, and ESCRT-I subunit Vps37a are depleted from livers of mice *in vivo*. In addition, *in vitro* knockdowns in primary hepatocytes using siRNA address the mechanisms underlying alterations elicited by depletion of those proteins. These approaches uncover broad metabolic changes, ranging from accelerated fibrosis in NASH upon Ap4e1 reduction to altered lipid and glucose parameters in Vps33b depleted livers, and disturbed Glucagon receptor signaling when Vps37a is removed.

Together, this work attributes thus far unknown roles to the examined proteins within the liver. Furthermore, these data highlight the broad importance of endosomal trafficking complexes in metabolic regulation with implications for metabolic disease.

ZUSAMMENFASSUNG

Das endosomale Transportsystem wird zunehmend als wesentlicher Teil des Energiestoffwechsels wahrgenommen. Organe, die wichtige Funktionen im Stoffwechsel übernehmen, wie die Leber, müssen schnell und effektiv auf veränderte Nährstoffgegebenheiten reagieren können, um das Energiegleichgewicht aufrechtzuerhalten. Dabei unterstützt das endosomale Transportsystem, indem es die Lokalisation von beispielsweise Hormonrezeptoren und Metabolit-Transportern reguliert. Leberzellen benötigen eine besonders komplexe regulation des endosomalen Systems, um die polare Verteilung von basolateralen Protein, die mit dem Blut interagieren, und apikalen Membranen, die an Gallensäure grenzen, beizubehalten. Diese Arbeit beleuchtet im Speziellen drei Komponenten dieses Systems und deren Auswirkungen auf den Stoffwechsel im Allgemeinen und in der Leber: Adaptor Protein Bestandteil Ap4e1, Membran-Verknüpfung Vps33b und ESCRT-I Bestandteil Vps37a werden mittels Adeno-assoziierten Viren und Lipid Nanopartikeln in Lebern von Mäusen *in vivo* herunterreguliert und mithilfe von siRNAs *in vitro* in primären Leberzellen. Mithilfe dieser Systeme lassen sich weitreichende metabolische Veränderungen feststellen. Diese reichen von beschleunigter Entstehung von Fibrose in NASH bei Ap4e1-Reduktion, über veränderte Lipid- und Glukoseparameter in Tieren mit reduziertem hepatischem Vps33b, bis hin zu einer Störung des Glukagon-Rezeptor Signalweges nach Entfernung von Vps37a.

Zusammenfassend präsentiert diese Arbeit bislang unbekannte Funktionen der untersuchten endosomalen Proteine in der Leber. Darüber hinaus heben diese Daten die umfangreiche und wichtige Rolle des endosomalen Transportsystems in der Stoffwechselregulation hervor, auch im Bezug auf Stoffwechselerkrankungen.

ACKNOWLEDGEMENTS

This work is the present culmination of my continued interest in metabolic research. My scientific journey began together with Blaž in the lab of Dr. Kathrin Mädler in Bremen, who both sparked my curiosity in physiology and metabolism. After that, I was able to deepen my interest during two fun years in the institute of Prof. Dr. Alexander Pfeifer in Bonn, until I then joined PD Dr. Anja Zeigerers group in Munich. Throughout my work in her group, I experienced extensive support and encouragement, as well as trust, allowing for independence and growth. Thank you, Anja, for exciting research and discussions, and your wonderful supervision.

Of course, I am also deeply thankful to my Thesis Advisory Committee members, Prof. Dr. Stephan Herzig and Prof. Dr. Nina-Henriette Uhlenhaut, who assisted this dissertation with valuable discussions. In addition, thanks to all members of the Institute for Diabetes and Cancer and the group Endocytosis and Metabolism for creating a supportive environment. Here, I would like to highlight especially Dani, the best technician a lab has ever seen; Adriano, the institute's doubtless treasure; and Revathi, my initial tutor. Importantly, huge thank you to my dear desk mate Alina, for all the discussions, laughs and (most vital) sneaky eye rolls over the cupboard.

I would like to further express my deep gratitude to family and friends, who went on this journey with me. Thanks Mama und Papa for taking good care of me and enabling me to pursue my interests.

Finally, words cannot express my sincere appreciation for you, Christina. Thank you so much for your patience, your uplifting character, and your ever-lasting support. You have been a huge part of this work and I am extremely lucky you are at my side.

TABLE OF CONTENTS

LIST OF PUBLICATIONS

ACCEPTED:

Sekar, R. #, **Motzler, K. #**, Kwon, Y., Novikoff, A., Jülg, J., Najafi, B., Wang, S., Warnke, A. L., Seitz, S., Hass, D., Gancheva, S., Kahl, S., Yang, B., Finan, B., Schwarz, K., Okun, J. G., Roden, M., Blüher, M., Müller, T. D., Krahmer, N., Behrends, C., Plettenburg, O., Miaczynska, M., Herzig, S., Zeigerer, A. (2022). Vps37a regulates hepatic glucose production by controlling glucagon receptor localization to endosomes. Cell Metabolism, 34(11), 1824-1842.e9. https://doi.org/10.1016/j.cmet.2022.09.022 (# equal contribution)

UNDER REVISION:

Jimena, A., Nunez, A., Dittner, C., Becker, J., Loft, A., Mhamane, A., Maida, A., Georgiadi, A., Tsokanos, P., Klepac, K., Molocea, E., Merahbi, R., **Motzler, K.**, Geppert, J., Karikari, R. A., Szendrödi, J., Feuchtinger, A., Hofmann, S., Melchior, F., Herzig, S. (under revision). Fasting-sensitive SUMO-switch on Prox1 controls hepatic cholesterol metabolism.

Nieborak, A., Lukauskas, S., Capellades, J., Heyn, P., Santos, G.S., **Motzler, K.**, Zeigerer, A., Bester, R., Protzer, U., Schelter, F., Wagner, M., Carell, T., Hruscha, A., Schmid, B., Yanes, O., Schneider, R. (under revision). Depletion of pyruvate kinase (PK) activity causes glycolytic intermediate imbalances and reveals a PK-TXNIP regulatory axis.

1 INTRODUCTION

Energy metabolism is one of the seven signs defining “life” (Koshland, 2002). Accordingly, metabolic processes are constantly happening within every cell, organ and creature. Given the utmost importance of these processes, a tight regulation developed that maintains proper function. Upon metabolic disturbances, however, such as obesity and associated comorbidities, these well-balanced processes become dysregulated. The following chapters summarize aspects of these developments and focus in particular on the role of the endosomal trafficking system in relation to the liver and the implications this association has for physiology.

1.1 THE OBESITY PANDEMIC

During evolution of the modern human, our species had to survive periods of famine, cold, and other forms of privation. In these times, when food was scarcely available, individuals that could absorb and store energy more effectively than others, while using low amounts of energy during rest, had evolutionary advantages over less effective conspecifics (Yanovski, 2018). Therefore, most of today's living humans share these impressive qualities. However, nowadays, this genotype turns out to be troublesome: A major problem in western civilizations is the increasing prevalence of obesity, caused mainly by lessened physical activity and the calorie-dense western diet, together with permanent access to food. The human body is still optimized for energy uptake and storage, while availability and demand are vigorously changed (Blüher, 2019; James, 2004).

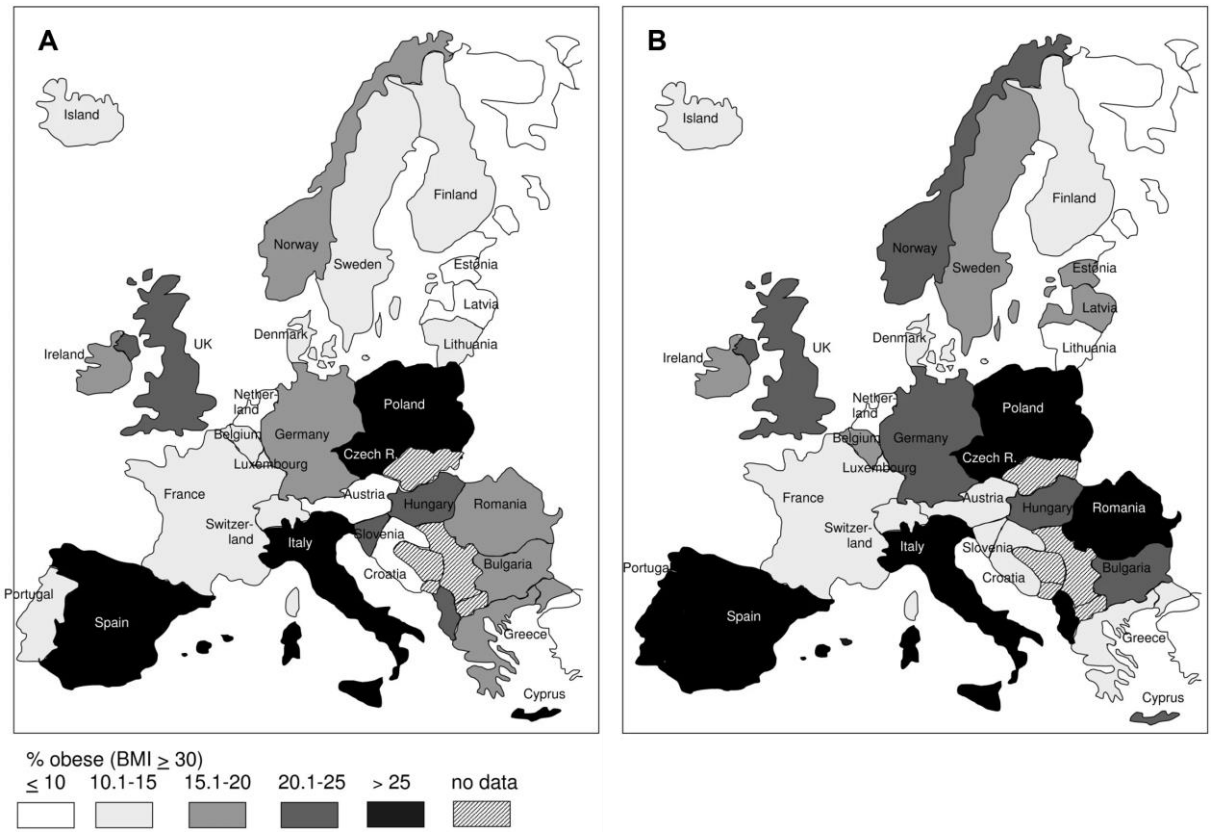

Figure 1 – Obesity prevalence throughout Europe.
Percentage of obesity prevalence in European countries for men (A) and women (B). Percentages are based on studies published between 1990 and 2008, representative for the overall population in each country. Images are reused under CC BY 2.0 license (Berghöfer et al., 2008). BMI: Body Mass Index.

The occurrence of obesity, defined by a Body Mass Index (BMI) > 30 kg/m^2 (James, 2004), has increased dramatically in recent years. In the early 2000s, obesity prevalence amasses to > 20 % for more than half of European countries (**Figure 1**) (Berghöfer et al., 2008; Fry & Finley, 2005), and projections for 2030 and 2060 predict a continued increase to 25-30 % (Janssen et al., 2020; Kelly et al., 2008; Pineda et al., 2018).

In addition, a variety of comorbidities such as type 2 diabetes, cardiovascular disease (CVD), or non-alcoholic fatty liver disease and non-alcoholic steatohepatitis are closely associated with obesity (Roden & Shulman, 2019). Importantly, obesity and linked comorbidities are not only a threat to the health of each affected individual, but also a substantial burden for public healthcare systems (Y. C. Wang et al., 2011), with US$327 billion estimated costs in the US in 2017 (Yanovski, 2018) and 10 billion Euros for Germany in 2002 (Fry & Finley, 2005). Therefore, fighting further spreading of the disease, as well as finding effective therapies is of tremendous importance.

1.1.1 Type 2 Diabetes

Concomitantly to increasing obesity prevalence, worldwide diabetes mellitus cases are expected to rise by 50 % until 2040 (Ogurtsova et al., 2017). Most diabetes mellitus cases, however, are accounted for by type 2 diabetes (T2D). Type 1 diabetes (T1D) is an autoimmune disease, resulting in the destruction of insulin-producing β-cells in the endocrine pancreas and an absolute lack of insulin (Atkinson et al., 2014). T2D instead manifests with a relative lack of insulin, as insulin is still produced, yet not enough to make up for decreased sensitivity of peripheral tissue to insulin. Thus, blood glucose excursions cannot be controlled anymore, resulting in additional complications such as diabetic nephropathies or neuropathies (Forbes & Cooper, 2013).

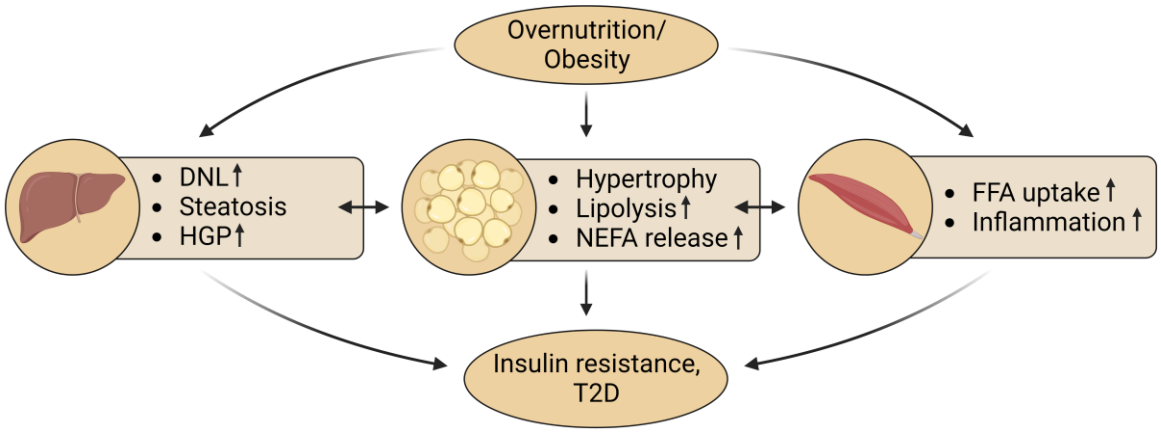

Figure 2 – Metabolic alterations in liver, adipose tissue and skeletal muscle upon overnutrition.
Chronic overnutrition can lead to obesity, which both result in drastic metabolic alterations, exemplified in this figure. In the liver, these changes include enhanced *de novo* lipogenesis (DNL), steatosis, and increased hepatic glucose production (HGP). In adipose tissue, overnutrition induces tissue hypertrophy, as well as increased lipolysis and release of non-esterified fatty acids (NEFAs), whereas in muscle, free fatty acid uptake and inflammation are increased. Moreover, tissue crosstalk and metabolite exchange between organs contributes to systemic disturbances. Ultimately, these changes can result in insulin resistance and type 2 diabetes (T2D). Created with BioRender.com

Pancreatic β-cells secrete insulin postprandially to facilitate anabolic processes as storage of lipids and inhibition of lipolysis. In addition, insulin stimulates the uptake of glucose into peripheral tissue such as muscle and white adipose tissue (WAT) to reduce blood glucose (Roden & Shulman, 2019). Precisely, insulin inhibits lipolysis in WAT, thereby decreasing circulating and hepatic levels of Non-esterified fatty acids (NEFAs). Thus, acetyl-CoA levels in the liver decrease which leads to lowered pyruvate carboxylase activity, hence reducing glycerol-to-glucose conversion and hepatic gluconeogenesis. Moreover, direct action of insulin and hepatic insulin receptor (InsR) mediate reducing glycogenolysis which further contributes to decreased hepatic glucose production (HGP) (Perry et al., 2015). Under conditions of overnutrition, however, diacylglycerol accumulates intracellularly in the liver during *de novo* lipogenesis (DNL), which promotes translocation of protein kinase C-ε (PKCε) to the plasma membrane, where it phosphorylates and inhibits InsR (Petersen et al., 2016). Thus, these well-balanced processes become ineffective due to reduced sensitivity of insulin-responsive tissue to insulin, termed insulin resistance (IR) (Petersen & Shulman, 2018) (**Figure 2**). Finally, IR necessitates increased insulin production to compensate for lowered insulin-responsiveness, resulting eventually in β-cell-failure and -apoptosis with diminished insulin secretion and an absolute lack of insulin, defining T2D.

T2D annunciates as prediabetes with raised blood glucose levels (termed intermediate hyperglycemia) and IR, which can progress to T2D with further elevations in blood glucose (hyperglycemia) (Tabák et al., 2012). However, risk associations for the development of T2D differ between 6 defined subclusters of patients with prediabetes, as well as risks for the development of other complications. For example, patients in clusters 1, 2, and 4 have a low risk for T2D with low mortality despite diagnosed prediabetes. Interestingly though, patients in cluster 6 possess a relatively low risk for T2D as well, yet mortality is higher due to an increased risk of developing nephropathies. Patients in clusters 3 and 5 are at high risk of developing T2D, and patients specifically in cluster 5 have IR and are very likely to have Non-alcoholic fatty liver disease (Wagner et al., 2021).

1.1.2 NON-ALCOHOLIC FATTY LIVER DISEASE AND NON-ALCOHOLIC STEATOHEPATITIS

Non-alcoholic fatty liver disease (NAFLD) is tightly associated with obesity, insulin resistance, and T2D (Li et al., 2016; Williams et al., 2011; Yki-Järvinen, 2014). NAFLD appears in various forms, ranging from simple hepatic lipid deposition (i.e. steatosis) to non-alcoholic steatohepatitis (NASH) and cirrhosis (Ekstedt et al., 2017) (**Figure 3**). NASH is characterized by hepatocellular ballooning, lobular inflammation, and collagen deposition within the liver, thus impeding proper liver function. Fibrotic lesions upon NASH liver injury can lead to

cirrhosis, i.e. disturbed blood flow through the liver. In addition, NAFLD and NASH are strong risk factors for the development of hepatocellular carcinoma (HCC) (Younossi, 2019).

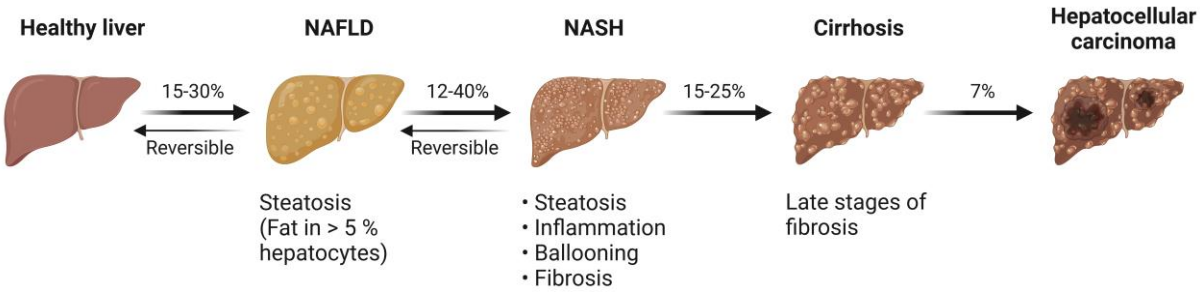

Figure 3 – Transition from NAFLD to late-stage diseases NASH, cirrhosis, and HCC.
Schematic depiction of NAFLD (Non-alcoholic fatty liver disease), NASH (Non-alcoholic steatohepatitis), cirrhosis, and hepatocellular carcinoma (HCC) with prevalence to continue to more severe disease. Adapted from "Non-Alcoholic Fatty Liver Disease (NAFLD) Spectrum", by BioRender.com (2023). Retrieved from https://app.biorender.com/biorender-templates

NAFLD develops due to chronic overnutrition, leading to steatosis. Decreased inhibition of DNL from fructose, but also other carbohydrates, due to IR contributes to excessive lipid deposition within the liver and hence accelerates disease progression (Friedman et al., 2018; Petersen & Shulman, 2018; Sánchez-Lozada et al., 2010). Development from NAFLD to NASH has long been described by a "two-hit"-theory, where hepatic lipid accumulation would pose the "first hit", causing NAFLD, ensued by a "second hit", such as oxidative stress, causing NASH (Day & James, 1998). However, due to the diversity of NASH pathogenesis, this theory is now considered outdated. Instead, multiple events, or "hits", are now seen as contributors to NASH development (Friedman et al., 2018; Malaguarnera et al., 2009). Combined, these events result in the accumulation of toxic lipid species that induce hepatocellular stress and cytokine release, causing apoptosis, immune cell activation, and fibrosis (Mota et al., 2016; Neuschwander-Tetri, 2010).

Given the rapid increase in NAFLD prevalence, NAFLD is expected to become the main cause for liver transplantation (Pais et al., 2016). However, due to the variety of comorbidities associated with NAFLD, NAFLD patients are currently often removed from transplantation lists (O'Leary et al., 2011), further highlighting the importance of finding effective treatment strategies.

1.2 LIVER ANATOMY AND FUNCTION

The liver is a central metabolic organ, facilitating various functions to maintain energy homeostasis. In humans, the liver consists of two highly vascularized lobes that receive blood mainly from the gastrointestinal tract and the pancreas *via* the portal vein (Abdel-Misih & Bloomston, 2010). Thus, the liver integrates hormonal and nutritional signals coming from these organs.

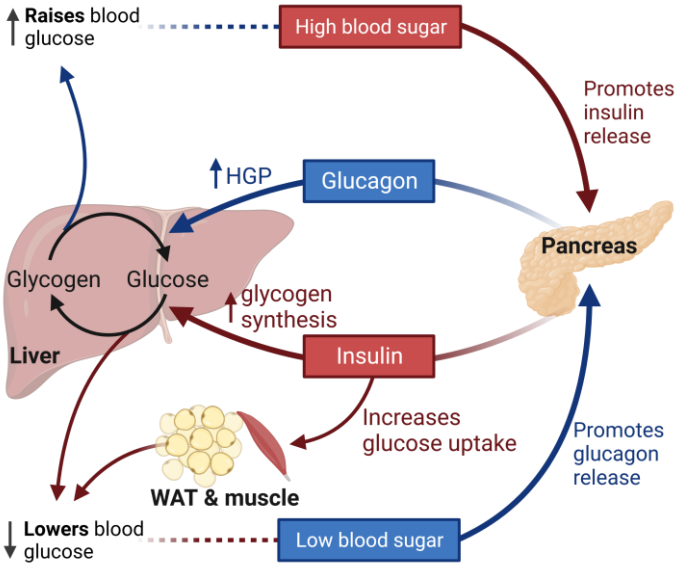

Figure 4 – Glucose-centered hepatic actions of insulin and glucagon on blood glucose levels.
Insulin is secreted postprandially when blood glucose levels are high to regulate the reduction of blood glucose by inducing hepatic glycogen production and decreasing hepatic glucose output, while also enhancing glucose uptake in white adipose tissue (WAT) and muscle. In contrast, when blood glucose levels are low, glucagon is secreted by the pancreas and induces hepatic glucose production (HGP) to raise blood glucose levels. Adapted from "Regulation of blood glucose", by BioRender.com (2023). Retrieved from https://app.biorender.com/biorender-templates

Upon ingestion of a meal, nutrient-rich blood, containing, carbohydrates, proteins, amino acids, and lipids reaches the liver, together with hormones, such as pancreatic insulin. Here, insulin facilitates the disposal of glucose by activating glycogen synthesis and glycolysis, and inhibits hepatic glucose production (Petersen & Shulman, 2018) (**Figure 4**). Moreover, insulin induces fatty acid synthesis, thus facilitating the removal of nutrients from the blood. Importantly, during periods of fasting, the liver contributes to energy homeostasis by secreting glucose and fatty acids into the blood stream (Zeigerer et al., 2021). These effects are largely mediated by glucagon, a hormone secreted by the pancreas when blood glucose levels are low (Frizzell et al., 1988; Müller et al., 2017) (**Figure 4**). In addition, the liver secretes bile into the stomach to aid the uptake of e.g. lipids (De Aguiar Vallim et al., 2013). Combined, these functions position the liver as crucial metabolic organ for the maintenance of energy homeostasis.

The main cell type within the liver are hepatocytes that contribute 60 % in cell number and 80 % of cellular mass (Gebhardt, 1992). Other cell types include endothelial cells, surrounding

the vasculature, liver-resident immune cells, such as hepatic stellate cells (HSCs) and Kupffer cells, and cholangiocytes, forming the bile duct (Trefts et al., 2017). The liver is organized in lobules that allow a tight connection between hepatocytes and blood flow, as well as bile ducts (**Figure 5**).

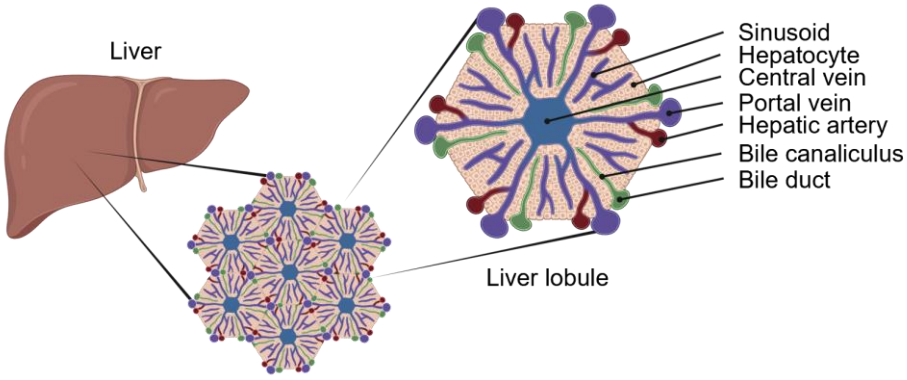

Figure 5 – Lobular organization of the liver.
The liver is composed of liver lobules that allow thorough perfusion and close contact of hepatocytes with blood. Hepatocytes are surrounded by blood vessels connected to the central vein and portal vein, called sinusoids. Bile canaliculi facilitate the flow of bile acids, secreted by hepatocytes, to the bile duct. Created with BioRender.com

Hepatocytes are highly polarized cells with membranes separated by tight junctions into distinct basolateral and apical domains. The basolateral membrane is facing the blood stream or sinusoid, whereas the apical membrane forms the bile canaliculus (Schulze et al., 2019). This separation allows for the specific transport of e.g. bile acid transporters to the apical membrane for bile acid secretion, while simultaneously enabling e.g. protein secretion into the blood stream (L. Wang & Boyer, 2004). Quick alterations in protein localization upon changes in nutrient availability, e.g. upon ingestion of a meal, are in part facilitated by the endosomal trafficking system and its components (Gilleron et al., 2019), such as endosomal trafficking complexes.

1.3 ENDOSOMAL TRAFFICKING COMPLEXES

Upon changes in nutrient status, the liver has to adapt quickly by sensing and integrating these signals to either provide or store energy. These adjustments are in part facilitated by the endosomal trafficking system (Gilleron et al., 2019), enabling multi-directional protein transport (Guidotti et al., 2003; Margall-Ducos et al., 2007), and the maintenance of membrane polarity (Müsch, 2004). Importantly, this connection between individual parts of the endosomal system within the liver and related implications for whole body metabolism have already been shown by different groups (Bartuzi et al., 2016; Fedoseienko et al., 2018; Seitz et al., 2019; Sekar et al., 2022; Zeigerer et al., 2015).

The endosomal trafficking system is responsible for all directed protein transport within the cell, mediated by fusion and fission of organellar membranes. Based on the direction of traffic, the endosomal system can be divided into endocytosis, i.e. inward transport, and exocytosis, i.e. outwards transport. The former includes the engulfment and transport of e.g. activated signaling receptors from the plasma membrane (PM) into the cell, whereas the latter comprises e.g. the shuttling of newly synthesized proteins to the PM (Bonifacino & Glick, 2004; Miaczynska et al., 2004). Both, endo- and exocytosis, require a complex arrangement of components, mediating transport along different organelles and endosomal compartments (Gilleron et al., 2019).

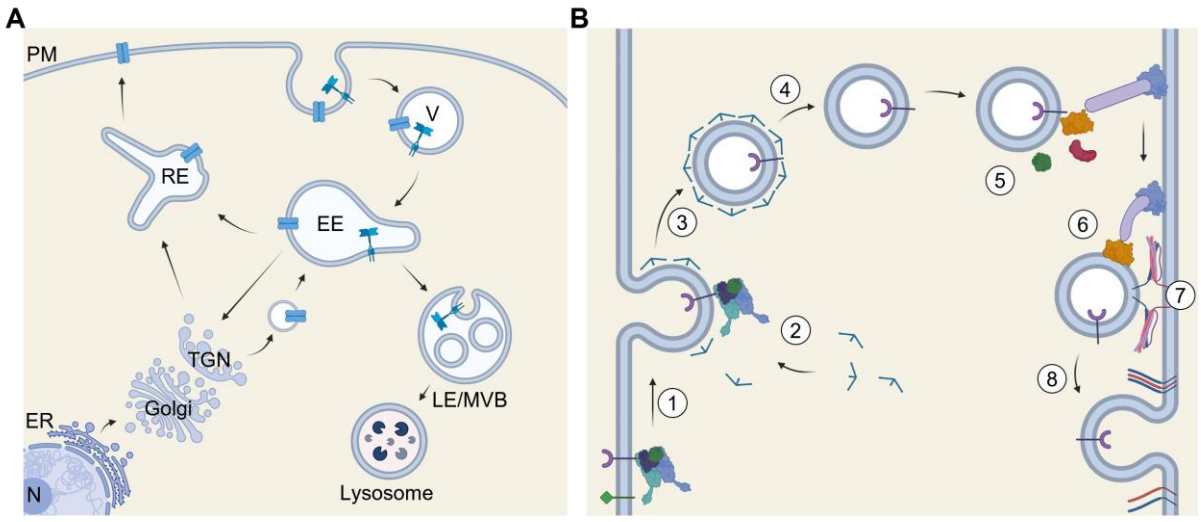

Figure 6 – Endo-lysosomal compartments, vesicle budding and membrane fusion.
(A) Proteins are newly synthetized at the endoplasmic reticulum (ER) and transported *via* the Golgi and *trans*-Golgi network (TGN) to early endosomes (EE) or recycling endosomes (RE). Similarly, transmembrane proteins such as signaling receptors or transporters at the plasma membrane (PM) are directed to EEs in vesicles (V) after internalization. From EEs, proteins can directly be recycled back to the PM *via* REs or through the TGN. In addition, transmembrane cargos can be degraded in lysosomes by trafficking through late endosomes (LE) and multivesicular bodies (MVB).
(B) Heterotetrameric adaptor proteins specifically bind and enrich transmembrane cargo proteins (1) and recruit coat components to form the vesicle bud (2). The vesicle is pinched off from the host membrane (3) and adaptor proteins and coat components are released from the vesicle membrane (4). For fusion with the destination membrane, effector proteins, such as RabGTPases, assemble on the vesicle (5), allowing tethering factors to establish a first contact between the opposing membranes (6). SNARE protein assembly (7) then facilitates the fusion of the two membranes (8). (A-B) Created with BioRender.com

Endosomal compartments comprise early and late endosomes, recycling endosomes, and lysosomes, collectively referred to as endo-lysosomal system (Gilleron & Zeigerer, 2022) (**Figure 6A**). Individual cellular membranes within the endo-lysosomal system are characterized by distinct phosphatidylinositol phosphate (PIP) and protein compositions (Krahmer et al., 2018; Paolo & Camilli, 2006; Segev, 2001). PIPs define organelle identity and aid the specific attraction of certain proteins. Phosphatidylinositol 3-phosphate (PI3P), for example, is enriched at early endosomal membranes (Gillooly et al., 2000), where it is bound by soluble proteins destined for early endosomal localization, such as early endosomal antigen 1 (EEA1) (Simonsen et al., 1998). Enhancing binding specificity for early endosomes, EEA1 binds membrane-bound early endosomal Rab5 (ras-related in brain 5) (Simonsen et al., 1998). Hence, recognition of markers specific for distinct membrane entities allows to distinguish between endosomal compartments, specific fusion of their membranes, and for the correct localization of proteins (**Figure 6B**).

1.3.1 Adaptor protein complexes

For the targeted delivery of transmembrane proteins to a destination organelle, cargo proteins are enriched in dedicated regions within the donor organelle, called coated pits, where they are packed into developing vesicles. The nascent vesicle then pinches off and is transported to the target organelle to be tethered and fused with the opposing membrane (Bonifacino & Glick, 2004; Nakatsu & Ohno, 2003) (**Figure 6B**). Among the variety of cytosolic proteins involved are adaptor protein (AP) complexes, mediating cargo selection and vesicle coat assembly.

Thus far, five adaptor protein complexes have been described (AP-1-5) (Hirst et al., 2013; Park & Guo, 2014), with AP-1 and AP-3 having cell type-specific isoforms (Bonifacino, 2014). The AP-4 and AP-5 complexes are the least well studied complexes, with the former being discovered in 1999 and the latter in 2011 (Dell'Angelica et al., 1999; Hirst et al., 1999, 2011). All APs are heterotetrametric complexes composed of two large subunits (β1-5 and either α, γ, δ, ε, or ζ for AP-1-5, respectively), one medium-sized subunit (μ1-5), and one small subunit (σ1-5) (Park & Guo, 2014). Each subunit within the complex is assigned a specific role: α, γ, δ, and ε are suggested to mediate membrane binding (Brodsky et al., 2001) and β1-3 are responsible to bind and recruit the clathrin coat through a N-terminal clathrin-box (Boehm & Bonifacino, 2001; Dell'Angelica et al., 1998; Shih et al., 1995). Interestingly, β4 from the AP-4 complex is lacking the clathrin-box, hence no clathrin-recruitment has been reported for AP-4 (Dell'Angelica et al., 1999) and the scaffolding proteins for AP-4 are unknown. The small subunit of AP-2, σ2, has been attributed a role in stabilizing the complex together with μ2 (Collins et al., 2002), and it is expected that σ1 and σ3-5 fulfill a similar function. Lastly, the μ-

subunits are responsible for cargo recognition by binding specific motifs within the cytoplasmic tail of transmembrane cargo proteins (Bonifacino & Traub, 2003).

The first motif for endocytosis was found based on the landmark reports by Goldstein and Brown that identified a single point mutation within the cytoplasmic tail of the low-density lipoprotein (LDL) receptor (LDLR) causative of one form of familiar hypercholesterinemia (Anderson et al., 1977; Brown & Goldstein, 1976). The peptide sequence affected by this mutation, NPXY (Asn-Pro-X-Tyr, where X is any amino acid), was then also found in other transmembrane proteins and amino acid substitutions in NPXY resulted in increased serum LDL cholesterol levels due to decreased endocytosis of LDLR (Chen et al., 1990). Later, another tyrosine-based motif YXXØ (Ø as bulky, hydrophobic amino acid (i.e. leucine, isoleucine, phenylalanine, methionine, or valine)) was found that is recognized by all µ-subunits (Aguilar et al., 2001; Boll et al., 1996; Hirst et al., 2013; Ohno et al., 1998). Thus, additional selectivity is provided by distinct cellular localization of the APs (Park & Guo, 2014).

Polarized sorting by APs is mainly distinguished into sorting of transmembrane proteins endocytosed from the plasma membrane at recycling endosomes and sorting of newly synthetized proteins from the *trans*-Golgi network (TGN) (Bonifacino, 2014). The AP-4 complex, one of the main targets of this study, is located at the TGN (Dell'Angelica et al., 1999; Hirst et al., 1999) and the directions of sorting events mediated by AP-4 are controversially discussed. In HeLa cells, AP-4 was shown to regulate sorting from the TGN to both, late endosomes (Aguilar et al., 2001) and early endosomes (Burgos et al., 2010; Toh et al., 2017). In polarized MDCK cells, however, AP-4 regulates sorting of transmembrane proteins towards basolateral membranes (Simmen et al., 2002).

AP-4 subunits are ubiquitously expressed (Dell'Angelica et al., 1999; Hirst et al., 1999), suggesting universally important functions, albeit very low expression levels compared to other APs: In HeLa cells, estimates for AP-4-positive vesicles per cell are 30- and 60-fold lower compared to AP-1 and AP-2, respectively (Hirst et al., 2013). However, defects in any subunit of AP-4 result in a severe recessive neurological disorder with early onset progressive spastic paraplegia (SPG) and intellectual disability, also named hereditary spastic paraplegia (HSP) (Abou Jamra et al., 2011; Behne et al., 2020; Ebrahimi-Fakhari et al., 2018; Verkerk et al., 2009) and thus, AP-4 function is mainly studied in regards to SPG and HSP.

Early studies on AP-4 have suggested a variety of basolateral receptors to be trafficked by AP-4 in polarized MDCK cells, including the metabolically relevant LDLR (Simmen et al., 2002). In addition, mislocalized LDLR was also reported in brains of β4-deficient mice (Matsuda et al., 2008). Yet, the metabolic relevance of these findings are questionable, as endocytosis of LDLR in the liver is mainly attributed to LDLR associated protein 1 (LDLRAP1) and AP-2 (He et al., 2002; Mishra et al., 2002).

Recent research on AP-4 and its subunits was until now limited to function in neurons, given the direct causal relationship with HSP. Involvement in other diseases, however, such as obesity and associated comorbidities, has thus far been neglected. Here, this work reveals a novel role for Ap-4 ε1 (Ap4e1) in NAFLD and NASH, thereby broadening the functional spectrum of AP-4 to metabolic disease.

1.3.2 MEMBRANE TETHERING COMPLEXES

APs, described in the previous chapter, mediate the generation of specialized vesicles through the recruitment of coat components and fall off the nascent vesicle after release from the host membrane. Thus, other cytosolic proteins regulate the fusion process of the vesicle membrane with that of the target organelle (**Figure 6B**). In order for two opposing membranes to fuse, three key components are required: Rab GTPases, membrane tethers, and SNARE proteins (van der Beek et al., 2019).

Fusion is initiated by proteins of the Rab-family of GTPases. The exchange of guanosine diphosphate (GDP) for guanosine triphosphate (GTP) recruits a range of proteins needed to facilitate membrane fusion further (Segev, 2001), including membrane tethers. Finally, soluble N-ethylmaleimide-sensitive fusion protein (NSF) attachment protein receptors (SNAREs) on both membranes mediate the actual fusion (Südhof & Rothman, 2009). Interestingly though, Rothman and colleagues have shown that in artificial vesicles, SNARE proteins alone are able to facilitate membrane fusion (Weber et al., 1998), while still providing specificity (McNew et al., 2000; Paumet et al., 2004), hence questioning the need for membrane tethers *per se*. However, membrane tethers hold features that are indispensable for membrane fusion in actual cells, some of them detailed below.

Tethers comprise are diverse group of proteins or protein complexes that span long distances within cells, thus establishing a first distant contact between two opposing membranes (Yu & Hughson, 2010). Early endosome tether EEA1, for example, was shown to span around 200 nm distance (Murray et al., 2016), whereas SNARE proteins are only around 12 nm in length (Duman & Forte, 2003). EEA1 pulls opposing membranes closer together through a conformational change initiated by the GTPase Rab5 (Murray et al., 2016), thus enabling actual membrane fusion through SNAREs (Bonifacino & Glick, 2004). Moreover, SNARE-only mediated membrane fusion is largely inefficient (Ohya et al., 2009), thus tethers, given their length, promote more efficient membrane fusion (Yu & Hughson, 2010).

Besides single-protein membrane tethers such as EEA1, multisubunit tethering complexes (MTCs) introduce additional layers of complexity and specificity for membrane fusion (Spang, 2016). Among these are three related complexes, HOPS (homotypic fusion and vacuole

protein sorting), CORVET (class C core vacuole/endosome tethering), and CHEVI (class C homologs in endosome-vesicle interaction), regulating transport within the endo-lysosomal trafficking system (Spang, 2016; van der Beek et al., 2019). More specifically, HOPS regulates homo- and heterotypic fusion of late endosomes and lysosomes, while CORVET aids homotypic fusion of early endosomes (van der Beek et al., 2019; Yu & Hughson, 2010). Fusion events mediated by the most recently discovered CHEVI complex, however, are less clear. Interestingly, expanding their tethering function to SNARE assembly, HOPS, CORVET, and CHEVI contain one isoform of Sec1/Munc18-family (SM) member vacuolar protein sorting 33A/B (VPS33A: HOPS and CORVET; VPS33B: CHEVI) (van der Beek et al., 2019). SM proteins, such as yeast Vps33, were shown to bind SNAREs on opposing membranes, thus acting as chaperones for SNARE complex assembly (Baker et al., 2015; Krämer & Ungermann, 2011). In addition to VPS33B, the CHEVI complex comprises VIPAS-39 (Spang, 2016) and its function is detailed below as Vps33b is one of the main targets in this study.

In polarized cells, such as epithelial cells or hepatocytes, CHEVI mediates recycling of apical proteins through Rab11a positive recycling endosomes (Cullinane et al., 2010; Hanley et al., 2017). Besides, CHEVI was shown important for the generation of lysosome related organelles (LROs) in megakaryocytes, where deficiencies in CHEVI result in impaired trafficking from the Golgi to LROs (Bem et al., 2015; Rogerson & Gissen, 2016). An additional role for Vps33b has been established in HeLa cells, where CHEVI can be recruited to late endosomes and lysosomes, aiding their heterotypic fusion (Galmes et al., 2015). Thus, the variety of functions suggest cell type-specific roles for the CHEVI complex. Importantly, mutations within either VPS33B or VIPAS-39 result in arthrogryposis-renal dysfunction-cholestasis (ARC) syndrome, a severe autosomal recessive disorder (Cullinane et al., 2010; Gissen et al., 2004, 2006; Zhou & Zhang, 2014), further underlining the importance of the CHEVI complex and its subunits.

1.3.3 Endosomal sorting complex required for transport

Another important step in endosomal trafficking is mediated by the endosomal sorting complex required for transport (ESCRT) machinery. The ESCRT multisubunit machinery comprises ESCRT-0 to ESCRT-III and the Vps4/SKD1 complex (Schmidt & Teis, 2012). In contrast to mechanisms involving the proteins and complexes described in previous chapters, ESCRTs mediate the inwards bending and abscission of vesicles away from the cytosol. This feature fulfils three major functions within cells: i) During cytokinesis at the end of cell division, ESCRTs mediate the membrane separation of two daughter cells (Dukes et al., 2008; Elia et al., 2011). ii) ESCRTs are required for budding and release of HIV (human immunodeficiency virus) particles from host cells (Garrus et al., 2001). iii) Lastly, the feature of enabling inwards budding is key for the generation of intraluminal vesicles (ILV) to form multivesicular bodies (MVB)

(Henne et al., 2011). MVB generation is a fundamental sorting process occurring on early endosomal membranes that serves the delivery of ubiquitinated transmembrane proteins to lysosomes for subsequent degradation (Bache et al., 2006). Here, the ESCRT machinery orchestrates the concentration of ubiquitinated cargo and the inwards budding of the endosomal membrane with ensuing fission thereof, thus generating ILVs that make up the MVB (Schmidt & Teis, 2012) (**Figure 6A**).

The sorting process is initiated by ESCRT-0 recruitment to endosomes by binding both, ubiquitin, attached to transmembrane proteins destined for lysosomal degradation, and PI3P within the endosomal membrane (Henne et al., 2011; Raiborg et al., 2001). Moreover, ESCRT-0 directs ESCRT-I to the endosome, which acts as a bridge between ESCRT-0 and ESCRT-II (Henne et al., 2011). This trimer of complexes facilitates the enrichment of ubiquitinated cargos, as well as the invagination of the endosomal membrane. Upon ESCRT-III assembly on the membrane, the cargos are collected into the nascent ILV and ILV formation is finalized by membrane scission (Wollert et al., 2009). Lastly, the Vps4/SKD1 complex mediates the disassembly of the ESCRTs and their return into the cytosol (Babst et al., 1998). Thus, the ESCRT machinery has an important role in the downregulation of transmembrane cargo proteins, such as ubiquitinylated signaling receptors (Szymanska et al., 2018).

The most prominent example of ESCRT-mediated receptor degradation is endosomal growth factor (EGF) receptor (EGFR) (Bache et al., 2006; Malerød et al., 2007). EGFR becomes ubiquitinated after activation, resulting in internalization and signal termination (Levkowitz et al., 1999). Upon depletion of ESCRT complex subunits, EGFR accumulates at early endosomal and MVB membranes and undergoes less degradation (Malerød et al., 2007). Despite decreased degradation upon ESCRT deficiencies, EGFR signaling activity is not necessarily reduced due to its endosomal localization (Bache et al., 2006). In interesting contrast, G protein coupled receptors (GPCRs) such as β_2 adrenergic receptor or parathyroid hormone receptor type 1 continue to signal from endosomal membranes (Ferrandon et al., 2009; Irannejad et al., 2013).

Thus far, ESCRT function in the downregulation of signaling receptors has not been addressed much in relation to metabolism. In fact, metabolic roles for ESCRT have mainly been connected to the generation of extracellular vesicles and their contribution to inter-organ communication during T2D (Liu et al., 2022). However, ESCRT-mediated MVB-formation was shown to regulate the development of NASH by mediating lysosomal Tlr4 degradation (Zhao et al., 2017). Precisely, ESCRT-I was attributed a prominent role through direct interaction of ESCRT-I subunit Tsg101 with Tmbim1, thereby increasing Tlr4 turnover (Zhao et al., 2017). Whether any of the other subunits, Vps37a-d, Vps28, or Ubap1 are contributing to similar metabolically relevant events is still unknown.

1.4 AIMS

This work aims at investigating the roles of three subunits of different endosomal trafficking complexes in relation to liver metabolism. Given the central role for endosomal trafficking in intracellular protein distribution and the dependency of metabolic adaptation on e.g. hormone receptor localization, it is no surprise that the endosomal system was already shown important for metabolic regulation. Increasing prevalence of obesity and associated comorbidities call for a thorough understanding of these diseases for the identification of novel treatment options. Despite tremendous advancements in this field in recent years, different patient characteristics and diverse responses to treatments require further developments. Among the organs widely affected by e.g. excessive fat accumulation is the liver, yet no treatment options are available for advanced stages of metabolic liver disease.

Here, the functions of three components of the endosomal trafficking system will be examined by liver-specific depletion *in vivo* and in isolated primary murine hepatocytes *in vitro*. Thorough metabolic phenotyping will be combined with functional and mechanistic assays to study the function of Ap4e1, Vps33b, and Vps37a all the way from whole body physiology to cell biology. Applied techniques range from confocal microscopy and proteomics to *in vivo* tolerance tests and tissue analyses. Using cohorts of human patients with metabolic disease and samples of different murine disease models, disease correlations of these proteins will be identified to address potential translatability. These studies are aimed at expanding the current knowledge on trafficking complexes in hepatic (patho-)physiology, hopefully providing novel targets to alter liver disease outcomes.

2 RESULTS

2.1 CHAPTER 1: AP4E1 REGULATES NAFLD-TO-NASH PROGRESSION

Members of the group generated preliminary data on endosomal adaptor protein subunit Ap4e1 based on published data from the International Mouse Phenotyping Consortium (IMPC), which suggested Ap4e1 as a potential metabolic regulator. Thus, my doctoral research started with studying the function of Ap4e1 in livers of mice.

2.1.1 WHOLE-BODY KNOCKOUT (KO) OF AP4E1 IN MICE REVEALS METABOLIC ALTERATIONS

The International Mouse Phenotyping Consortium (IMPC) is generating a comprehensive, publicly available catalog of murine gene function by producing and phenotyping whole-body knockout (KO) mice (Dickinson et al., 2016). In a recent publication, the consortium assessed metabolic abnormalities upon gene deletions in a high-throughput fashion, measuring e.g. bodyweight, glucose tolerance, and serum parameters (Rozman et al., 2018). Among the phenotyped KO mice, mice depleted of Ap-4 subunit ε (Ap4e1) presented with a broad variety of significant metabolic disturbances, summarized from the publication and IMPC website in **Table 1**. Mice with Ap4e1$^{-/-}$ KO showed e.g. impaired glucose tolerance and alterations in blood glucose levels, but also increased serum transaminases and decreased serum albumin (**Table 1**). These liver-related disturbances of whole-body Ap4e1 deletion suggest a functional role for Ap4e1 in liver metabolic function. In addition, the authors connected Ap4e1 with other genes already known to be involved in metabolic regulation by common regulatory elements within the promotor region (Rozman et al., 2018).

Table 1 – Whole-body KO of Ap4e1 results in broad metabolic alterations.
Listing of significant phenotypes, categorized as "homeostasis/metabolism or adipose tissue", analyzed by and obtained from the website of the International Mouse Phenotyping Consortium (IMPC) (Dickinson et al., 2016). Mouselines Tm1a and Tm1b have a KO of first allele or a reporter tagged deletion allele, respectively. Mice with Em2 background have non-functional Ap4e1 due to an indel. Table continues on the next page.

Measurement	Gender	Mouseline
Abnormal cholesterol homeostasis	Female	Tm1b
Decreased circulating chloride level	Female	Tm1b
Increased circulating creatine kinase level	Male	Tm1b
Increased circulating aspartate transaminase level	Female	Em2
Increased circulating aspartate transaminase level	Female	Tm1b
Decreased circulating alanine transaminase level	Male	Tm1b

Decreased circulating creatinine	Male	Tm1a
Increased circulating amylase level	Male	Tm1b
Impaired glucose tolerance	Female	Tm1b
Decreased circulating glucose level	Male	Tm1b
Increased fasting circulating glucose level	Male	Tm1b
Decreased respiratory quotient	Female	Tm1b
Decreased total body fat amount	Female/male	Tm1b
Increased circulating alkaline phosphatase level	Female/male	Tm1b
Decreased circulating serum albumin level	Male	Tm1a
Decreased circulating total protein level	Male	Tm1a

2.1.2 *AP4E1* IS UPREGULATED IN PATIENTS AND MICE WITH NASH

Given the alterations of liver-related metabolic markers upon whole-body KO of Ap4e1 in mice, members of the Zeigerer group assessed the mRNA levels of *AP4E1* in livers of patients with T2D. Interestingly, *AP4E1* is increased in livers of male T2D patients (**Figure 7A**). The corresponding group of females, however, consisted of only four control patients and did not show a significant increase. Within the whole patient cohort, *AP4E1* levels are negatively correlated with hepatic mitochondrial biogenesis markers PGC1A (Peroxisome proliferator-activated receptor gamma coactivator 1-α) and TFAM (mitochondrial transcription factor A) (Heilbronn et al., 2007), suggesting an association of *AP4E1* with mitochondrial impairments.

In human livers of another cohort of patients with NASH (Koliaki et al., 2015), *AP4E1* mRNA showed an almost-significant increase (**Figure 7B**). Therefore, I assessed the expression levels of all Ap-4 subunits in livers of mice fed a NASH-inducing methionine-choline deficient (MCD) diet (Hebbard & George, 2011), used in Seitz et al. (Seitz et al., 2019). In line with human NASH, *Ap4e1* mRNA is increased in MCD-induced NASH (**Figure 7C**). Ap-4 subunit *Ap4s1* showed a tendency for increased expression, while *Ap4m1* and *Ap4b1* remained unchanged (**Figure 7C**). Next, to assess Ap4e1 expression in NASH mouse models resembling the human disease more realistically than the MCD model (Gallage et al., 2022), I utilized livers from mice fed Gubra Amylin NASH (GAN) diet or a diet rich in fructose, palmitate and cholesterol (FPC). In a collaboration between Anja Zeigerers and Natalie Krahmers groups, mice were fed GAN diet for 12 weeks. Here, consistent with the mRNA expression of

Ap4e1 in human and murine MCD-NASH livers, Ap4e1 protein is significantly increased (**Figure 7D, E**).

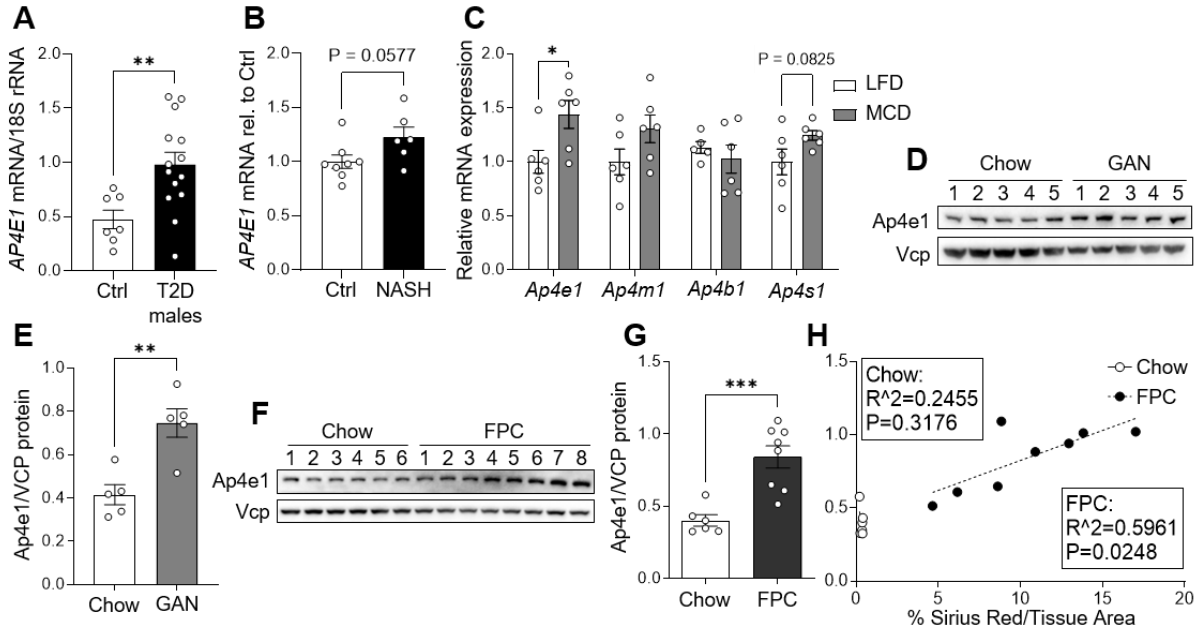

Figure 7 – Ap4e1 is upregulated in NASH.
(A) *AP4E1* mRNA expression in livers of patients with T2D or in healthy controls.
(B) Relative expression of *AP4E1* in livers of patients with NASH or in healthy controls.
(C) Relative mRNA expression of Ap-4 subunits in livers of mice fed a low-fat diet control or NASH-inducing methionine-choline deficient diet for 5 weeks.
(D-E) Western blot of livers of mice fed normal chow diet or GAN for 12 weeks (D) with quantification in (E).
(F-H) Western blot of liver samples from mice fed chow or FPC for 20 weeks. FPC samples 1-8 are sorted by degree of hepatic fibrosis from low (1) to high (8) (F) with quantification thereof in (F). (H) Linear regression of Ap4e1 protein with degree of hepatic fibrosis, assessed by % Sirius Red/Tissue Area.
Data are presented as mean ± SEM (standard error of the mean). *P < 0.05, ** P < 0.01 by two-tailed unpaired Student's t test.

Lastly, in livers of mice fed FPC for 20 weeks (used in Loft et al., 2021), Ap4e1 protein levels were similarly elevated (**Figure 7F, G**). Intriguingly, Ap4e1 protein is positively correlated with the degree of hepatic fibrosis in those livers, as assessed by Sirius red staining (**Figure 7F, H**), indicating a direct relationship between Ap4e1 levels and hepatic fibrosis.

Together, these data strengthen the notion attained from the IMPC data in which Ap4e1 might be involved in hepatic metabolism and liver metabolic disease.

2.1.3 AP4E1 DEPLETION FROM THE LIVER HAS NO EFFECT ON WHOLE-BODY METABOLISM

To investigate the metabolic role of Ap4e1, I performed liver-specific KO using the loxP-Cre system (Schwenk et al., 1995). In brief, homozygous Ap4e1 floxed mice ($Ap4e1^{fl/fl}$) were injected with recombinant adeno-associated virus serotype 8 (rAAV8) for the liver-specific expression of functional wildtype Cre^{WT} ($Ap4e1^{liver\text{-}KO}$) or mutated, non-functional Cre^{mut}

(Control) under the LP1 promotor (Jimena et al., 2022) (**Figure 8A**). Control and Ap4e1$^{liver\text{-}KO}$ mice were extensively phenotyped on standard chow diet, before the mice were fed 60 % High Fat Diet (HFD). On chow diet, Ap4e1 depleted mice showed no alterations in weightgain and random blood glucose, as well as glucose, insulin, and pyruvate tolerance tests (**Figure 8B-F**), rendering glucose utilization unaffected by hepatic Ap4e1 depletion. However, plasma total cholesterol was significantly reduced while plasma LDL cholesterol showed a trend for reduction (**Figure 8G, H**). Interestingly, plasma alanine and aspartate aminotransferase (ALT, AST) were elevated in blood plasma, drawn before the start of HFD (**Figure 8I, J**), indicative of mild liver damage upon Ap4e1 depletion. Based on these results, I aimed at metabolically challenging Ap4e1$^{liver\text{-}KO}$ mice with 60 % HFD.

As observed under chow diet, depletion of Ap4e1 from livers of mice had no effect on bodyweight and random blood glucose (**Figure 8B, C**). Similarly, Ap4e1$^{liver\text{-}KO}$ mice had no alterations in glucose, insulin, and pyruvate tolerance tests (**Figure 8K-M**). After 12 weeks of HFD, the effects on aminotransferases and circulating cholesterol entities were alleviated (**Figure 8N-Q**). In addition, haematoxylin-eosin (HE) staining in sections of Ap4e1$^{liver\text{-}KO}$ livers, performed by the Helmholtz Munich pathology core facility, revealed no alterations in liver tissue structure (**Figure 8R**). Thus, Ap4e1$^{liver\text{-}KO}$ has no effect on *in vivo* glucose and lipid utilization while serum parameters suggest mild signs of liver damage.

(Figure on following page)
(A) Schematic depicting the generation of mice depleted of Ap4e1 from the liver. Homozygous Ap4e1 floxed mice were injected with Adeno Associated Viruses (AAV) serotype 8, expressing either non-functional mutated (mut) Cre (Control) or fully functional wild-type Cre (WT) under the liver-specific LP1 promotor.
(B) Bodyweight development of Control and Ap4e1$^{liver\text{-}KO}$ mice under chow and 60 % High-fat diet (HFD). Mice injected with AAVs at 10 weeks of age were maintained on chow diet for 6 weeks. Then, mice were fed HFD for 12 more weeks.
(C) Random blood glucose of Control and Ap4e1$^{liver\text{-}KO}$ mice under chow and HFD.
(D) Intraperitoneal Glucose tolerance test (ipGTT) in chow-fed mice with 2 g/kg glucose after 6 hours fasting.
(E) Intraperitoneal Insulin tolerance test (ipITT) in chow-fed mice with 1 IU/kg after 6 hours fasting.
(F) Intraperitoneal Pyruvate tolerance test (ipPTT) in chow-fed mice with 2 g/kg pyruvate after 16 hours fasting.
(G-J) Plasma levels of cholesterol (G), LDL cholesterol (H), ALT (I), and AST (J) 6 weeks after AAV injection in Control (Ctrl) and Ap4e1$^{liver\text{-}KO}$ (KO) chow-fed mice.
(K) Intraperitoneal Glucose tolerance test (ipGTT) in HFD-fed mice with 2 g/kg glucose after 6 hours fasting.
(L) Intraperitoneal Insulin tolerance test (ipITT) in HFD-fed mice with 1 IU/kg after 6 hours fasting.
(M) Intraperitoneal Pyruvate tolerance test (ipPTT) in HFD-fed mice with 2 g/kg pyruvate after 16 hours fasting.
(N-Q) Serum levels of HFD-fed mice, sacrificed after 6 hours of fasting for ALT (N), AST (O), cholesterol (P), and LDL cholesterol (Q).
(R) Haematoxylin-eosin (HE) staining in livers of female Control and Ap4e1$^{liver\text{-}KO}$ mice 4 weeks after AAV injection. Scale bar = 100 µM.
Data are presented as mean ± SEM. *P < 0.05, ** P < 0.01 by two-tailed unpaired Student's t test.

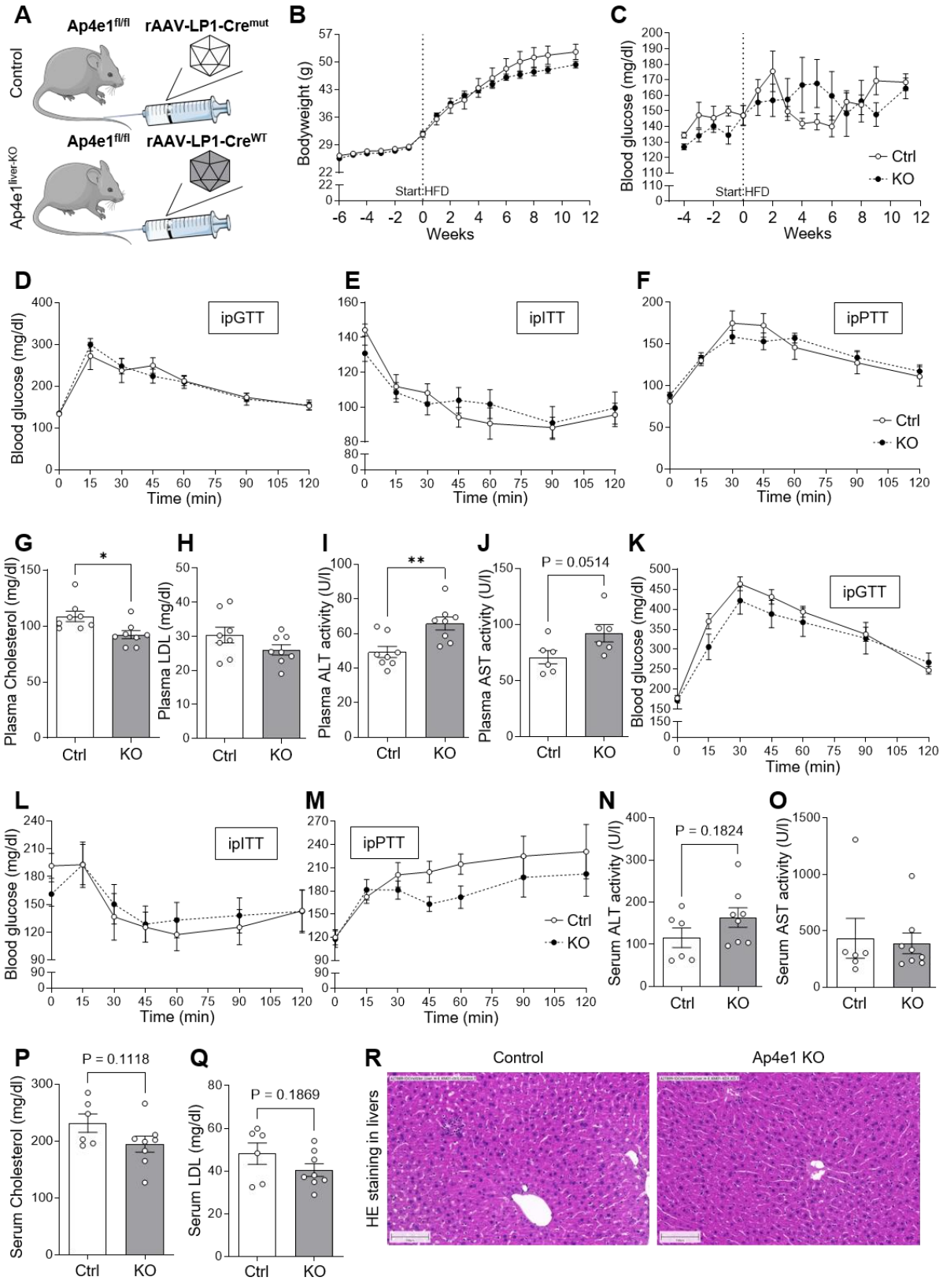

Figure 8 – Ap4e1$^{liver\text{-}KO}$ mice are metabolically healthy on chow diet and HFD.

2.1.4 LIVER-KO OF AP4E1 IN NASH MODELS EXACERBATES FIBROSIS DEVELOPMENT

Given the increased expression of *AP4E1* in livers of patients with NASH (**Figure 7B**) and in mice fed NASH diets (**Figure 7C-H**), I wondered whether depletion of Ap4e1 in mice fed NASH-inducing diets alters disease outcome. Thus, $Ap4e1^{fl/fl}$ mice were put on MCD diet 4 weeks after injection of either control or KO-inducing AAV and sacrificed after 5 weeks of MCD feeding with no alterations in bodyweight (**Figure 9A**). *Ap4e1* mRNA was reduced 59 % in the MCD KO group, compared to control-injected low-fat diet fed mice (**Figure 9B**). KO-efficiency on mRNA under MCD was markedly lower than in chow or HFD fed mice but this might be due to tissue regeneration and tissue remodeling upon MCD (Oz et al., 2006), hence diluting the hepatocyte portion with *Ap4e1* reduction. However, protein levels of Ap4e1 were still reduced by 92 % (**Figure 9C, D**). Interestingly, $Ap4e1^{liver\text{-}KO}$ led to an initial elevation in plasma ALT in blood drawn from the tail vein after 2 weeks on diet. After 4 weeks, however, this effect was alleviated (**Figure 9E**). Moreover, reduction of Ap4e1 resulted in a slight and almost significant increase in liver/bodyweight (**Figure 9F**). Histological examination of hepatic lipid content, performed by the Helmholtz Munich pathology core facility, showed a dramatic increase in lipid droplets in MCD samples, compared to LFD, yet revealed no changes between control and KO MCD (**Figure 9G, H**). Hence, Ap4e1 depletion does not affect lipid utilization in MCD, and this can therefore not explain elevated liver weight. Surprisingly, the degree of hepatic fibrosis, stained by Sirius Red staining, showed a close-to-significant increase in Sirius Red positive tissue area (**Figure 9G, I**). This is especially interesting in light of the observed positive correlation of Ap4e1 protein with hepatic fibrosis in livers of FPC fed mice (**Figure 7F, H**), as this suggested an ameliorating effect of Ap4e1 reduction on fibrosis. However, this is in line with elevated aminotransferase levels seen under different diets.

(Figure on following page)
(A) Bodyweight of mice fed methionine-choline deficient (MCD) or control low-fat (LFD) diet. MCD/LFD feeding started 3 weeks after AAV injection.
(B) Relative mRNA expression of *Ap4e1* in livers of LFD- or MCD-fed mice.
(C-D) Quantified protein expression of Ap4e1 in (C) and immunoblot in (D).
(E) Plasma ALT levels in mice fed LFD or MCD for 2 and 4 weeks.
(F) Liver/bodyweight ratio from LFD- or MCD-fed mice.
(G-I) Liver sections of LFD- or MCD-fed mice, stained with Sirius Red (G) with quantifications of lipid area (H), and Sirius Red positive area (I).
(J) Bodyweight of mice fed chow control or fructose, palmitate, cholesterol rich diet (FPC). Six weeks old mice were put on diet for 4 weeks before AAV injection. After the initiation of KO, the mice were kept on diet for 12 more weeks before sacrificed.
(K) Liver/bodyweight ratio from chow- or FPC-fed mice.
(L-M) Plasma levels for AST (L) and ALT (M) in chow- or FPC-fed control and $Ap4e1^{liver\text{-}KO}$ mice, 8 weeks after initiation of KO.
(N-P) Sirius Red stained liver sections of chow- or FPC-fed mice (N) with quantifications of lipid area (O), and Sirius Red positive area (P).
(Q) Percentage of mice per treatment group assigned to different inflammation scores, defined by the number of inflammatory foci per tissue area.
Data are presented as mean ± SEM. *P < 0.05, **P < 0.01, ***P < 0.001, ****P < 0.0001 by ordinary one-way ANOVA with Šídák's multiple comparisons test.

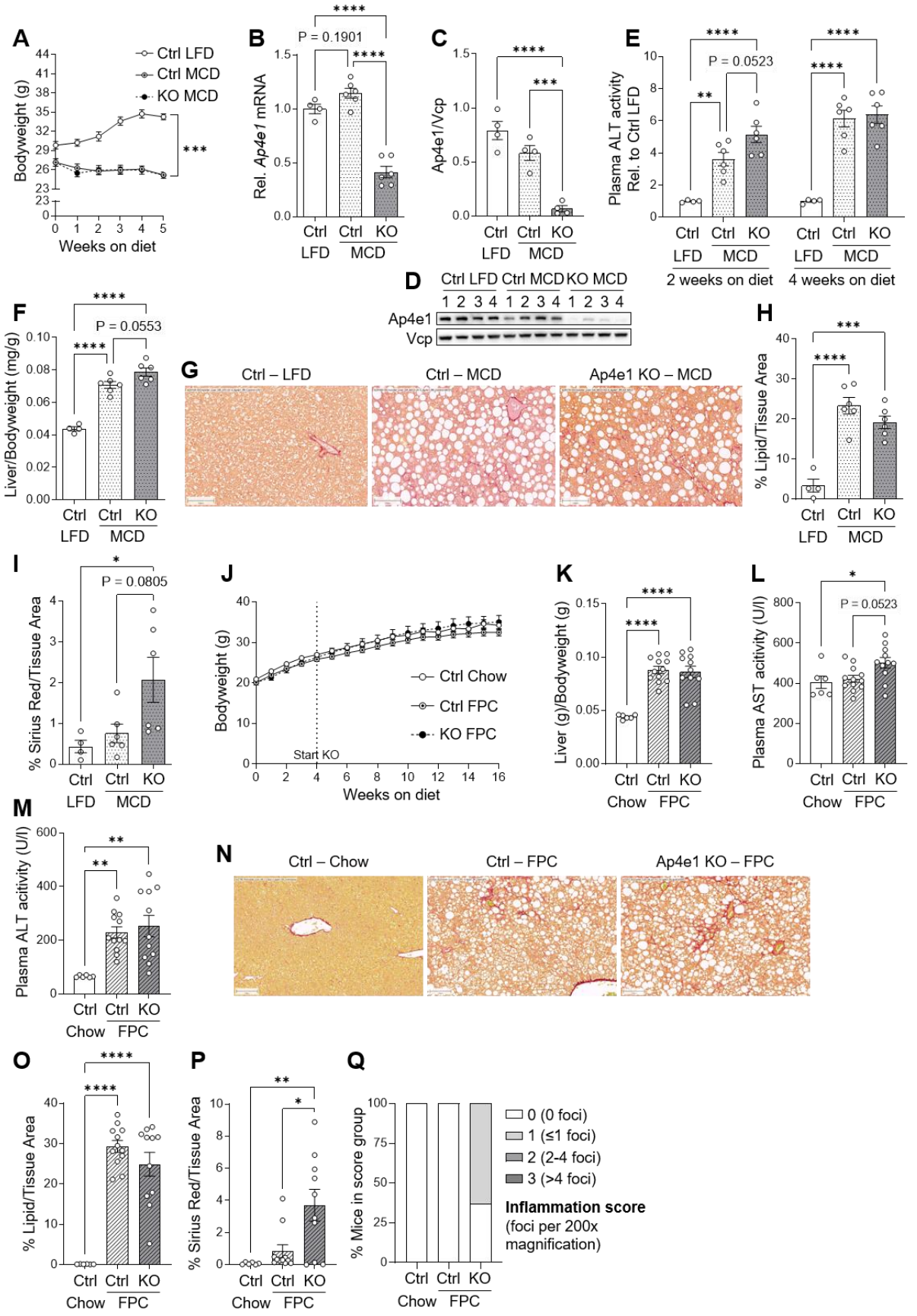

Figure 9 – Ap4e1 depletion exacerbates fibrosis development in NASH.

To explore the connection of Ap4e1 and fibrosis development, Ap4e1$^{liver\text{-}KO}$ mice were fed FPC, a considerably realistic murine model of fibrosis development (Xiaobo Wang et al., 2016). FPC diet is rich in fructose and cholesterol, both strongly contributing to NASH development (Ioannou, 2016; Sánchez-Lozada et al., 2010). Here, Ap4e1$^{fl/fl}$ mice were fed FPC or chow diet for 4 weeks, before AAVs were injected for control or to initiate KO. Mice were kept on diet for another 12 weeks. Again, Ap4e1$^{liver\text{-}KO}$ had no effect on bodyweight (**Figure 9J**). Interestingly, also under FPC diet, depletion of Ap4e1 resulted in elevated aminotransferases, though under this diet AST instead of ALT was changed (**Figure 9L, M**). Markedly, while increased lipid content upon FPC was again unchanged between control and Ap4e1$^{liver\text{-}KO}$ (**Figure 9N, O**), Sirius Red staining revealed once more a significant increase in hepatic fibrosis upon Ap4e1 KO in FPC-induced NASH (**Figure 9N, P**). In addition, while both, control chow and control FPC, had no histologically detectable inflammatory foci (score 0), 63 % of the mice with Ap4e1$^{liver\text{-}KO}$ were given score 1 (**Figure 9Q**). Therefore, this work reveals that depletion of Ap4e1 from livers in a NAFLD/NASH setting accelerates disease progression as it increases hepatic fibrosis and deteriorates liver inflammation.

2.2 CHAPTER 2: REGULATION OF METABOLISM BY ENDOSOMAL MEMBRANE TETHER VPS33B

As the phenotypes upon Ap4e1$^{liver\text{-}KO}$ rely on long-lasting NASH-inducing diets, I studied another potential endosomal regulator of metabolism, Vps33b, in parallel. Vps33b turned out to be an interesting candidate with a broad variety of metabolic phenotypes. Therefore, the focus of my work shifted more towards studying Vps33b, despite Ap4e1 remaining an interesting target in NASH disease progression.

2.2.1 VPS33B IS RECRUITED TO ENDOSOMES UPON REFEEDING IN MURINE LIVERS

Data presented in this chapter (2.2.1) was generated by Dr. Yun Kwon and Dr. Bahar Najafi.

For the identification of novel endosomal regulators of hepatic metabolism, the group of PD Dr. Anja Zeigerer performed organelle proteomics in a fasting/refeeding setting in mice. Upon changes in nutritional status, cells and organs need to adapt to altered nutrient availabilities to maintain proper function. The immediate changes are in part facilitated by the endosomal trafficking system (Gilleron et al., 2019). For the identification of proteins involved, Dr. Yun Kwon and Dr. Bahar Najafi collected livers of mice that were either 14 hours fasted, or 12 hours fasted and 2 hours refed and performed organelle separation using a sucrose gradient (**Figure 10A**). From this gradient, 16 organellar fractions were directed to liquid chromatography mass spectrometry (LC-MS) for the detection of proteins enriched in these fractions (Krahmer et al., 2018). Using sets of organellar marker proteins, the different fractions were assigned to specific organelles and the movement of proteins from one fraction/organelle to another upon refeeding was monitored (**Figure 10B, C**). Intriguingly, membrane tether Vacuolar protein sorting 33b (Vps33b) was the protein most significantly recruited to endosomes upon refeeding, thus implicating an important involvement of Vps33b in the hepatic response to changes in nutritional status.

(Figure on following page)
(A) Representative western blot showing organelle separation in samples subjected to a 10-40 % sucrose gradient. Different organelles are indicated by corresponding marker proteins. PNS = post nuclear supernatant (i.e. whole lysate input).
(B-C) Distribution of organellar marker proteins within different fractions of the sucrose gradient in livers of fasted (B) and refed (C) mice, identified by LC-MS proteomics.
ER: Endoplasmatic reticulum, VCP: Valosin-containing protein, VDAC1: Voltage-dependent anion-selective channel 1.

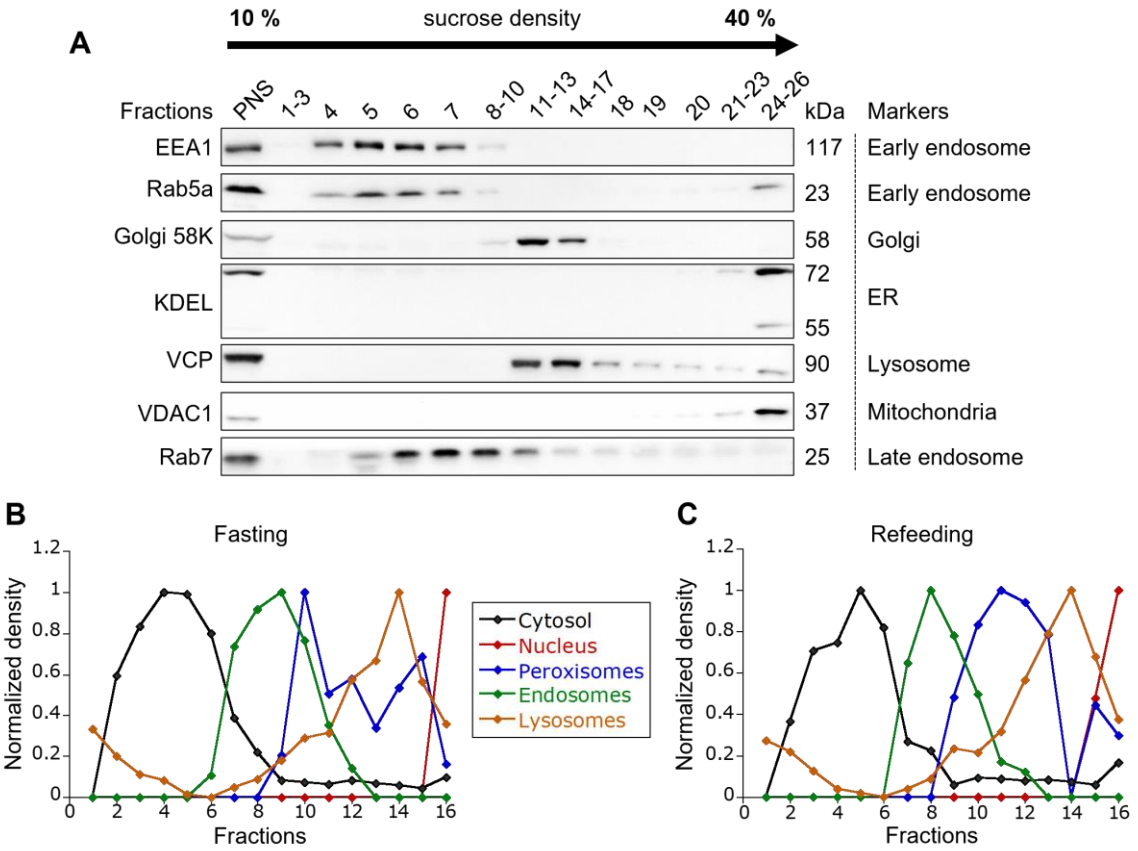

Figure 10 – Organelle proteomics for the detection of proteins recruited to distinct organelles upon refeeding.

2.2.2 VPS33B IS DIFFERENTIALLY REGULATED IN LIVERS OF DIABETIC MICE

To assess whether the recruitment of Vps33b to membranes upon feeding could contribute to metabolically associated diseases such as fatty liver and diabetes (Roden & Shulman, 2019), I measured Vps33b levels in livers of a time course cohort of diabetic *db*/*db* mice, operated by PD Dr. Anja Zeigerer. In leptin receptor deficient *db/db* mice (Hummel et al., 1966), *Vps33b* mRNA levels were increased starting from 8 weeks of age (**Figure 11A**). A trend for elevated *Vps33b* mRNA persisted throughout the duration of the cohort up until 24 weeks of age (**Figure 11A**). Interestingly though, while increased on mRNA, Vps33b protein was unchanged at 8 weeks of age (**Figure 11B, D**) and significantly decreased at 12 weeks of age (**Figure 11C, D**). Thus, Vps33b mRNA and protein regulation is oppositional, indicative of counterregulatory mechanisms regulating Vps33b abundancy.

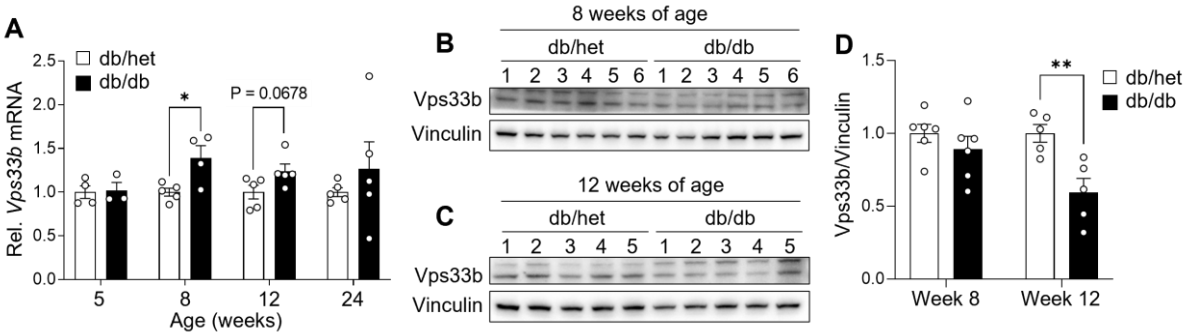

Figure 11 – Vps33b mRNA and protein are differentially regulated in livers of *db/db* mice.
(A) mRNA expression of *Vps33b* in livers of heterozygous control and homozygous diabetic *db/db* mice at indicated age.
(B-D) Western blots showing protein levels of Vps33b in 8 weeks (B) and 12 weeks (C) control (db/het) and diabetic (db/db) mice with quantification thereof in (D).
Data are presented as mean ± SEM. *P < 0.05, **P < 0.01 by two-tailed unpaired Student's t test.

2.2.3 HEPATIC KNOCKDOWN (KD) OF VPS33B IN MICE ALTERS CHOLESTEROL AND LIPID UTILIZATION *IN VITRO* AND *IN VIVO*

To further study the potential role of Vps33b in metabolism, I searched for VPS33B-interacting proteins on BioGRID (Oughtred et al., 2021), a publicly available interactome database. Interestingly, VPS33B was shown to interact with, among others, CCDC22, COMMD1, and COMMD6 in HEK293T cells (Huttlin et al., 2017), three proteins already known to be required for LDL receptor (Ldlr) recycling and serum cholesterol homeostasis (Fedoseienko et al., 2018; Wijers et al., 2019). Therefore, I wondered how Vps33b depletion alters Ldlr distribution in livers. First, polarized primary murine hepatocytes in a collagen sandwich were depleted of Vps33b using siRNA knockdown (KD) (Seitz et al., 2019; Sekar et al., 2022; Zeigerer et al., 2017). Fluorescence staining for Ldlr and imaging using confocal microscopy revealed a significant reduction of total Ldlr levels (**Figure 12A, B**). In line, surface levels of Ldlr, labeled with a fluorescent LDL probe on ice to block endocytosis, were similarly reduced (**Figure 12C, D**). Remarkably, while *Ldlr* protein was reduced 70-80 %, *Ldlr* mRNA remained unaffected (**Figure 12E**). To investigate whether these effects on Ldlr are receptor-specific or due to wider-scale dysregulation of cholesterol metabolism (Goldstein et al., 2006), secretion of cholesterol by hepatocytes into the cell culture supernatant was measured. However, cholesterol secretion remained unchanged (**Figure 12F**).

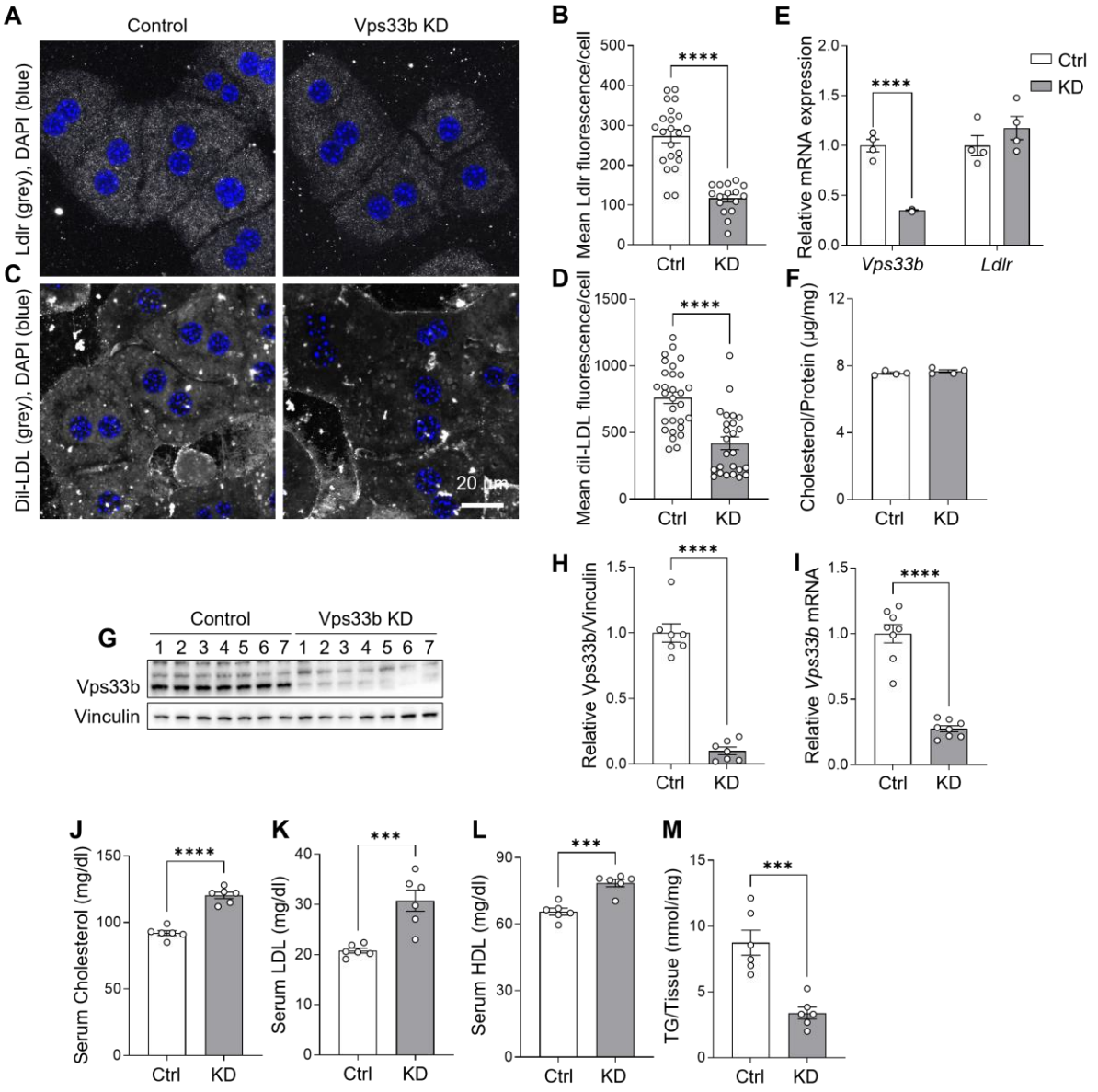

Figure 12 – Vps33b KD increases serum cholesterol.
(A-B) Immunofluorescent images of Ldlr (grey, A) in primary murine hepatocytes after siRNA-mediated Vps33b KD *in vitro*, quantified in (B).
(C-D) Primary murine control and Vps33b KD hepatocytes were treated with fluorescently labeled dil-LDL on ice for 2 hours after 2 hours serum starvation (grey, C). Quantifications in (D).
(E) Relative mRNA expression of *Vps33b* and *Ldlr* in primary murine hepatocytes upon Vps33b KD *in vitro*.
(F) Cholesterol secretion in control- and Vps33b-siRNA treated primary hepatocytes into the cell culture medium. Hepatocytes were serum starved for 5 hours and medium was collected for the detection of secreted cholesterol, presented as portion per hepatocyte protein content.
(G-I) Immunoblot for Vps33b from livers of control or Vps33b KD LNP injected mice after three weeks of continued KD. Quantifications in (H). Relative *Vps33b* mRNA expression in those livers in (I).
(J-L) Serum levels of cholesterol (J), LDL cholesterol (K), and HDL cholesterol (L) of control and Vps33b KD mice after 3 weeks of KD.
(M) Liver triglyceride content in control and Vps33b KD mice.
Data are presented as mean ± SEM. ***P < 0.001, ****P < 0.0001 by two-tailed unpaired Student's t test. Scale bar = 20 µm.

Next, to investigate hepatic Vps33b KD effects *in vivo*, I performed injections of lipid nanoparticles (LNPs) encapsulating siRNA into mice *via* the tail vein (Sekar et al., 2022; Zeigerer et al., 2012, 2015). This approach was shown to KD proteins of interest specifically

from hepatocytes *in vivo* (Gilleron et al., 2013) while allowing to study acute effects of Vps33b depletion in normally developed adult mice. After three weekly injections, Vps33b protein was decreased ~85 % (**Figure 12G, H**) and mRNA ~73 % (**Figure 12I**). Intriguingly, KD of Vps33b *in vivo* led to increased serum levels of total free cholesterol, LDL cholesterol, and HDL cholesterol (**Figure 12J-L**). Thus, the observed reduction in Ldlr protein *in vitro* after Vps33b KD translated into elevated serum cholesterol, potentially due to decreased uptake. Importantly, mice depleted of Vps33b had drastically reduced liver triglyceride (TG) levels (**Figure 12M**). Combined, these data reveal altered cholesterol and lipid utilization in livers with Vps33b KD.

2.2.4 LNP-INDUCED VPS33B KD-PHENOTYPE DIFFERS FROM GENETIC DEPLETION MODELS

Vps33b-deficiency is mainly studied in the context of arthrogryposis renal dysfunction and cholestasis syndrome (ARC) (Gissen et al., 2004). Within the liver, mutations in either CHEVI subunit, *VPS33B* or *VIPAS39*, were shown responsible for cholestatic jaundice and hepatomegaly, two main features of ARC (Zhou & Zhang, 2014). Interestingly, in patients with ARC, ARC-related cholestatic liver injury results in elevated serum alkaline phosphatase (ALP) but unchanged ALT and AST (Gissen et al., 2006). Similarly, Vps33b$^{fl/fl}$-AlfpCre mice also present with elevated plasma ALP levels and increased liver/bodyweight but unchanged plasma ALT levels (Hanley et al., 2017).

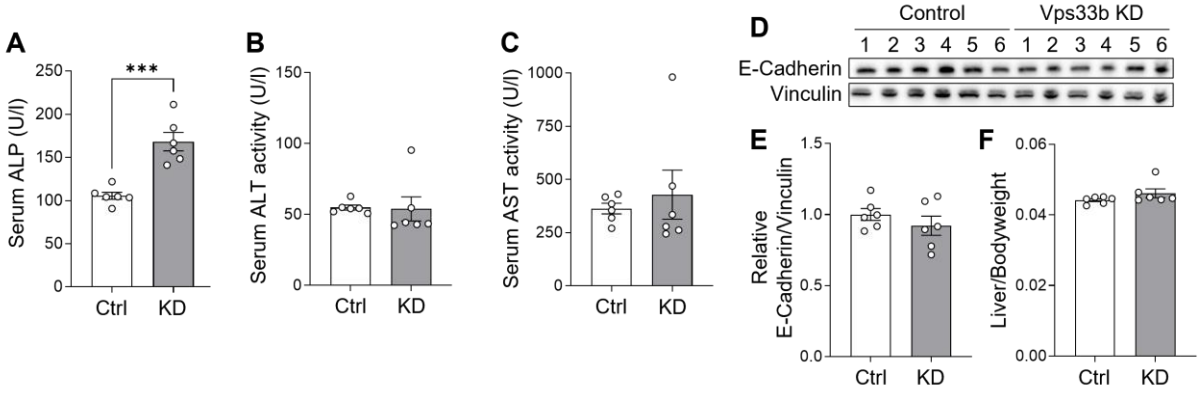

Figure 13 – LNP-mediated Vps33b KD in adult mice only partially recapitulates ARC syndrome.
(A-C) Serum levels of ALP (A), ALT (B), and AST (C) of control and Vps33b KD mice after 3 weeks of KD.
(D-E) Western blot for E-Cadherin from livers of control or Vps33b KD LNP mice after three weeks of continued KD (D) with quantifications in (E).
(F) Liver (g) per bodyweight (g) after three weeks of LNP-induced Vps33b KD.
Data are presented as mean ± SEM. ***P < 0.001 by two-tailed unpaired Student's t test.

Likewise, LNP-mediated depletion of Vps33b from livers of adult mice resulted in elevated serum levels of alkaline phosphatase (ALP) (**Figure 13A**), without altering aminotransferase levels (**Figure 13B, C**). Interestingly, deficiencies upon Vps33b have been associated with polarity defects with concomitant reductions in e.g. adherens-junction protein E-Cadherin

(Cullinane et al., 2010; C. Wang et al., 2018). While one conflicting publication reported on increased E-Cadherin levels upon Vps33b depletion (Fu et al., 2019), Vps33b KD by LNP-mediated siRNA delivery had no effect on E-Cadherin protein levels after 3 weeks of KD (**Figure 13D, E**). In addition, liver/bodyweight ratio, published to increase in other settings of Vps33b deficiency (Hanley et al., 2017; Zhou & Zhang, 2014), remained similarly unchanged in LNP-induced KD (**Figure 13F**). Thus, LNP-induced KD of Vps33b only partially recapitulates characteristics of ARC syndrome.

2.2.5 VPS33B DEPLETION FROM MOUSE LIVERS REDUCES BLOOD GLUCOSE LEVELS AND HEPATIC INSULIN SENSITIVITY

To expand the understanding of the role of Vps33b in metabolism from cholesterol and lipids to glucose, I measured blood glucose levels in mice with liver-KD of Vps33b. Here, blood glucose levels were significantly reduced both at random (fed) and 6 hours fasted state (**Figure 14A, B**). To understand how Vps33b could reduce blood glucose, I performed glucose tolerance tests (GTT) in mice and observed no significant changes (**Figure 14C**). Despite slight tendencies for improved glucose handling upon liver-KD of Vps33b in two independent mouse cohorts, this did not reach statistical significance in neither of the cohorts. Importantly, liver glycogen content was unchanged (**Figure 14D**), indicating that decreased blood glucose levels are unlikely due to decreased uptake into the liver or altered glycogenolysis. In addition, plasma insulin levels measured before and after glucose injection during a GTT were similarly unchanged (**Figure 14E**), rendering changes in glucose levels independent of insulin-mediated uptake into peripheral tissues.

However, while insulin levels were unchanged, insulin sensitivity in hepatocytes *in vitro* was significantly reduced (**Figure 14F, G**), assessed by measuring Akt phosphorylation at Serine 473 upon acute stimulations with insulin. This decrease in insulin sensitivity resulted in a mild but significant decline in the initial slope of blood glucose reduction after insulin injections (K_{ITT}) in an insulin tolerance test (ITT) (Müller et al., 2021) (**Figure 14H, I**), while the area of the curve (AOC) was unchanged (quantification not shown). However, slightly reduced hepatic insulin sensitivity together with unchanged plasma insulin levels cannot explain reduced blood glucose levels and are instead contradicting.

Furthermore, to investigate hepatic gluconeogenesis as potential mediator of blood glucose levels (Roden & Shulman, 2019), I measured plasma glucose levels in response to acute injections of pyruvate but observed no alterations in gluconeogenesis (**Figure 14J**). Thus, neither glucose utilization and storage, alterations in insulin sensitivity, nor changes in

gluconeogenesis could explain reduced blood glucose levels in mice depleted of Vps33b from the liver.

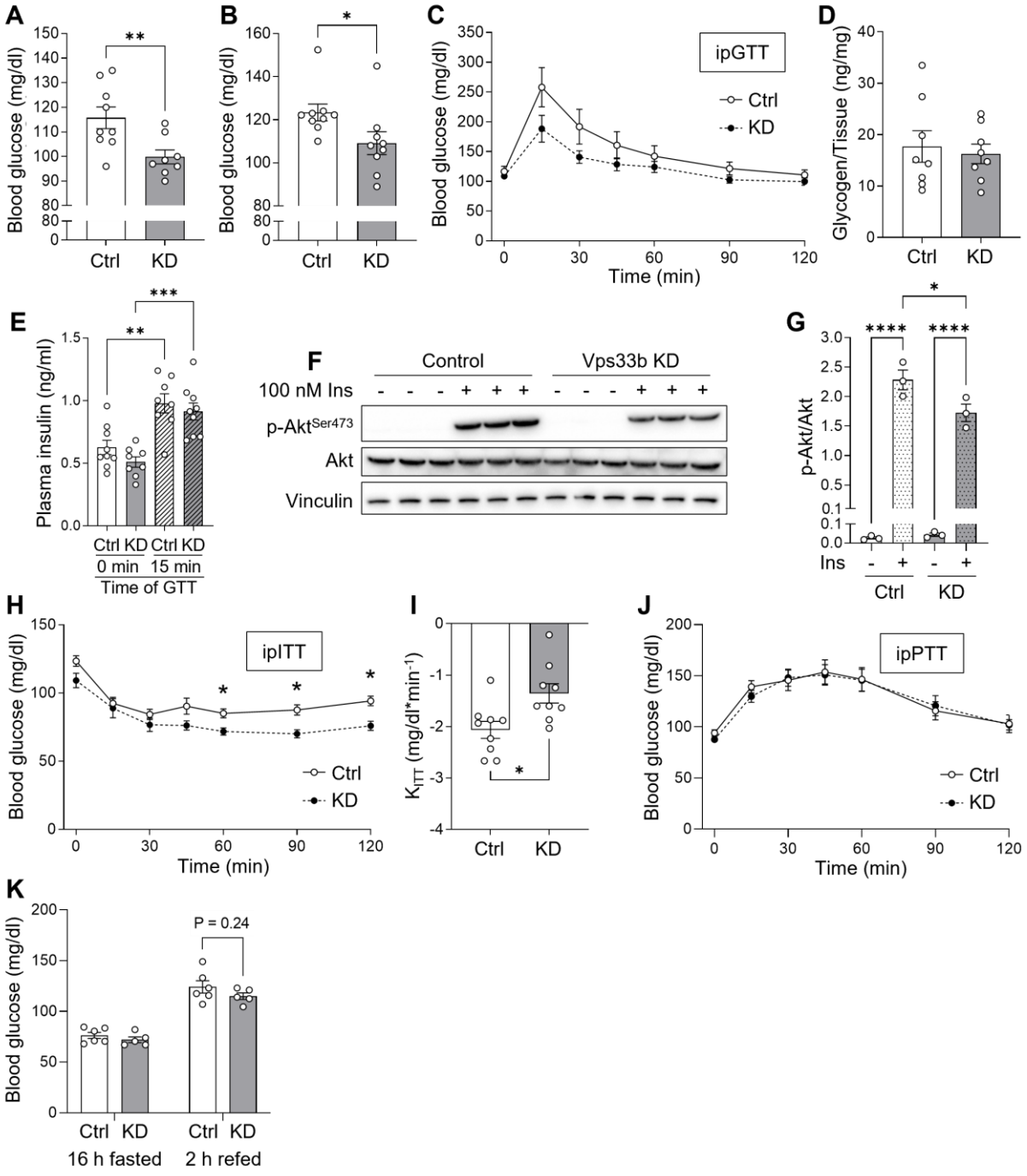

Figure 14 – Hepatic KD of Vps33b alters glucose utilization and insulin sensitivity.
(A-B) Random (A) and 6 hours fasted (B) blood glucose of mice depleted of Vps33b from the livers for 3 weeks by consecutive LNP injections.
(C) Intraperitoneal Glucose tolerance test (ipGTT) in chow-fed control and Vps33b KD mice with 2 g/kg glucose after 6 hours fasting.
(D) Hepatic glycogen content, measured in livers collected from control and Vps33b KD mice after 6 hours of fasting. Mice had three weeks of Vps33b KD by weekly LNP injections.
(E) Plasma insulin levels in control and Vps33b KD mice. Plasma was collected from mice during an ipGTT at 0 min (before glucose injection) and 15 min (after glucose injection).
(F-G) Western blot showing Akt phosphorylation upon insulin stimulations in primary murine hepatocytes *in vitro* (F) with quantifications in (G). Hepatocytes cultured in collagen sandwich were treated with 100 nM insulin for 15 min, 3 days after induction of RNAi by siRNA transfection.

(H-I) Intraperitoneal Insulin tolerance test (ipITT) in chow-fed mice with 1 IU/kg after 6 hours fasting (H). K_{ITT} as the slope of initial reduction in blood glucose upon insulin injection was calculated as difference in blood glucose from 0 to 15 min, relative to time (15 min) (I).
(J) Intraperitoneal Pyruvate tolerance test (ipPTT) in chow-fed mice with 2 g/kg pyruvate after 16 hours fasting.
(K) Blood glucose levels in Vps33b KD and control mice after 16 hours of fasting and after 2 hours of subsequent refeeding.
Data are presented as mean ± SEM. *P < 0.05, **P < 0.01, ***P < 0.001 by two-tailed unpaired Student's t test or ordinary one-way ANOVA with Šídák's multiple comparisons test (E, G).

Intriguingly, after 16 hours of fasting before the ipPTT, the reduction in blood glucose levels observed at random fed and 6 hours fasted state, is no longer significant (**Figure 14J**). Given the discovery of Vps33b as potential metabolic regulator recruited in a fasting-refeeding setting (chapter 2.2.1), I aimed at investigating the specific role of Vps33b under these conditions. Therefore, blood glucose levels of control and Vps33b KD mice were assessed after 16 hours of fasting and again after 2 hours of refeeding (**Figure 14K**). Interestingly, hepatic depletion of Vps33b has no effect on refed blood glucose levels, despite its enhanced recruitment to endosomal membranes upon refeeding in mouse livers.

2.2.6 VPS33B KD IS NOT SUFFICIENT TO LOWER BLOOD GLUCOSE IN DIABETIC *DB/DB* MICE

Given the reducing effects of Vps33b KD on blood glucose in adult mice, I wondered whether Vps33b depletion could reduce hyperglycemia in diabetic *db/db* mice. Hyperglycemia is a hallmark of T2D, contributing to various comorbidities (Forbes & Cooper, 2013). Thus, reducing blood glucose levels is beneficial. As expected, in lean, heterozygous control mice, depletion of Vps33b led to a reduction in blood glucose levels (**Figure 15A**). In diabetic *db/db* mice, however, Vps33b KD was not sufficient to alleviate hyperglycemia (**Figure 15A**). Moreover, while homozygous *db/db* mice had drastically increased bodyweight compared to heterozygous mice, Vps33b KD had no further effect on bodyweight (**Figure 15B**).

Interestingly, while blood glucose levels remained unchanged, liver TG content was also in homozygous *db/db* mice reduced, although only by trend (**Figure 15C**). In heterozygous mice, the absolute values of liver TG were lower, yet not significant (**Figure 15C**). As observed in wildtype mice upon Vps33b KD, serum ALP, total free cholesterol, and LDL cholesterol were increased in homozygous *db/db* mice and showed trends in heterozygous mice (**Figure 15D-F**).

As reported in chapter 2.2.4, genetic KO of hepatic Vps33b has been associated with hepatomegaly (Zhou & Zhang, 2014), which did not appear upon LNP-induced KD for 3 weeks (**Figure 13F**). In line, also prolonged Vps33b KD of 6 weeks using LNPs in hetero- and homozygous *db/db* mice did not result in hepatomegaly (**Figure 15G**). In addition, muscle weight and gonadal white adipose tissue weight remained unchanged (**Figure 15H-I**),

indicating that the metabolic alterations of Vps33b reduction have no additional effect in severely diseased homozygous *db/db* mice.

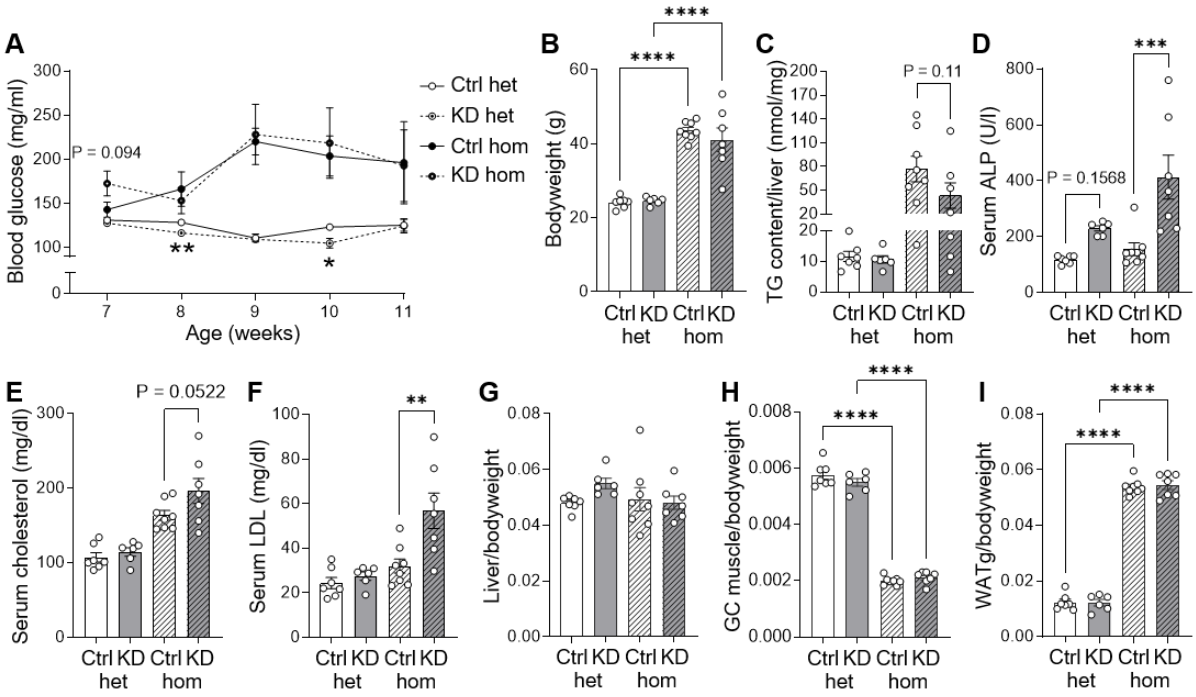

Figure 15 – Vps33b KD does not alleviate hyperglycemia in *db/db* mice.
(A) Weekly blood glucose levels at randomly fed state in lean heterozygous and obese/diabetic homozygous *db/db* mice. Mice were injected weekly with control or Vps33b KD LNPs, starting from 6 weeks of age.
(B) Bodyweight before organ withdrawal at 12 weeks of age.
(C) Liver triglyceride (TG) content.
(D-F) Serum ALP (D), free cholesterol (E), and LDL cholesterol levels (F).
(G-I) Liver (G), gastrocnemius muscle (H), and gonadal white adipose tissue (I) mass, relative to bodyweight.
Data are presented as mean ± SEM. *P < 0.05, **P < 0.01, ***P < 0.001, ****P < 0.0001 by two-tailed unpaired Student's t test.

2.2.7 Whole-liver proteomics reveal increased protein turnover upon Vps33b KD

To understand the broad variety of metabolic alterations upon Vps33b depletion, I performed quantitative proteomics in collaboration with Dr. Natalie Krahmer on whole-livers depleted of Vps33b for 3 weeks. Here, I found 498 significantly down- and 133 proteins significantly upregulated (t-test, P < 0.05) (**Figure 16A**). The upregulated proteins associated with KEGG terms such as "Metabolic pathways" and "Cytochrome P450 Drug Metabolism", whereas the bulk of downregulated proteins were linked to "NAFLD", "Fatty acid metabolism", and "Oxidative phosphorylation" (**Figure 16A**). For the identification of subclusters of functionally and physically interacting proteins within the set of downregulated proteins, I subjected those to STRING network analysis (Szklarczyk et al., 2021) and performed Markov clustering (MCL), resulting in 157 clusters (**Figure 16B**).

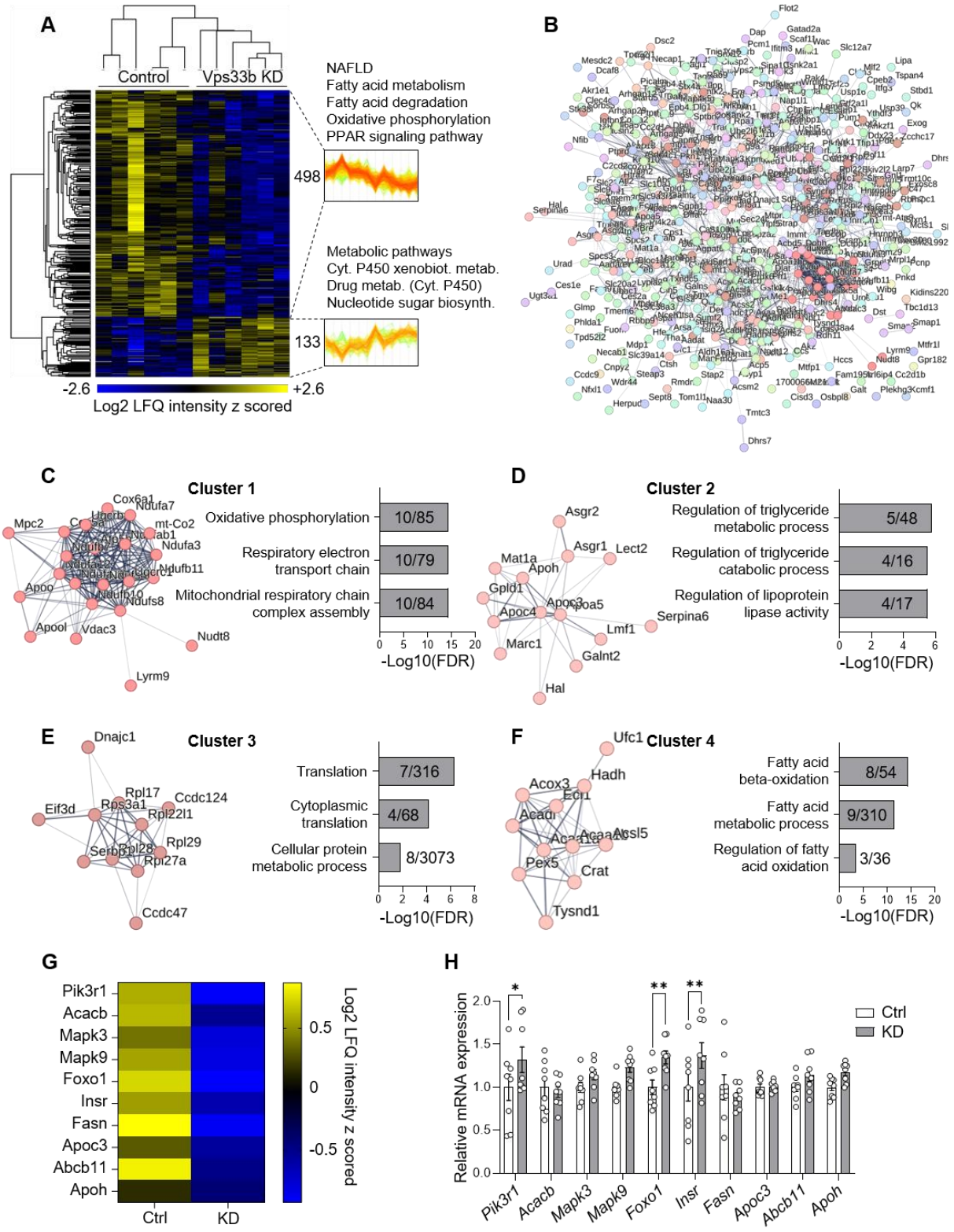

Figure 16 – Identification of metabolic clusters of downregulated proteins in Vps33b KD livers and enhanced protein turnover.
(A) Heatmap showing all significantly altered (t-test, P < 0.05) proteins, detected by LC-MS, in livers of control and Vps33b KD mice with associated KEGG terms.
(B) Markov clustering (MCL) of the downregulated protein portion presented in (A) using STRING network analysis of physically and functionally interacting proteins.
(C-F) Top 4 clusters (by size) of downregulated proteins, identified in (B). For each cluster (C-F), the 3 most significantly (FDR) associated GO-Terms from *GO:Biological Processes* are indicated. Numbers inside the bar graphs indicate the observed protein count associated with that term within the cluster, relative to the total number of proteins associated with that term within the whole dataset of downregulated proteins.

(G-H) Protein (by LC-MS) (G) and relative mRNA (H) expression of selected genes, associated with KEGG terms *Insulin signaling* and *Cholesterol metabolism* in livers of control and Vps33b KD mice.
Data are presented as mean ± SEM. *P < 0.05, **P < 0.01 by two-tailed unpaired Student's t test.

The four largest clusters are shown in **Figure 16C-F** together with their associations with Gene ontology "Biological Process" terms. Cluster 1 shows a strong mitochondrial association (**Figure 16C**). Cluster 2 is associated with decreased triglyceride and lipoprotein metabolism (**Figure 16D**), resembling the phenotypes of Vps33b depletion described in chapter 2.2.3. While the third largest cluster associates with translational processes (**Figure 16E**), Cluster 4 relates to beta-oxidation and fatty acid metabolism (**Figure 16F**). Thus, network analysis of proteomics of livers deficient in Vps33b uncover two of the top four clusters (cluster 2 and 4) to be directly connected with metabolic phenotypes identified in this work.

Interestingly, many of the proteins found downregulated in the proteomics, such as Foxo1 or Insr, are unchanged or even increased on mRNA level, as exemplified in **Figure 16G, H**. This indicates a posttranscriptional regulation of protein abundancy upon Vps33b depletion and is especially interesting in light of the discovery of downregulated Cluster 3, associated with translation (**Figure 16E**). Moreover, previous work has described Vps33b as required for late endosomal-lysosomal fusion and could thus link the effects of Vps33b with the lysosomal degradative system (Galmes et al., 2015; H. Xiang et al., 2022).

2.2.8 Asiaglycoprotein receptor as potential new cargo trafficked through Vps33b

Vps33b function, as part of the heterodimeric CHEVI tethering complex (Rogerson & Gissen, 2016), is thought to occur mainly in recycling. Specifically, CHEVI was suggested to mediate recycling from early to recycling endosomes, recycling endosomes to the plasma membrane, or potentially both pathways (van der Beek et al., 2019). Besides, Vps33b was shown to interact with the CCC complex through binding of Ccdc22 (Hunter et al., 2018), potentially enabling the recruitment of this complex to Rab11-positive recycling endosomes. Further studies on Vps33b revealed a broad variety of functions for Vps33b in different cell types, including integrin delivery (B. Xiang et al., 2015) and α-granule formation in megakaryocytes (Bem et al., 2015). In the liver, however, Vps33b deficiencies have thus far been associated with alterations in the delivery of apical proteins to bile canaliculi (Hanley et al., 2017).

Interestingly, among the most significantly downregulated proteins upon Vps33b KD by LNPs in the proteomics were Asiaglycoprotein receptor 1 (Asgr1) and Asgr2 (rank 3 and 10, respectively) (**Figure 17A**). Functional Asiaglycoprotein receptor is a complex composed of Asgr1 and Asgr2 (Harris et al., 2012), located at the basolateral hepatocyte membrane (Schulze et al., 2019). Thus, downregulation of both subunits highlights Asgr as potential novel

cargo dependent on Vps33b. Western blots confirmed a significant reduction in Asgr1 protein upon Vps33b KD (**Figure 17B, C**). In addition, immunofluorescent staining of Asgr1 in sections of PFA-perfused control and Vps33b KD livers revealed a remarkable reduction upon KD (**Figure 17D, E**). Intriguingly, Asgr1$^{liver\text{-}KO}$ was shown to reduce liver and serum lipids while enhancing cholesterol secretion into the bile (J.-Q. Wang et al., 2022). These effects were attributed to reduced uptake of asiaglycoproteins (AGP) upon Asgr1 KO, resulting in decreased lysosomal degradation of such, and inhibition of mTORC1 activity due to a lack in AGP-derived amino acids with concomitant Ampk (Adenosine monophosphate (AMP) activated kinase) activation (J.-Q. Wang et al., 2022). Therefore, L-amino acid content was measured in livers of Vps33b KD mice. However, a trend for slightly reduced hepatic amino acid content did not reach statistical significance in two independent mouse cohorts (**Figure 17F, G**).

Given the association of Vps33b with the CCC complex (Hunter et al., 2018) and the potential trafficking of Vps33b cargos through this pathway, I wondered whether components of this complex would alter their cellular distribution upon Vps33b depletion. Thus, primary hepatocytes in sandwich culture with siRNA-mediated KD of Vps33b were stained for Ccdc93 and localization was assessed by high-resolution confocal microscopy and particle analysis using Fiji (Schindelin et al., 2012). Interestingly, mean fluorescence intensity of Ccdc93 was unchanged between control and Vps33b KD (**Figure 17H, I**), indicating equal protein levels of Ccdc93 in both treatment groups. However, Ccdc93-positive structures were decreased in size (**Figure 17J**) and increased in abundance (**Figure 17K**). Possibly, this could be indicative of altered recruitment of Ccdc93 upon Vps33b depletion. The interaction of Vps33b with the CCC complex or components thereof, as well as associated functions, however, need further studies.

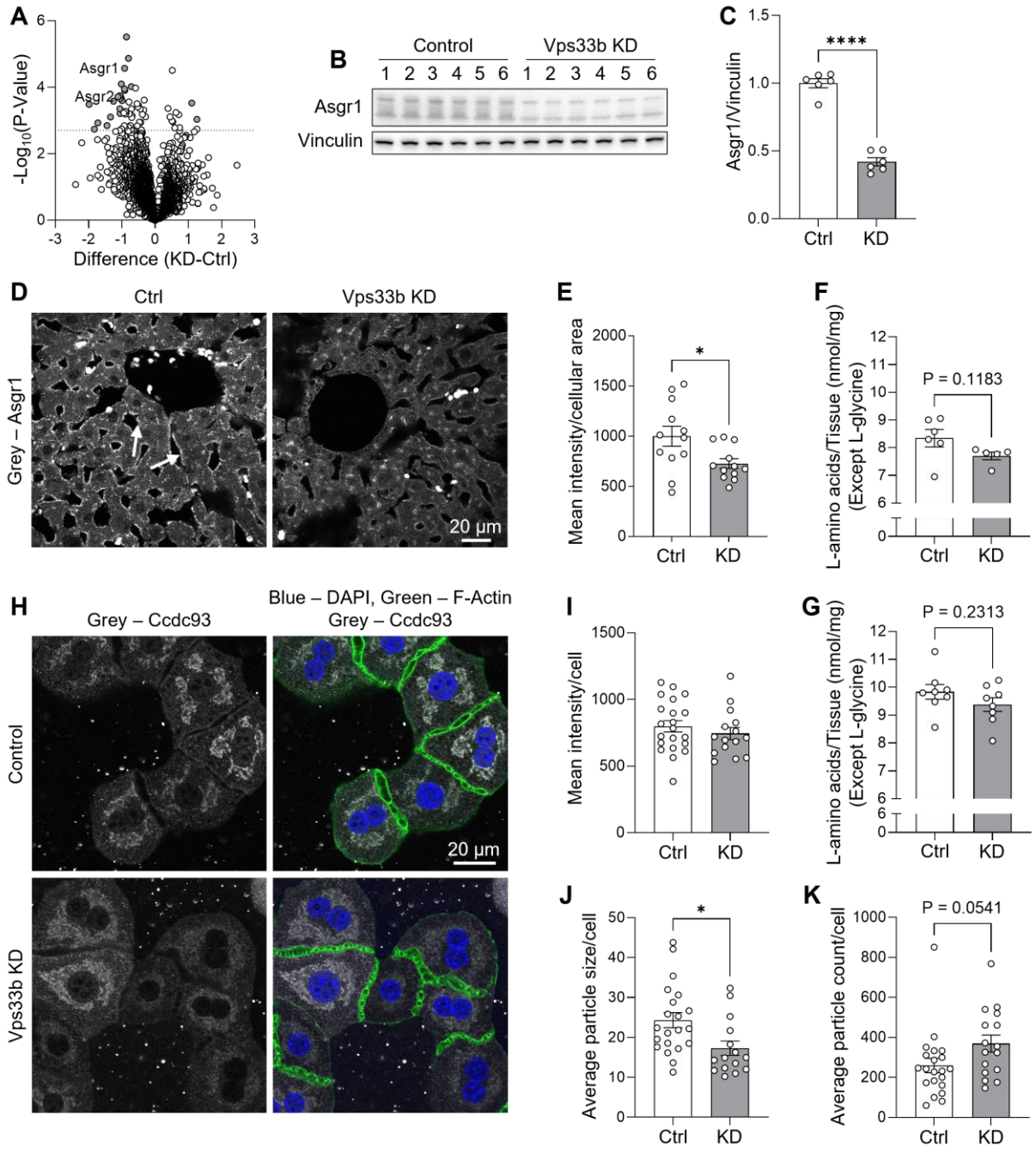

Figure 17 – Vps33b KD reduces Asgr1.
(A) Volcano plot of proteins detected by LC-MS in livers of control and Vps33b KD mice. Symbols of proteins changed significantly by s0 FDR are indicated by grey filling. Localization of Asgr1 and Asgr2 within the volcano plot are shown.
(B-C) Representative western blot of Asgr1 in livers of Vps33b KD and control mice (A), quantified in (B).
(D-E) Confocal microscopy image of liver sections from PFA-perfused livers of control and Vps33b KD mice, stained for Asgr1 in grey with arrows indicating basolateral localization of Asgr1 (D). Quantification of mean Asgr1 fluorescence intensity per cellular area in (E).
(F-G) Liver L-amino acid content from two independent mouse cohorts of three-weeks LNP-induced Vps33b KD.
(H-K) Representative confocal images of primary hepatocytes *in vitro*, stained for Coiled-coil domain-containing 93 (Ccdc93), F-actin (phalloidin), and DAPI (DNA), three days after Vps33b RNAi (H). Quantifications of mean fluorescence intensity in (I) and results of particle analysis using Fiji for particle size (J) and count (K).
Data are presented as mean ± SEM. *P < 0.05, ****P < 0.0001 by two-tailed unpaired Student's t test. Scale bar = 20 µm.

2.2.9 HEPATIC VPS33B KD RESULTS IN OVERACTIVATED AMPK

Given the dramatic effects of Vps33b on protein downregulation, together with the identified cluster of translation-related proteins decreased in abundance, I questioned whether Vps33b KD alters the signaling of pathways known to affect translational processes.

Ampk is a prominent regulator of translation, together with the mammalian target of rapamycin 1 (mTORC1), where Ampk inhibits and mTORC1 stimulates translation (Gleason et al., 2007). Moreover, increased p-Ampk has been reported for Asgr1$^{liver\text{-}KO}$ (J.-Q. Wang et al., 2022) and Vps33b KD reduces Asgr1 protein, presented in chapter 2.2.8. Thus, I measured Ampk phosphorylation in livers of mice depleted of Vps33b by LNPs and found a significant increase in p-Ampk (**Figure 18A, B**). To study whether this effect is hepatocyte specific, isolated primary mouse hepatocytes in sandwich culture (Zeigerer et al., 2017), depleted of Vps33b by siRNA, were treated with the Ampk activating AMP-mimetic AICAR (Drake et al., 2010). In line, primary hepatocytes *in vitro* showed a similar increase, both basally and when stimulated with AICAR (**Figure 18C**), hence rendering overactivated Ampk signaling as potential cause for decreased protein expression.

Ampk senses the cellular energy status as it is activated by AMP, which accumulates as ATP levels decrease (Garcia & Shaw, 2017). Therefore, to identify causes for elevated p-Ampk, hepatic ATP content was assessed. However, ATP levels in livers of Vps33b KD mice remained unchanged (**Figure 18D**). One of the nucleotide-independent upstream regulators of Ampk is Ca^{2+}/calmodulin-dependent protein kinase II (CaMKII) (Kim et al., 2022; Raney & Turcotte, 2008). Intriguingly, p-CaMKII levels were increased by trend in Vps33b KD livers (**Figure 18E, F**), thus hinting at a nucleotide-independent mode of Ampk activation upon Vps33b depletion.

Importantly, Ampk activation was shown to occur in parts at lysosomes (Carroll & Dunlop, 2017; C. S. Zhang et al., 2022) and Vps33b was shown to increase Lamp1-positive organelles in different cell types (Cullinane et al., 2010; Galmes et al., 2015; H. Xiang et al., 2022). Thus, I assessed lysosomal markers in livers and hepatocytes. Interestingly, also in murine livers, Lamp1 protein increased by 2.5-fold upon Vps33b KD (**Figure 18G, H**). Next, LysoTracker, a pH sensitive fluorescent probe to label acidic organelles (i.e. lysosomes), was used in primary hepatocytes isolated from Vps33b liver KD mice. Notably, Vps33b KD also increased LysoTracker fluorescence in isolated hepatocytes (**Figure 18I, J**), suggesting that increased Lamp1 is indeed representative of elevated lysosomal compartments.

Interestingly, Xiang et al. have linked increased numbers of lysosomes in regulatory T cells (Tregs) upon Vps33b KO with overactivated mTORC1 (H. Xiang et al., 2022). However, upregulated mTORC1 activity would oppose enhanced p-Ampk (Garcia & Shaw, 2017). Therefore, phosphorylation of p70 S6 kinase (p70 S6K) and S6 ribosomal protein (rpS6) was

assessed, two downstream targets of mTORC1 activity (Pullen & Thomas, 1997). Interestingly, in isolated hepatocytes at basal state, p-p70 S6K was significantly reduced whereas p-rpS6, downstream of p70 S6K, was unchanged (**Figure 18K-M**). In livers of control and Vps33b KD mice, both downstream effectors showed only tendencies for reduced phosphorylation (**Figure 18N-P**). Although the effects on mTORC1 inhibition upon hepatic Vps33b KD are only mild, they are in stark contrast to the overactivation of this pathway, reported in Vps33b deficient Tregs (H. Xiang et al., 2022). Thus, while the Vps33b KD effects on lysosomes seem general, the effects on either Ampk or mTORC1 activation seem cell type specific.

(Figure on following page)
(A-B) Representative western blots for p-Ampk and Ampk from mouse livers after three weeks LNP KD (A), quantified in (B).
(C) p-Ampk and Ampk western blots from primary hepatocytes in sandwich culture *in vitro*, stimulated with 200 µM AICAR for 1 hour three days after RNAi.
(D) Hepatic ATP content from mice after three weeks Vps33b KD.
(E-F) Western blots for p-CaMKII and CaMKII from mouse livers after three weeks LNP KD (E), quantified in (F).
(G-H) Immunoblot for Lamp1 from mouse livers after Vps33b KD (G) with quantifications in (H).
(I-J) LysoTracker labeled lysosomes in primary hepatocytes in monolayer, isolated from mice after 3 weeks of Vps33b KD (I) with quantifications thereof in (J). Hepatocytes were treated with 500 nM LysoTracker for 30 min before fixation.
(K-M) Western blots for p- and total p70 S6K and p-rpS6 in primary hepatocytes *in vitro* after siRNA KD (K) with quantifications in (L) and (M).
(N-P) Western blots for p- and total p70 S6K and p-rpS6 in livers of LNP-induced KD (N) with quantifications in (O) and (P).
Data are presented as mean ± SEM. *P < 0.05, **P < 0.01, ***P < 0.001, ****P < 0.0001 by two-tailed unpaired Student's t test. Scale bar = 20 µm.

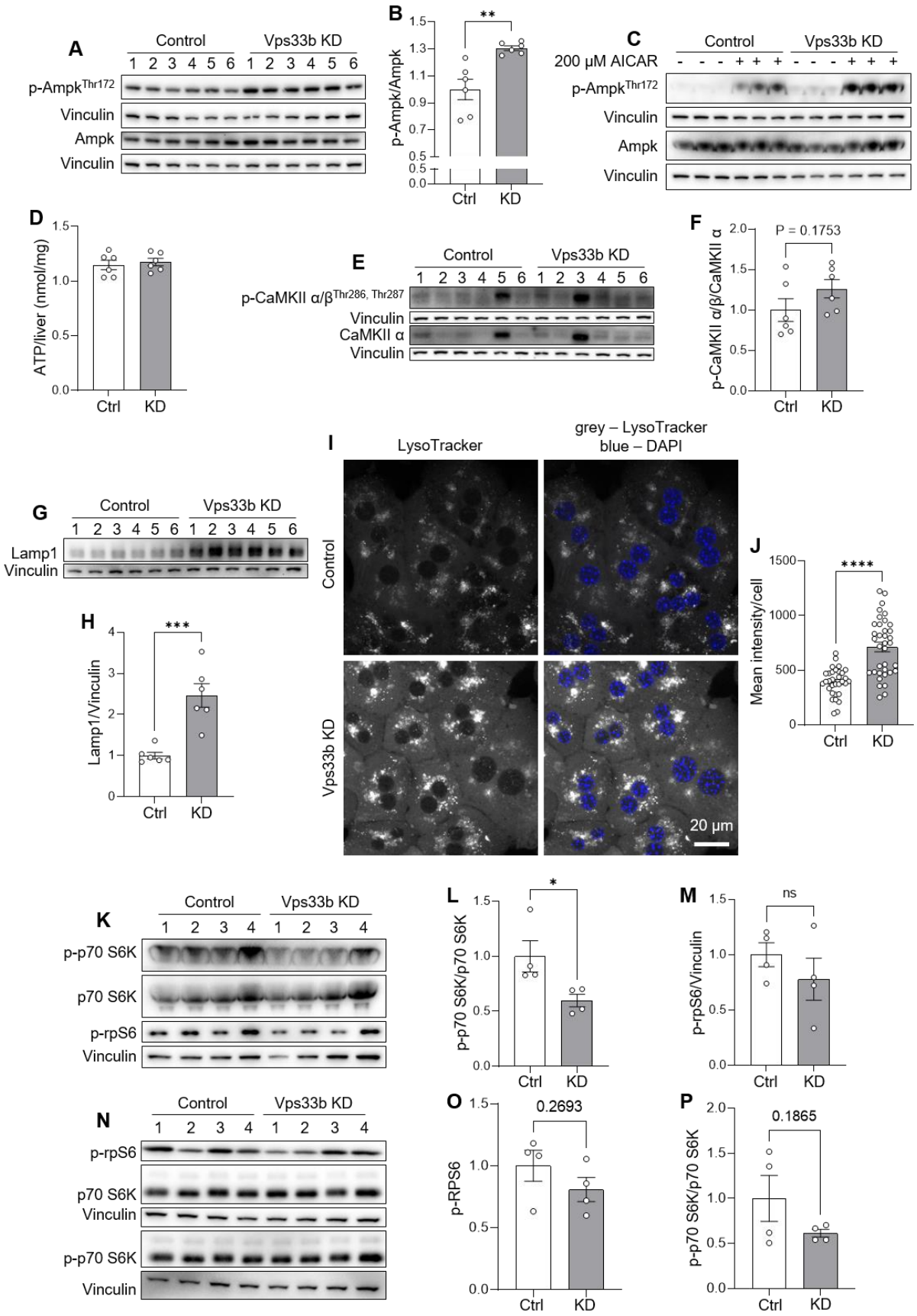

Figure 18 – Vps33b KD results in overactivated p-Ampk.

2.2.10 VPS33B KD EFFECTS ARE DEPENDENT ON THE DURATION OF KD

When assessing several phenotypes of Vps33b depletion at different time points after initiation of KD, it appeared that the occurrence of certain phenotypes is time-dependent. Importantly, Vps33b protein levels were already depleted 5 days after LNP injection, the earliest time point investigated (**Figure 19A**). Reduction of Asgr1 protein levels, for example, started 2 weeks after initiation of KD (**Figure 19B-D, E-F**) and was highest at the last time point (**Figure 19D, G**). This late occurrence of Asgr1-depletion is resembled by the fact that siRNA KD of Vps33b in primary hepatocytes *in vitro* does not result in altered Asgr1 levels 3 days after RNAi, assessed by immunofluorescence (data not shown). In contrast, as described in chapter 2.2.9, p-Ampk is already induced on that day *in vitro*. Yet in livers *in vivo*, induction of p-Ampk occurs from day 10 after LNP injection onwards (**Figure 19B-D, H, J**), though not significantly on day 14 (**Figure 19C, I**), likely due to variability between samples.

Interestingly, although elevated Lamp1 upon Vps33b depletion was already shown in other cell types (Galmes et al., 2015; H. Xiang et al., 2022), this increase occurs robustly only after 3 weeks of KD. Lamp1 protein seems to fluctuate mildly upon KD initially and is stably increased after 3 weeks in livers *in vivo* (**Figure 19B-D, K-M**), and LysoTracker-positive lysosomes in primary hepatocytes isolated from mice after KD-initiation *in vivo* (**Figure 18I**). However, in hepatocytes with siRNA-induced KD of Vps33b *in vitro*, LysoTracker staining of lysosomes is significantly reduced 2 days after RNAi (**Figure 19N, O**), thus mirroring the fluctuations of Lamp1 protein seen *in vivo*. Interestingly, the time-dependent occurrence of phenotypes is further highlighted by a delay in the blood glucose-reducing effects of Vps33b KD *in vivo* (**Figure 19P**). Thus, it appears that the diverse alterations within the liver accumulate only over time into phenotypes affecting whole-body metabolism, such as blood glucose levels.

(Figure on following page)
(A) Western blot images for Vps33b protein levels in livers of mice 5, 10, and 14 days after a single LNP injection, or after 3 weeks of once weekly LNP injections.
(B-D) Representative western blots for Asgr1, Lamp1, p-Ampk and Ampk from livers of mice. (B, C) Mice were injected a single dose of LNP and sacrificed 5, 10, and 14 days later. (D) LNPs were injected once weekly and mice were sacrificed after 3 weeks of KD.
(E-G) Quantifications of (B-D) for Asgr1.
(H-J) Quantifications of (B-D) for p-Ampk relative to Ampk.
(K-M) Quantifications of (B-D) for Lamp1.
(N-O) LysoTracker and DAPI fluorescence in primary hepatocytes *in vitro*, two days after RNAi by siRNA (N) with quantifications in (O). Hepatocytes were treated with 500 nM LysoTracker for 30 min prior to fixation.
(P) Blood glucose levels in LNP-injected control and Vps33b KD mice with weekly LNP injections.
Data are presented as mean ± SEM. *P < 0.05, **P < 0.01, ***P < 0.001, ****P < 0.0001 by two-tailed unpaired Student's t test. Scale bar = 20 µm.

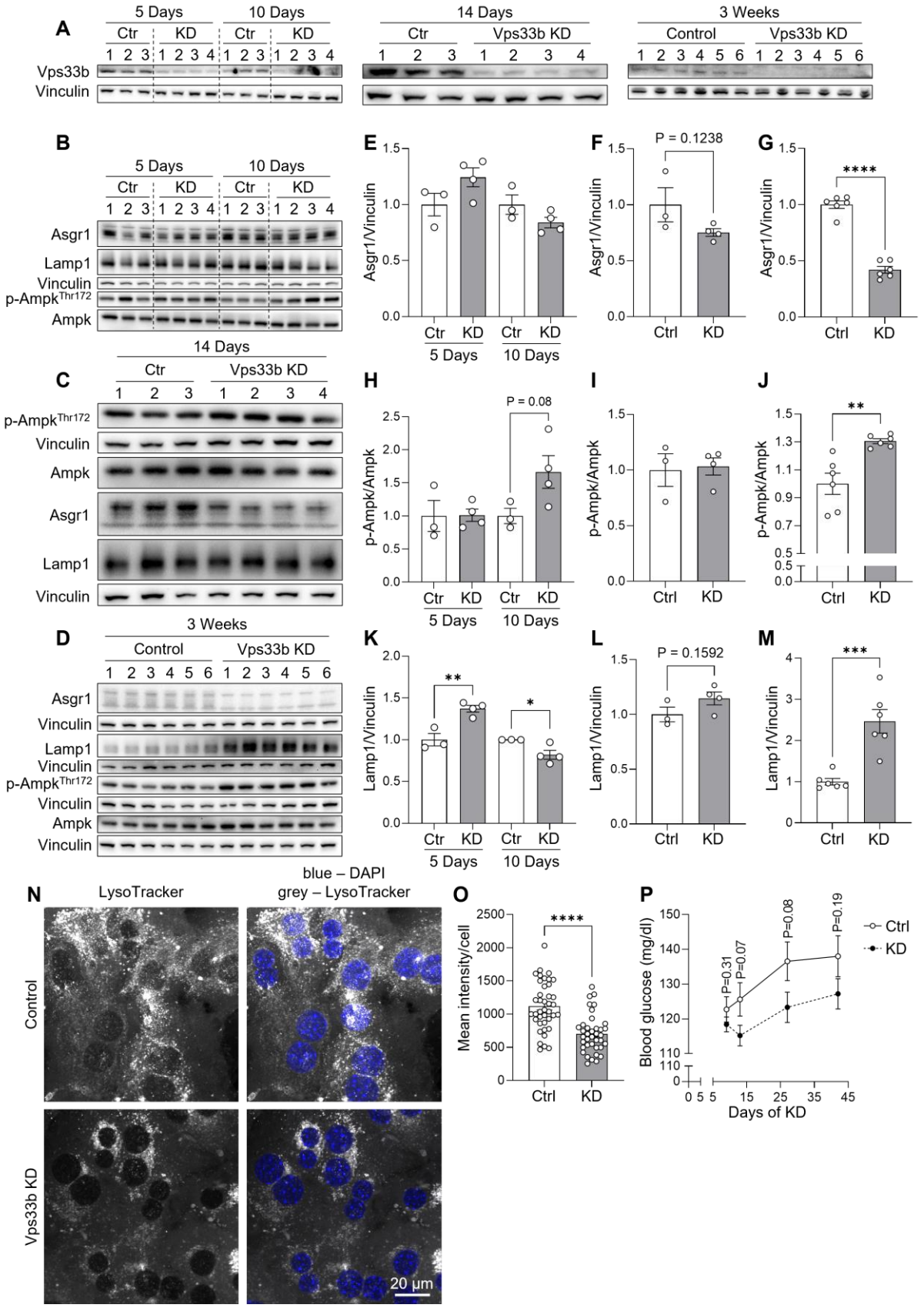

Figure 19 – Time course-dependent effects of Vps33b KD.

2.3 Chapter 3: Vps37a Regulates Hepatic Glucose Production by Controlling Glucagon Receptor Localization to Endosomes

In parallel to the work described in the previous chapters, I was involved in the project of Dr. Revathi Sekar, a former postdoctoral researcher of the lab, studying the function of ESCRT-I complex member Vps37a on hepatic glucose production. Fragments of her findings achieved before I joined the project are summarized in the next chapter (2.3.1). Parts of my work leading to the completion of the project, including work for the revision that I took care of, are presented in chapters 2.3.2-2.3.5. Our collaborative work was published in 2022 and the graphs presented in chapters 2.3.1-2.3.4 are reproductions of figures from Sekar & Motzler et al. (2022), *Cell Metabolism*.

2.3.1 Vps37a enhances hepatic gluconeogenesis *via* overactivation of cAMP/PKA/p-Creb signaling

Published first in Sekar & Motzler et al. (2022), *Cell Metabolism*. Work presented in this chapter (2.3.1) was performed by Dr. Revathi Sekar.

Based on a publication suggesting ESCRT-I involvement in NAFLD to NASH progression (Zhao et al., 2017), the group screened for the expression of ESCRT-I subunits in livers of patients with NAFLD with and without hepatic ballooning and NASH (Koliaki et al., 2015). Interestingly, ESCRT-I complex subunit VPS37A showed the strongest reduction on mRNA levels in patients with NAFLD with hepatic ballooning (**Figure 20A**), implicating an involvement of VPS37A specifically in this stage of NAFLD. In addition to NAFLD, *VPS37A* was strongly reduced in livers of patients with obesity and type 2 diabetes (T2D) (**Figure 20B**), two diseases closely linked with NAFLD (Mantovani et al., 2018). Combined, these data suggest an important role for VPS37A in both, NAFLD and T2D.

To understand the connection of VPS37A and metabolic liver disease, Vps37a was silenced in mouse livers using LNPs (Seitz et al., 2019; Zeigerer et al., 2012, 2015). Strikingly, reduction of Vps37a was specifically enhancing hepatic glucose production (HGP) in an ipPTT (**Figure 20C**), without effects on other metabolic parameters (data not shown, see Sekar & Motzler et al., 2022). In line with elevated HGP, mRNA expression of gluconeogenic genes *G6pc*, *Pck1*, *Foxo1*, and *Gcgr* were similarly increased in Vps37a KD livers (**Figure 20D**). To understand how Vps37a depletion is inducing gluconeogenesis and gluconeogenic gene expression, basal phosphorylation status of cAMP response element-binding protein (Creb) was assessed in livers, a known factor for the induction of gluconeogenesis (Herzig et al., 2001). Interestingly, KD of Vps37a resulted in elevated p-Creb (**Figure 20E, F**), suggesting an overactivation of p-Creb as responsible for increased gluconeogenesis.

As Creb phosphorylation is mediated by activation of cAMP/PKA (protein kinase A) signaling, PKA substrate phosphorylation and hepatic cAMP content were assessed. Intriguingly, Vps37a KD resulted in a remarkable increase in PKA substrate phosphorylation (**Figure 20G, H**), as well as significantly elevated cAMP levels (**Figure 20I**). Thus, increased gluconeogenesis upon Vps37a KD is mediated by enhanced signaling along the cAMP/PKA/p-Creb signaling axis.

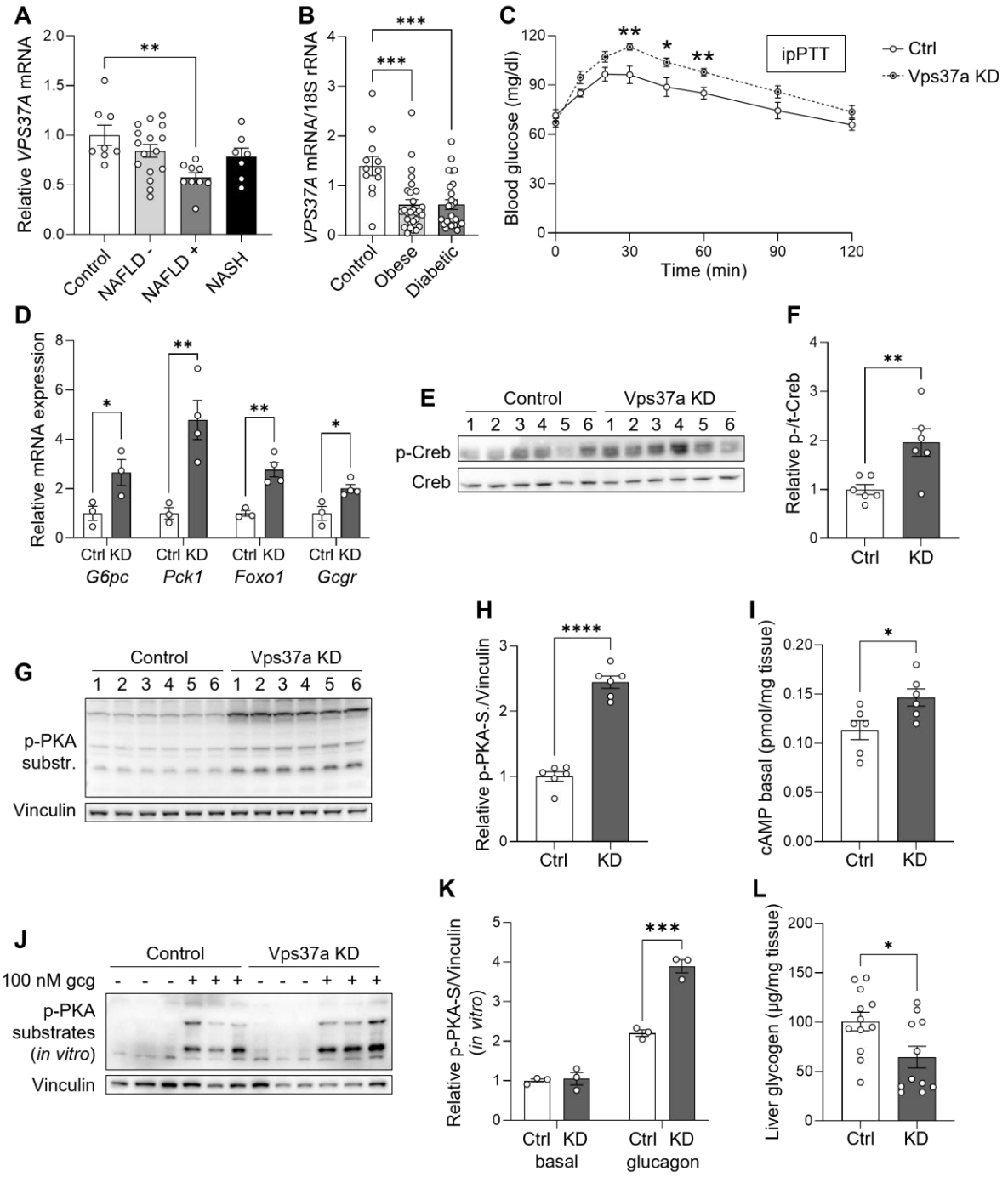

Figure 20 – Vps37a regulates hepatic glucose production through Gcgr/cAMP/PKA/Creb axis.
(A) Relative mRNA expression of *VPS37A* in livers of control patients and patients with NAFLD without and with ballooning, and NASH.
(B) *VPS37A* mRNA expression in livers of patients with obesity and type 2 diabetes (T2D).

(C) Intraperitoneal Pyruvate tolerance test (ipPTT) in chow-fed control and Vps37a KD mice with 2 g/kg pyruvate after 16 hours fasting.
(D) Relative hepatic gene expression of gluconeogenic genes *G6pc*, *Pck1*, *Foxo1*, and *Gcgr*.
(E-H) Western blots of livers with and without Vps37a KD of p-Creb (E) with quantifications in (F), and p-PKA substrates (G), quantified in (H).
(I) Liver cAMP in control and Vps37a KD mice.
(J-K) Representative western blots (J) and quantifications (K) for p-Creb in primary murine hepatocytes in sandwich culture three days after siRNA-mediated KD of Vps37a, stimulated with 100 nM glucagon (gcg) for 15 min.
(L) Liver glycogen content in control and Vps37a KD mice.
Data are presented as mean ± SEM. *P < 0.05, **P < 0.01, ***P < 0.001, ****P < 0.0001 by two-tailed unpaired Student's t test or ordinary one-way ANOVA with Šídák's multiple comparisons test (A, B).

A known regulator of gluconeogenesis along the cAMP/PKA/p-Creb signaling axis is glucagon via the G protein-coupled Glucagon receptor (Gcgr) (Perry et al., 2020; Petersen et al., 2017). To test whether glucagon is responsible for the observed effects, isolated mouse primary hepatocytes depleted of Vps37a by siRNA KD were acutely stimulated with glucagon *in vitro*. Intriguingly, KD of Vps37a resulted in significantly increased glucagon-induced p-PKA-substrates (**Figure 20J, K**). As expected for overactivated glucagon signaling (Habegger et al., 2010), hepatic glycogen content was significantly reduced (**Figure 20L**).

Taken together, these data show that KD of Vps37a results in overactivation of cAMP/PKA/p-Creb signaling of glucagon via Gcgr, leading to enhanced gluconeogenesis and HGP (Sekar et al., 2022). Moreover, data shown in Sekar & Motzler et al. reveal that this overactivation of Gcgr signaling is due to an accumulation of Gcgr at endosomes upon Vps37a KD. From endosomes, Gcgr preferentially signals to gluconeogenesis without affecting lipid utilization (Sekar et al., 2022).

2.3.2 Effects of ESCRT-I interference on p-Creb activation are Vps37a-specific

Data on Tsg101, Vps28, Vps37b, and Vps37c published first in Sekar & Motzler et al. (2022), *Cell Metabolism*. Data on Ubap1 has not yet been published.

ESCRT-I is a heterotetrametric complex of tumor susceptibility gene 101 (Tsg101), vacuolar protein sorting 28 (Vps28), ubiquitin associated protein 1 (Ubap1), and one of either Vps37a, Vps37b, Vps37c, or Vps37d (J. H. Hurley, 2010; Schmidt & Teis, 2012). In order for ESCRT-I to mediate its function in directing ubiquitinated cargo to lysosomes (Stuffers et al., 2009), the complex needs to be complete. Interestingly, previous work included in Sekar & Motzler et al. revealed a counterregulatory increase in Vps37c levels and a slight reduction in Vps37b upon Vps37a KD. Thus, to assess whether the gluconeogenic effects upon Vps37a KD are due to ESCRT-I complex destabilization or specific to Vps37a, I performed KDs of the other complex subunits in primary hepatocytes *in vitro* and measured p-Creb and gene expression changes upon glucagon stimulation. Remarkably, KD of none of the other ESCRT-I subunits resulted in elevated p-Creb (**Figure 21A, B, D, F, H, J**), as observed for Vps37a KD (Sekar et al., 2022).

Interestingly, while Tsg101 KD was shown to destabilize the ESCRT-I complex with concomitant reduction in Vps37a protein (Brunet et al., 2004; Sekar et al., 2022), no changes in transcript levels of *G6pc* and *Pck1* were observed (**Figure 21C**). Opposingly to increased *G6pc* and *Pck1* seen under Vps37a KD, KD of Vps28 and Vps37b led to reduced expression of *Pck1* under basal and glucagon-induced conditions, respectively (**Figure 21E, G**). Interestingly, depletion of Vps37c was able to slightly elevate glucagon-stimulated *G6pc* and *Pck1*, however, without reaching statistical significance (**Figure 21I**). In addition, Ubap1 KD increased *Pck1* expression upon treatment with glucagon (**Figure 21K**), however, none of the observed changes in mRNA expression upon KD of any ESCRT-I subunit except Vps37a were linked to altered Creb phosphorylation, thus indicating that the effects on PKA/p-Creb axis are specific to Vps37a reduction.

(Figure on following page)
(A) Representative western blots for p-Creb and Creb from KDs of indicated ESCRT-I subunits (Tsg101, Vps28, Vps37b, Vps37c, Ubap1) after gcg stimulation (100 nM glucagon for 15 min).
(B-C) Quantifications of (A) in (B). Relative gene expression of *Tsg101*, *G6pc*, and *Pck1* upon Tsg101 KD at basal and glucagon-stimulated condition (C).
(D-E) Quantifications of (A) in (D). Relative gene expression of *Vps28*, *G6pc*, and *Pck1* upon Vps28 KD at basal and glucagon-stimulated condition (E).
(F-G) Quantifications of (A) in (F). Relative gene expression of *Vps37b*, *G6pc*, and *Pck1* upon Vps37b KD at basal and glucagon-stimulated condition (G).
(H-I) Quantifications of (A) in (H). Relative gene expression of *Vps37c*, *G6pc*, and *Pck1* upon Vps37c KD at basal and glucagon-stimulated condition (I).
(J-K) Quantifications of (A) in (J). Relative gene expression of *Ubap1*, *G6pc*, and *Pck1* upon Ubap1 KD at basal and glucagon-stimulated condition (K).
For gene expression analysis, hepatocytes were treated with 100 nM glucagon for 5 hours. Data are presented as mean ± SEM. *P < 0.05, **P < 0.01, ***P < 0.001, ****P < 0.0001 by two-tailed unpaired Student's t test or ordinary one-way ANOVA with Šídák's multiple comparisons test.

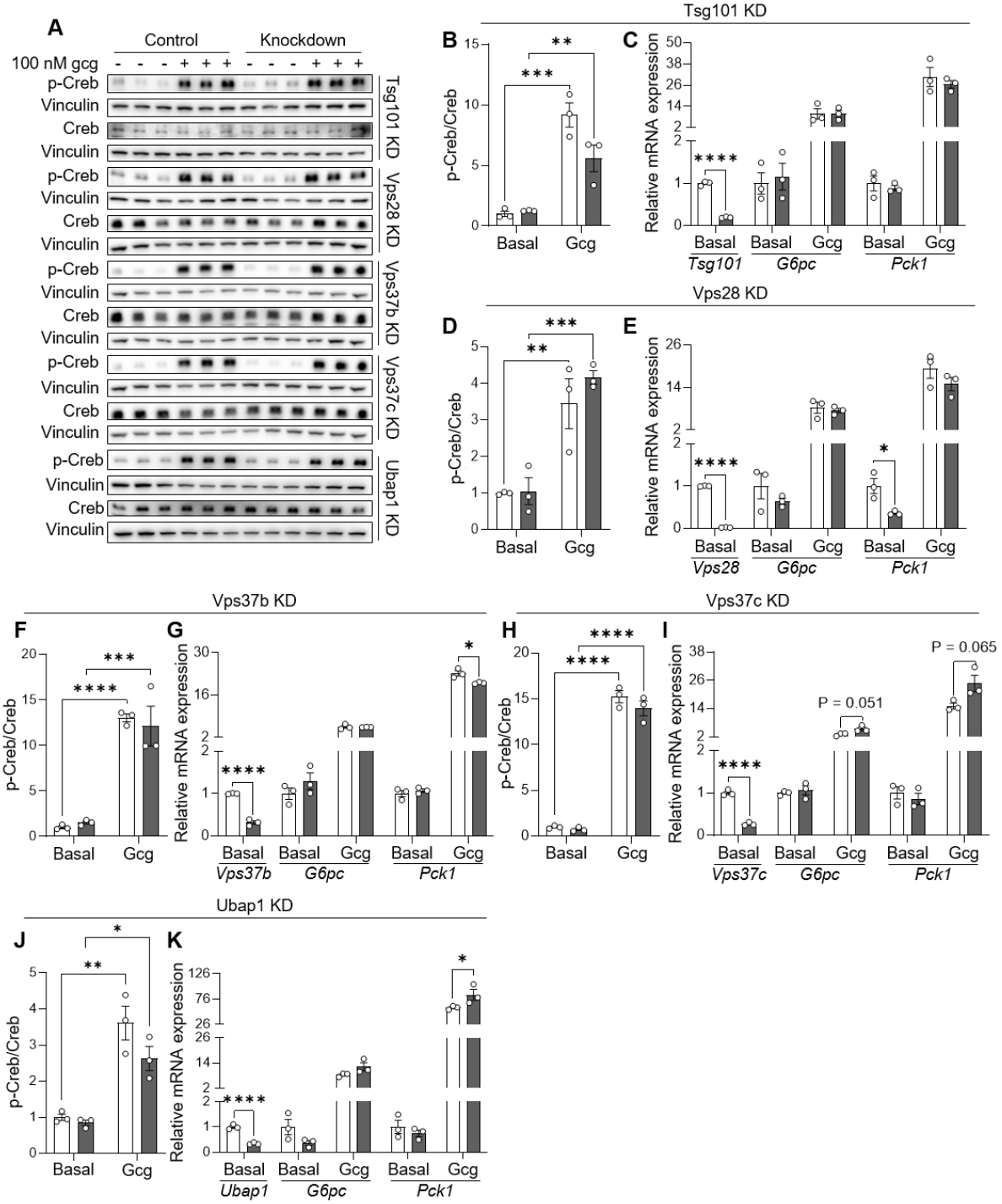

Figure 21 – Enhanced p-Creb and gluconeogenic gene expression are specific to Vps37a KD.

2.3.3 VPS37A OVEREXPRESSION IN LIVERS HAS THE POTENTIAL TO LOWER BLOOD GLUCOSE

Published first in Sekar & Motzler et al. (2022), *Cell Metabolism* unless indicated otherwise. Parts of the presented western blots were performed by Dr. Yun Kwon.

Given that Vps37a depletion increases blood glucose production through enhanced cAMP/PKA/Creb-mediated gluconeogenesis, it was interesting whether increasing Vps37a

levels would oppose these effects. Thus, I generated an adeno-associated virus (AAV) construct for the expression of murine Vps37a under the liver protein 1 promotor (AAV8-LP1-mVps37a) and used a mutated, translation deficient GFP AAV8 as control (Bühler et al., 2021). This approach allows the liver-specific overexpression (OE) by two means: first, AAVs from serotype 8 were shown to have high liver specificity (Gao et al., 2002). Second, using a hepatocyte specific promotor, off-target effects are reduced. Seven weeks after injection of AAVs through the tail vein, Vps37a protein levels were increased by 60 % (**Figure 22A, B**), indicating stable overexpression over a prolonged timeframe. OE of Vps37a resulted in a parallel increase in protein levels of Vps37c, Vps28, and Tsg101 (**Figure 22A, B**), hence suggesting that the whole ESCRT-I complex has been stabilized. Vps37b levels, however remained unchanged (**Figure 22A, B**). Remarkably, increased ESCRT-I complex abundancy led to both decreased p-PKA-substrates and p-Creb (**Figure 22C, D**), thus reversing the phenotypes seen upon Vps37a KD (Sekar et al., 2022). In line, basal cAMP levels in livers of Vps37a OE mice, upstream of PKA activation (Krebs et al., 1959; Yang & Yang, 2016), were significantly reduced (**Figure 22E**). Excitingly, these changes in cAMP/PKA/Creb activation were sufficient to increase liver glycogen content (**Figure 22F**) and to result in a tendency for reduced blood glucose (**Figure 22G**).

It is important to note, however, that the success of using Vps37a OE for the reduction of blood glucose levels due to changes in cAMP/PKA/Creb is highly dependent on the degree of overexpression achieved. In a separate cohort of mice, Vps37a protein was only increased by 30 %, which was not sufficient to stabilize ESCRT-I (**Figure 22H, I**), hence no change in hepatic cAMP levels was observed (**Figure 22J**). Interestingly, livers of diabetic leptin-deficient mice (*db/db*) (Hummel et al., 1966) after AAV8-LP1-mVps37a injection revealed a strong counterregulatory mechanism, preventing Vps37a mRNA to be translated into protein. Here, despite a 30 % increase on *Vps37a* transcript levels (**Figure 22K**), protein levels remained completely unaltered (**Figure 22L, M**) **(previously unpublished)**. This observation could be linked to reduced *VPS37A* expression in livers of patients with NAFLD and T2D, described above (**Figure 20A, B**).

Despite these hurdles in overexpressing Vps37a, however, in another cohort of *db/db* mice, Vps37a overexpression of 70 % was achieved (**Figure 22N, O**). This led again to reduced PKA-substrate and Creb phosphorylation (**Figure 22N, O**), with a concomitant reduction in liver cAMP (**Figure 22P**) and a trend for reduced blood glucose in diabetic mice (**Figure 22Q**).

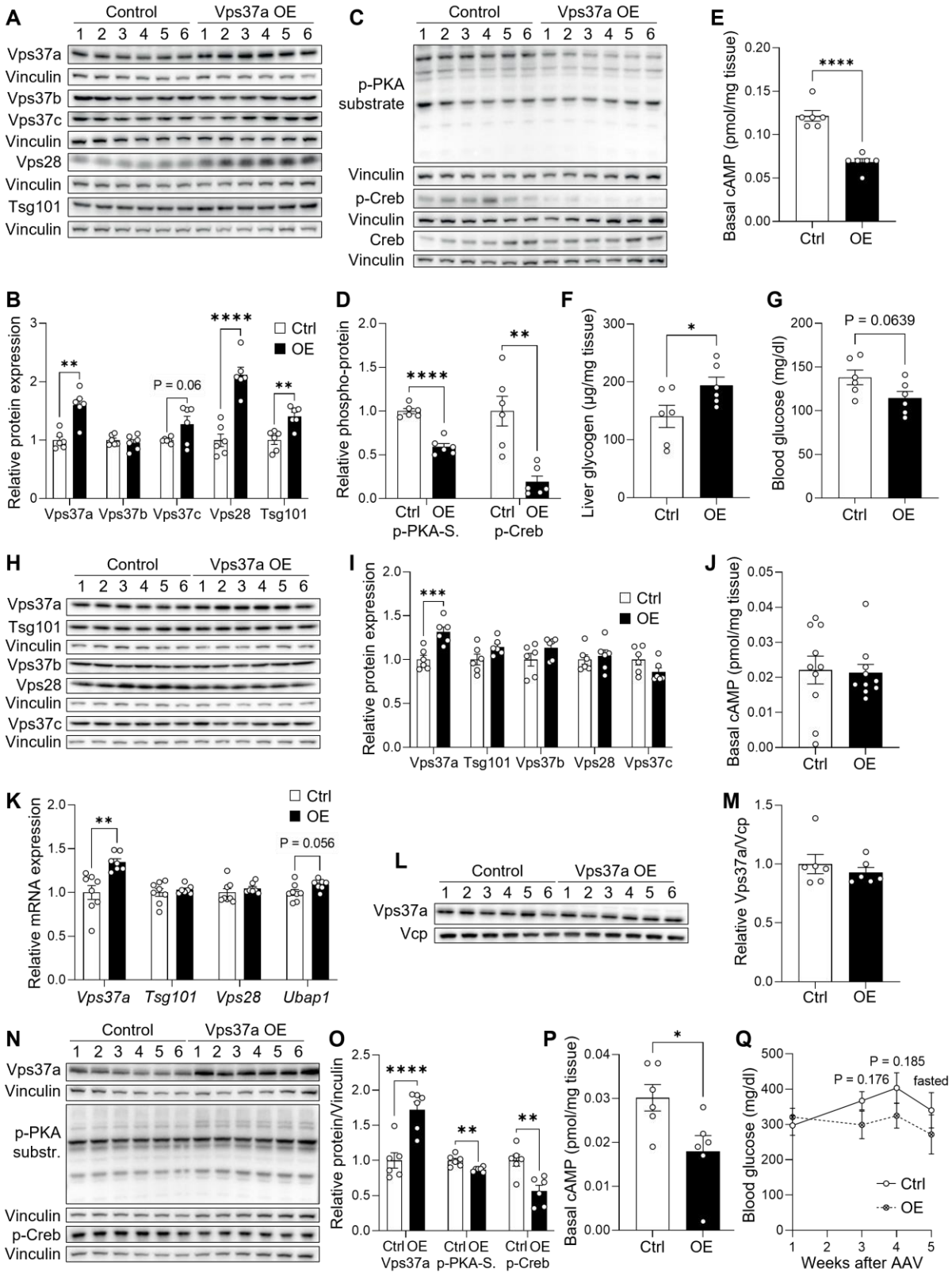

Figure 22 – OE of Vps37a in livers has the potential to lower blood glucose.
(A-B) Representative western blots for ESCRT-I subunits Vps37a, Vps37b, Vps37c, Vps28, and Tsg101 in livers of chow-fed WT mice, seven weeks after injection of control or Vps37a overexpression AAV (A) with quantifications in (B).
(C-D) Immunoblot for p-PKA substrates and p-Creb in control and Vps37a OE mice in (C), quantified in (D).
(E-G) Liver cAMP (E) and glycogen (F) levels, and blood glucose levels (G) in control and Vps37a OE mice.
(H-I) Representative western blots (H) and quantification (I) of a second cohort of control and Vps37a OE mice for ESCRT-I subunits.
(J) Hepatic cAMP content in control and OE mice in (H) and (I).

(K-M) mRNA expression for *Vps37a*, *Tsg101*, *Vps28*, and *Ubap1* in livers of 12 weeks old *db/db* mice, 6 weeks after initiation of OE. (L) Representative western blot for Vps37a with quantifications in (M).
(N-O) Representative western blots for Vps37a, p-PKA substrates, and p-Creb in livers of another cohort of *db/db* mice, quantified in (O).
(P-Q) Liver cAMP (P) and blood glucose levels (Q) in *db/db* mice with Vps37a OE from (N-O).
Data are presented as mean ± SEM. *P < 0.05, **P < 0.01, ***P < 0.001 ****P < 0.0001 by two-tailed unpaired Student's t test.

2.3.4 GLUCAGON ENHANCES COLOCALIZATION OF GCGR WITH UBIQUITIN IN HEPATOCYTES

Published first in Sekar & Motzler et al. (2022), *Cell Metabolism*. Fiji colocalization analysis was performed by Dr. Yun Kwon.

ESCRT-I mediates the sorting of ubiquitinated transmembrane receptors towards degradation (Szymanska et al., 2018). It is generally accepted that ubiquitin-binding by ESCRT-I is mediated by Tsg101 (Henne et al., 2011). Interestingly though, Vps37a possesses a N-terminus weakly similar to the ubiquitin E2 variant (UEV) sequence of Tsg101 (Brunet et al., 2004), used to bind ubiquitinated cargo. Thus far, however, ubiquitin-binding through Vps37a could not be shown.

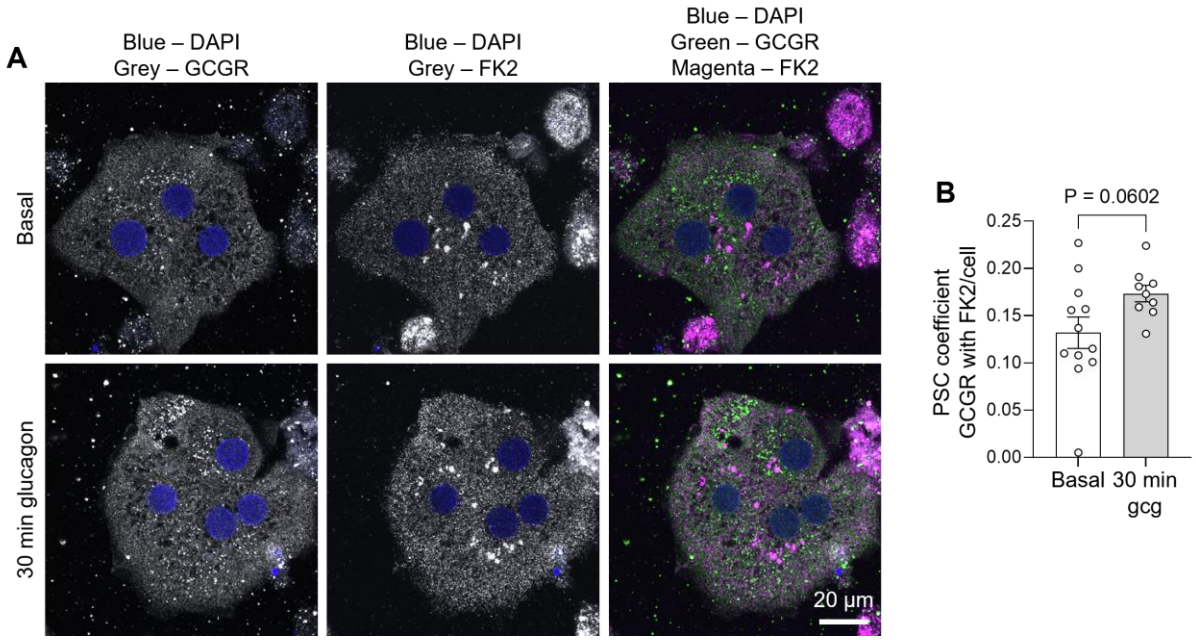

Figure 23 – Activated glucagon receptor colocalizes with ubiquitin.
(A-B) Primary human hepatocytes in collagen sandwich culture were stimulated with 100 nM glucagon for 30 min and co-stained with GCGR and FK2-ubiquitin. Representative confocal images in (A) and quantification of GCGR-FK2 colocalization with particle analysis using Fiji in (B).
Data are presented as mean ± SEM. Significance assessed by two-tailed unpaired Student's t test. Scale bar = 20 µm.

Given the direct interaction of Vps37a with Gcgr, identified by collaborators (Julia Jülg and Christian Behrends) (Figure 5J in Sekar et al., 2022), it was of interest whether Gcgr is indeed internalized in ubiquitin-dependent manner. Therefore, I treated primary human hepatocytes for 30 min with glucagon to induce receptor internalization and stained for GCGR and FK2

Ubiquitin. For this assay, human hepatocytes were used due to poor GCGR antibody quality for murine specimen (Bomholt et al., 2022). Interestingly, colocalization analysis of high-resolution confocal microscopy images using Fiji **(performed by Dr. Yun Kwon)** (French et al., 2008) revealed a close-to-significant increase in colocalization of GCGR and ubiquitin (**Figure 23A, B**), thus pointing towards a portion of internalized GCGR being ubiquitinated, potentially for degradation.

2.3.5 GCGR ABUNDANCY IS INCREASED IN MURINE AND HUMAN STEATOTIC HEPATOCYTES

Our work published in Sekar & Motzler et al. (2022) suggests that downregulation of *VPS37A* in NAFLD and T2D could potentially contribute to hyperglycemia, a common feature of both diseases (Petersen et al., 2017; Pouwels et al., 2022), through the regulation of GCGR intracellular localization and signaling. Interestingly, RNA-seq data of livers from rats with NAFLD revealed a 35 % reduction in *Gcgr* transcript levels (Zhu et al., 2017), thus questioning the importance of altered Gcgr signaling in the setting of NAFLD. To assess whether the regulation of Gcgr trafficking by Vps37a could indeed be relevant in this setting, I assessed GCGR protein levels in steatotic primary human and murine hepatocytes by confocal fluorescence microscopy. Steatosis in both murine and human hepatocytes was induced by treatment with oleate and palmitate. The surface portion of Gcgr was labeled by treating steatotic murine primary hepatocytes with a fluorescently labeled Cy5-glucagon analogue (**provided by Dr. Oliver Plettenburg**) on ice to halt receptor internalization (Sekar et al., 2022). Interestingly, surface binding of Cy5-gcg to Gcgr in steatotic hepatocytes was increased (**Figure 24A, B**). In addition, total GCGR levels were assessed in similarly steatotic primary human hepatocytes by immunofluorescence. Here, total GCGR levels were increased with steatosis (**Figure 24C, D**). Thus, while decreased on mRNA (Zhu et al., 2017), both total and surface Gcgr levels seem to increase upon steatosis. In contrast, Vps37a reduction in metabolically diseased livers occurs both, on mRNA and protein (Sekar et al., 2022). This renders altered trafficking of Gcgr upon Vps37a reduction as potential disease-contributing mechanism.

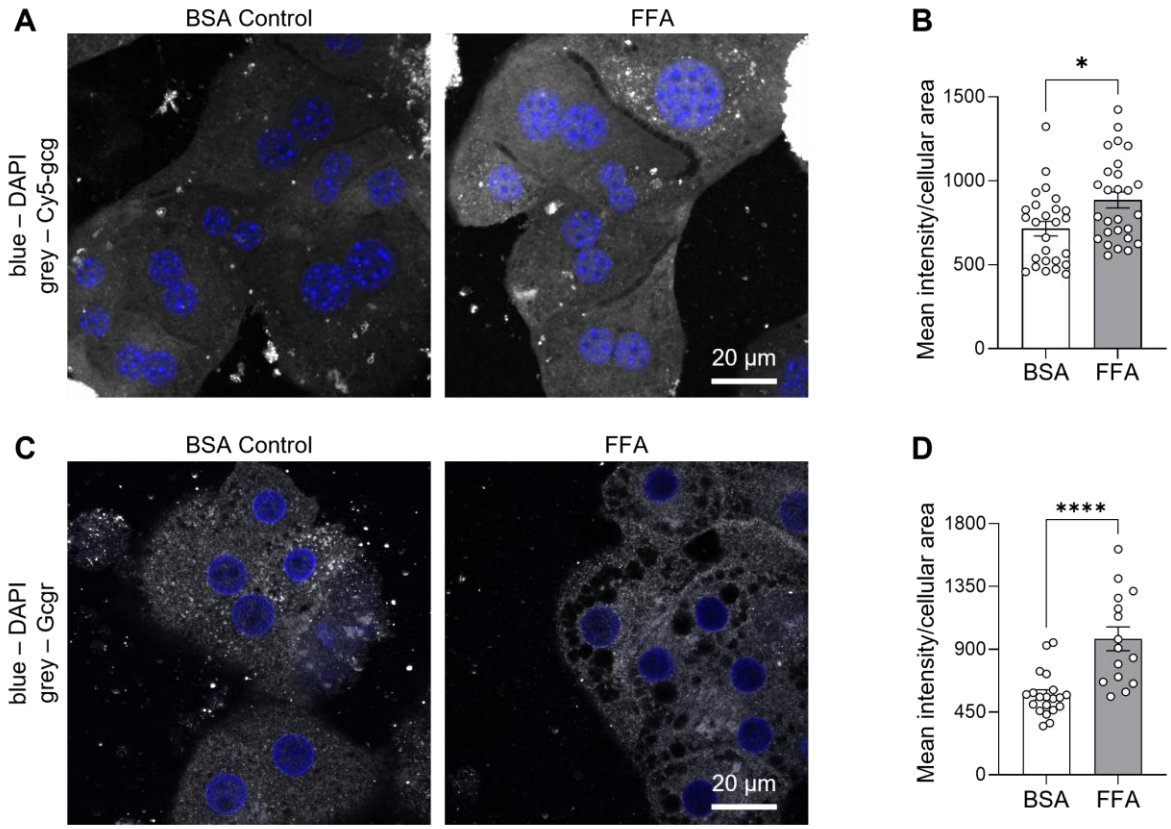

Figure 24 – Glucagon receptor protein levels are increased in steatotic hepatocytes.
Primary murine and human hepatocytes were cultured in a collagen sandwich and treated with medium supplemented with either BSA-conjugated 50 µM palmitate + 250 µM oleate (FFA) or a corresponding amount of BSA (BSA control).
(A-B) For surface labeling of Gcgr, murine hepatocytes were serum starved for 2 hours, three days after seeding, and Cy5-gcg was added in cold medium for 2 hours on ice. Quantifications in (B).
(C-D) Total GCGR levels in human hepatocytes were determined by staining with a Gcgr antibody after permeabilization (C) with quantifications thereof in (D).
Data are presented as mean ± SEM. *P < 0.05, ****P < 0.0001 by two-tailed unpaired Student's t test. Scale bar = 20 µm.

3 DISCUSSION

3.1 CHAPTER 1: AP4E1 REGULATES NAFLD-TO-NASH PROGRESSION

The present work demonstrates a functional relationship between hepatic Ap4e1 and NAFLD to NASH transition. While in healthy livers, Ap4e1 ablation has no apparent metabolic effects, Ap4e1 KO exacerbates NASH development in mice under NASH-inducing diets.

Building on the strong metabolic implications of phenotyping data reported for whole-body KO Ap4e1$^{-/-}$ mice, such as altered glucose tolerance and serum triglycerides (Rozman et al., 2018), this study reports significantly elevated *AP4E1* transcript levels in diseased livers of patients with T2D and NASH. Surprisingly, liver-specific KO of Ap4e1 in male mice did not reproduce all of the phenotypes published on whole-body KO. For example, random and fasted blood glucose levels in Ap4e1$^{liver\text{-}KO}$ mice were unchanged, while whole-body KO mice showed decreased random and increased fasting blood glucose (Rozman et al., 2018). Moreover, impaired glucose tolerance observed by Rozman and colleagues was not observed in Ap4e1$^{liver\text{-}KO}$ mice, neither on chow, nor on HFD. In line with a small cohort of human HSP patients deficient in AP4E1 in which no incidence of obesity was reported (Abou Jamra et al., 2011) and unchanged bodyweight in mice phenotyped by IMPC, Ap4e1$^{liver\text{-}KO}$ did not cause any alterations in bodyweight either, both on regular chow and HFD.

Differences between the data presented here and full-body KO models of Ap-4-subunit depletion, however, might originate from other organs affected in such models. Ap4e1$^{-/-}$ mice largely resemble the human HSP syndrome, including motor neuron deficiencies and weakened grip strength (De Pace et al., 2018), as well as retina and kidney abnormalities (Higgins et al., 2022). Moreover, multiple brain defects, such as axonal swelling in various areas of the brain, were reported both for mice (De Pace et al., 2018; Ivankovic et al., 2020; Majumder et al., 2022) and humans (Behne et al., 2020; Ebrahimi-Fakhari et al., 2020, 2021). The potential metabolic aspects of these Ap4e1 deficiency-derived alterations have thus far not been studied.

Interestingly, the IMPC data revealed a significant increase in serum AST in female mice upon Ap4e1$^{-/-}$ KO and a reduction of serum ALT in male mice. However, other metabolic parameters measured by the IMPC did not show additional gender specificity. Altered serum transaminases in those mice are especially interesting considering the positive correlation between Ap4e1 protein levels and degree of hepatic fibrosis, seen in livers of FPC diet fed mice. This correlation suggests an alleviating effect of Ap4e1 reduction on liver damage, as reported for other genes regulated in such fashion (Loft et al., 2021; Mridha et al., 2017). Yet, Ap4e1$^{liver\text{-}KO}$ mice on chow diet showed increased plasma transaminases, hence questioning this relationship.

In addition to elevated transaminases on chow diet, Ap4e1$^{liver\text{-}KO}$ resulted in elevated ALT and AST levels upon feeding of NASH-inducing MCD and FPC diets, respectively. Interestingly, increased ALT upon MCD feeding was only apparent after two weeks of MCD-feeding and disappeared later, possibly indicating an initially faster disease progression. The key determinant for long-term survival in patients with NAFLD is fibrosis (Angulo et al., 2015). Thus, it is striking that besides the counterintuitive initial elevation of transaminases, Ap4e1$^{liver\text{-}KO}$ also exacerbates fibrosis development under two different NASH-inducing diets. These findings again oppose the positive correlation of Ap4e1 protein with fibrosis under FPC diet which suggests an ameliorating effect of Ap4e1 KO on NASH progression. Instead, increased Ap4e1 upon NASH appears to be counterregulatory to decelerate NAFLD to NASH transition and fibrosis development. Thus, next experiments will include overexpression studies aimed at preventing fibrosis in NASH. Of note, the Ap-4 complex consists of four subunits (Dell'Angelica et al., 1999; Hirst et al., 1999), and in HSP, deficiencies in any of the subunits result in spastic paraplegia (Behne et al., 2020; Ebrahimi-Fakhari et al., 2021). Therefore, it will be interesting to address whether the observed effects on NASH are specific to the ε subunit or rather due to disruption of the whole Ap-4 complex.

Given the function of the Ap-4 complex in protein sorting at the TGN (Park & Guo, 2014) and the potentially counterregulatory increase in Ap4e1 upon NASH, mechanistic studies aiming at identifying the proteins trafficked by Ap-4 under these conditions could unveil novel druggable disease modifiers. Theoretically, these protein cargos could be destined for membrane localization or secretion, where they could interact with other cells within the liver to slow down fibrosis development. Potential techniques to dissect these mechanisms include membranome assessment (Nalbach et al., 2022), or single-nucleus RNA sequencing (Loft et al., 2021; Richter et al., 2021) to study alterations in the crosstalk of hepatocytes with e.g. HSCs. Moreover, autophagy was suggested preventive for NASH development through initiation of lipophagy (Czaja, 2016) and Ap-4 deficiencies are associated with autophagy defects in the brain (De Pace et al., 2018; Mattera et al., 2017). Thus, further studies should aim to examine whether defective autophagosome formation could also occur in hepatocytes upon Ap4e1 KO and whether this contributes to NASH development.

In conclusion, this work has attributed a thus far unknown role for Ap4e1 in the development of NASH. Further mechanistic studies are required to examine this novel concept by which this endosomal adaptor protein subunit contributes to NAFLD to NASH transition

3.2 CHAPTER 2: REGULATION OF METABOLISM BY ENDOSOMAL MEMBRANE TETHER VPS33B

Vps33b has thus far mainly been studied in relation to the ARC syndrome. However, this work presents novel functions of Vps33b in liver metabolism. KD experiments *in vitro* and *in vivo* revealed a prominent effect on liver lipid and glucose metabolism, thus broadening the current understanding of Vps33b action.

LNP-induced KD of Vps33b revealed inconsistencies with previously published studies using $Vps33b^{fl/fl}$-AlfpCre (Cullinane et al., 2010) or -AlbCre (Fu et al., 2019; C. Wang et al., 2018) Vps33b liver-KO mice. These could potentially originate from different durations of Vps33b-depletion and from the cell types affected: LNP injections are here only performed in adult mice, thus allowing for normal tissue development and hepatocyte growth. In contrast, genetic models result in a perpetual loss of Vps33b throughout all developmental stages. Moreover, inducing Cre expression in $Vps33b^{fl/fl}$ mice under α-fetoprotein (Alfp) or albumin (Alb) promotors not only affects hepatocytes but also biliary duct cells (Kellendonk et al., 2000; Pruniau et al., 2013). LNPs instead were shown to be specific for hepatocytes without affecting other liver-resident cells (Gilleron et al., 2013; Woitok et al., 2020).

Strikingly, hepatic KD of Vps33b in mice resulted in increased serum cholesterol levels. These effects could be attributed to decreased Ldlr protein expression observed in isolated hepatocytes after siRNA-mediated Vps33b KD, as was anticipated based on a previously published interaction of Vps33b with CCC complex components CCDC22 and COMMD1 and 6 (Hunter et al., 2018; Huttlin et al., 2017). The CCC complex, involving Ccdc22, Ccdc93, and Commd proteins (Phillips-Krawczak et al., 2015), was shown important for the recycling of Ldlr (Bartuzi et al., 2016; Fedoseienko et al., 2018), and Vps33b together with Vipas39 have previously been described to function in recycling (Cullinane et al., 2010). Of note, the magnitude of 20 % increased total serum cholesterol levels in mice on chow diet after hepatic Vps33b reduction is comparable to hepatic Commd1 and Commd6 KO with 40 % and 30 % increase in serum cholesterol, respectively (Bartuzi et al., 2016; Fedoseienko et al., 2018). As Ccdc22, Ccdc93 also interacts with Vps33b in co-immunoprecipitation assays, although much weaker (Hunter et al., 2018). Interestingly, the present work suggests altered recruitment of Ccdc93 upon Vps33b KD *in vitro*, further strengthening the notion that hepatic Vps33b can work together with the CCC complex to regulate recycling of e.g. Ldlr. However, whether an increased number and smaller size of Ccdc93-positive structures in hepatocytes upon Vps33b KD should be translated into increased recruitment from intracellular pools, thus resulting in a more dispersed distribution, or whether this means decreased recruitment indicated by smaller structure size, requires further studies. Moreover, proteomics analysis revealed a broad downregulation of various proteins, not only limited to transmembrane receptors. Thus, further studies are needed to understand whether indeed Vps33b-dependent trafficking affects specifically Ldlr abundancy or whether these effects are more general.

The results presented in this work raise the question, how Vps33b KD decreases insulin sensitivity and blood glucose levels, in addition to altered lipid metabolism. Whole-liver proteomics revealed that Vps33b depletion reduced Insr protein, thus resulting in decreased downstream Akt phosphorylation. Interestingly, while there were no obvious alterations during ITT, more thorough analysis of the initial response in blood-glucose reduction upon insulin injection, as suggested by Müller, Klingenspor & Tschöp (2021), indicated mildly decreased insulin sensitivity also *in vivo*. These effects were masked, however, by significantly lowered blood glucose in Vps33b KD mice already prior to insulin injection and at randomly fed state. In T2D, insulin insensitivity is contributing to hyperglycemia (Demir et al., 2021), thus reduced blood glucose in Vps33b KD mice despite decreased insulin signaling appears counterintuitive. However, the effects of Vps33b KD *in vivo* by LNPs are liver-specific, thus insulin signaling in other organs is likely not affected, and the reduction in p-Akt upon Vps33b KD *in vitro* is rather mild. Furthermore, the effects of Vps33b KD on blood glucose were not able to reduce hyperglycemia in homozygous *db/db* mice. Importantly though, *db/db* mice used in this study were already hyperglycemic before initiation of Vps33b KD. Thus, it will be interesting to assess the blood glucose-lowering effects in other models, such as high fat diet-fed mice, but also to investigate the differential regulation of Vps33b mRNA and protein observed in livers of *db/db* mice.

Reduced blood glucose with simultaneously unchanged liver glycogen content and gluconeogenesis, as assessed by PTT, raises the question for alternative causes. Interestingly, it was shown that inducible liver-specific overactivation of Ampk in mice, as observed under Vps33b KD, also leads to reduced blood glucose levels (Garcia et al., 2019). Moreover, Ampk activation in these mice induced plasma hypercholesterinemia and reduced liver TG levels (Garcia et al., 2019), two features associated with hepatic Vps33b ablation as well. Similarly, also small-molecule Ampk-activators were shown to decrease liver TGs and blood glucose (C. S. Zhang et al., 2022). Thus, p-Ampk induction upon Vps33b KD could potentially explain some of the metabolic phenotypes reported here, such as reduced liver TGs or blood glucose.

Ampk activation was suggested to occur on membranes, as Ampk-myristoylation induces membrane localization (Oakhill et al., 2010), as well as farnesylation of the major upstream kinase, LKB1 (Houde et al., 2014). Precisely, activation of Ampk has been located to lysosomal membranes, where Ampk associates with LKB1 upon nutrient starvation (Morrison et al., 2022; C. S. Zhang et al., 2014; Y. L. Zhang et al., 2013). This is especially interesting in light of increased amounts of Lamp1 protein and LysoTracker-positive structures (i.e. lysosomes), that could potentially contribute to increased lysosomal activation of Ampk. Lysosomal LKB1 activation of Ampk, however, is considered as nucleotide-dependent Ampk-activation pathway (Morrison et al., 2022), yet ATP levels in Vps33b KD livers were unchanged. Therefore, not

only ATP levels, but also ADP:ATP and AMP:ATP ratios, as well as phosphorylation status of LKB1 need to be assessed in further studies. Interestingly, an analogous mechanism has already been reported for Vps33b KO, where accumulation of lysosomes resulted in enhanced activation of lysosome-resident proteins. In contrast to the results described here in livers and hepatocytes though, Vps33b KO in regulatory T cells led to hyperactivation of mTORC1 at lysosomes (H. Xiang et al., 2022), the adversary of Ampk (Carroll & Dunlop, 2017). In fact, accumulation of Lamp1-positive compartments upon Vps33b depletion has been reported in different cell types already (Galmes et al., 2015; H. Xiang et al., 2022), and KD of Vps33b impairs late endosomal-lysosomal fusion (Galmes et al., 2015). Whether these compartments actually account for lysosomes, as the LysoTracker results here suggest, is yet unclear.

In search for potential causes of increased p-Ampk upon Vps33b KD, activated CaMKII in Vps33b KD livers is an interesting hint towards a nucleotide-independent, calcium-sensitive activation mechanism (Garcia & Shaw, 2017). Ampk activation by CaMKII was shown both in muscle and hepatocyte cell lines (Kim et al., 2022; Raney & Turcotte, 2008), however, the main calcium-dependent kinase activating Ampk is CaMKKII (Hawley et al., 2005; R. L. Hurley et al., 2005). Importantly, CaMKKII-mediated activation of Ampk also occurs during prolonged amino acid starvation (Ghislat et al., 2012; Pezze et al., 2016) and total hepatic L-amino acid levels upon Vps33b KD were slightly reduced, although not significant. Further studies will address whether such effects could contribute to Ampk activation seen here by addressing CaMKKII phosphorylation and measuring individual amino acids. Moreover, insulin signaling inhibits Ampk while activating mTORC1 (Haeusler et al., 2018; Hawley et al., 2014; Menon et al., 2014), thus reduced p-Akt as shown here upon Vps33b KD might additionally contribute to Ampk activation.

Data presented in this work, including the discovery of feeding-sensitive recruitment of Vps33b, various metabolic alterations upon Vps33b KD, and p-Ampk induction, position Vps33b potentially as endosomal nutrient sensor. In line, proteomics data show the post-transcriptional downregulation of numerous proteins and suggest Vps33b KD to reduce translation, a highly energy consuming process (Buttgereit & Brand, 1995). Further studies, including polysome profiling, are planned to shed light on these regulatory processes in Vps33b deficient hepatocytes. Of note, the phenotypes of Vps33b KD appear to be time dependent. Potentially, some events caused by altered trafficking upon Vps33b depletion require longer to accumulate to ultimately result in the observed phenotypes, or rely on a certain chronology. Thus, identifying the initial changes after Vps33b KD that possibly begin a cascade of ensuing alterations could provide mechanistic understanding of changes elicited by Vps33b KD.

Together, the current work opened a novel direction for further studies on Vps33b as potential regulator of liver metabolism. Inducible KD of Vps33b in livers of adult mice lacks some of the features associated with ARC and instead alters different aspects of liver metabolism. Thus,

further studies will aim at dissecting this connection and allow a deeper understanding of both Vps33b and liver function.

3.3 Chapter 3: Vps37a Regulates Hepatic Glucose Production by Controlling Glucagon Receptor Localization to Endosomes

The work presented here, together with additional data published in Sekar & Motzler et al. (2022), shows that glucagon *via* Gcgr can induce HGP independently of its effects on lipid oxidation when Gcgr localization is shifted to endosomes. These effects of Vps37a KD are mediated through enhanced signaling along the $G_{\alpha s}$ cAMP/PKA/p-Creb axis. Moreover, overexpression of Vps37a in livers of lean and obese mice suggests a novel strategy to lower blood glucose levels.

Enhanced gluconeogenic gene expression and HGP upon Vps37a KD are dependent on Gcgr, as $Gcgr^{liver\text{-}KO}$ mice or mice pretreated with Gcgr antagonists lack these phenotypes despite Vps37a ablation (Sekar et al., 2022). Importantly, like other transmembrane receptors (Seifert & Wenzel-Seifert, 2002), Gcgr undergoes constant endocytosis, also without ligands. This internalization at basal state is already sufficient to contribute to increased activation of cAMP/PKA/p-Creb and gluconeogenic gene expression. Moreover, gluconeogenesis from glycerol and pyruvate is increased upon hepatic Vps37a KD, and in obese HFD-fed mice, Vps37a KD exacerbates hyperglycemia (Sekar et al., 2022). Importantly, these effects are due to an accumulation of Gcgr at endosomal membranes. ESCRT-I, however, is not involved in receptor internalization but instead in sorting of internalized cargo from MVBs (Henne et al., 2011). In fact, blocking endocytosis by dynasore treatment inhibits the excessive gluconeogenic signaling of Gcgr at endosomes (Cajulao et al., 2022). Strikingly, enhanced signaling activity of Gcgr at endosomes is limited to gluconeogenic $G_{\alpha s}$ signaling, without altering $G_{\alpha q}$-mediated lipid utilization and storage (Sekar et al., 2022). These findings indicate distinct G protein recruitment to Gcgr at endosomes and plasma membrane. In fact, endosomal $G_{\alpha s}$ recruitment has already been shown for other GPCRs (Calebiro et al., 2009; Ferrandon et al., 2009), whereas $G_{\alpha q}$ has thus far not been shown to occur at endosomes (Sutkeviciute & Vilardaga, 2020). Therefore, differential G protein recruitment to Gcgr upon Vps37a depletion fosters selective signaling to gluconeogenesis, without altering lipid usage. As Gcgr antagonist treatment to ameliorate hyperglycemia in T2D was thus far challenging due to concomitant effects on lipid metabolism causing fatty liver (Janah et al., 2019), uncoupling of Gcgr signaling arms hence poses interesting therapeutic potential.

Given the disadvantageous hyperglycemic effects of Vps37a ablation in HFD-fed mice, it was interesting whether increasing Vps37a levels by AAV-mediated overexpression (OE) could reverse these effects, potentially leading to reduced blood glucose levels. Excitingly, overexpression of hepatic Vps37a in lean mice was indeed able to reduce blood glucose by lowering cAMP, PKA activity, and Creb phosphorylation. Moreover, also in diabetic *db/db* mice, Vps37a OE revealed similar changes and a non-significant trend to reduce blood glucose. Importantly, similar to the effects of Vps37a KD, overexpression affected only carbohydrate

metabolism and did not change liver triglyceride content (Sekar et al., 2022). Previously published experiments aiming to overexpress ESCRT-I subunit Tsg101, however, revealed a strong intrinsic counterregulation that prevent an increase of total Tsg101 protein (Hong Feng et al., 2000). Likewise, overexpressing Vps37a protein succeeded only at times, despite elevated mRNA levels. This indicates a strong counterregulation also for Vps37a expression and points to a tight control of ESCRT-I protein abundancy. In fact, a ~ 60 % increase of Vps37a protein was required, both in lean and obese mice, to elicit a concomitant increase of ESCRT-I proteins. This collective increase was required to lower cAMP, reduce PKA substrate and Creb phosphorylation, and ultimately to reduce blood glucose. Together, Vps37a overexpression and KD data reveal an uncoupling of Gcgr signaling arms *via* Vps37a and prevents a potential new strategy for Gcgr-antagonism in T2D.

During T2D, in addition to IR with increased but insufficient insulin secretion (Petersen & Shulman, 2018), hyperglucagonemia was suggested to be a contributing factor for hyperglycemia (Færch et al., 2016; Raskin & Unger, 1978). However, the exact mechanisms underlying the regulation of Gcgr levels in metabolically diseased liver were yet unknown. Interestingly, the current work found Gcgr protein to be increased upon steatosis, both in human and murine primary hepatocytes. Together with decreased expression of Vps37a under these conditions in patients with T2D and NASH, this suggests a counterregulatory increase of Gcgr to complement for altered trafficking modalities when Vps37a is reduced. In line, Vps37a KD revealed increased expression of *Gcgr* mRNA, further strengthening this notion.

ESCRT-I subunit Tsg101 was shown to be crucial for ESCRT-I stability, as upon Tsg101 depletion, the complex disassembles with degradation of its components (Kolmus et al., 2021). Hepatic Vps37a KD, however, did not result in complex degradation, yet elicited changes in the expression of other Vps37 isoforms (shown in Sekar et al., 2022). Despite these alterations suggesting substituting functions of different Vps37 isoforms, the effects on Creb activation are specific to Vps37a. Thus, it remains elusive what functions are mediated by Vps37b-d in particular, and whether distinct ESCRT-I compositions could contribute to tissue-specific functions, as suggested previously (Henne et al., 2011).

Sorting of internalized transmembrane receptors through ESCRTs is dependent on the ubiquitination status of these cargos (Szymanska et al., 2018). Whether GCGR is in fact ubiquitinated upon agonist binding, however, has thus far not been shown. Accordingly, I performed co-staining experiments of GCGR and ubiquitin to delineate these internalization details for a thorough understanding of VPS37A-mediated GCGR trafficking. Importantly, colocalization of GCGR with ubiquitin indeed increased upon glucagon treatment. This data, however, allows no conclusion yet as to whether the ubiquitination signal is directly attached to GCGR or to an adaptor as shown for other GPCRs (Shenoy et al., 2001, 2007), or whether the ubiquitin-signal is involved in Vps37a-Gcgr interaction.

Combined, these data highlight a novel and specific role for Vps37a in Gcgr trafficking. ESCRT-I mediated sorting of Gcgr towards degradation *via* Vps37a is required for signal termination. Precisely, Vps37a depletion shifts Gcgr localization to endosomes, where it signals exclusively to gluconeogenesis. Redirecting Gcgr back to the plasma membrane reestablishes signaling to lipid usage (shown in Sekar et al., 2022), thus strengthening the connection of endosomal localization with the uncoupling of Gcgr signaling arms. Ultimately, these results show that altering Gcgr trafficking allows distinct signaling activation with effects on whole-body physiology.

3.4 SUMMARY AND OUTLOOK

The present work aimed at studying endosomal trafficking complexes in the regulation of metabolism. Based on published data and preliminary work, three trafficking complex members were selected. Ap4e1, a subunit of the Ap-4 complex, has thus far mainly been studied in relation to a severe neurological disease caused by Ap-4 dysfunction. This work, however, expands the functional landscape associated of Ap4e1 to the development of fibrosis in NAFLD/NASH. Identifying novel cargos of Ap-4 in the liver will be of particular interest, as these cargos are potential mediators of disease progression. Furthermore, whether the observed effects are specific to Ap4e1 or facilitated by the whole Ap-4 complex needs to be addressed. Vps33b, member of the dimeric CHEVI complex, has until now also not been studied in a metabolic context. Importantly, however, Vps33b was found here to be an important regulator of liver metabolism with diverse metabolic alterations upon KD in liver. Further mechanistic studies will help to identify the initial and acute consequences of Vps33b loss and how these changes translate into altered whole-body physiology. Lastly, Vps37a-mediated Gcgr trafficking sets a prominent example of how alterations in the endosomal trafficking system can modify metabolism by changing the spatial distribution of a single signaling receptor. Whether Vps37a function is indeed limited to Gcgr or whether similar mechanisms exist with different receptors, maybe in different tissues, requires further studies. Importantly, follow-up studies on all three examined proteins must include experiments using female mice in search for gender-specific differences in the phenotypes described here. This will be especially important when aiming for potential therapeutic aspects of these targets, as new drugs should ideally have similar functions in both, women and men.

Conclusively, novel metabolic functions for Ap4e1, Vps33b, and Vps37a were identified here, thus expanding the current knowledge on the function of the endosomal system in health and disease (**Figure 25**). In addition, this work provides a basis for further functional characterizations of endosomal trafficking complexes in hepatic metabolism.

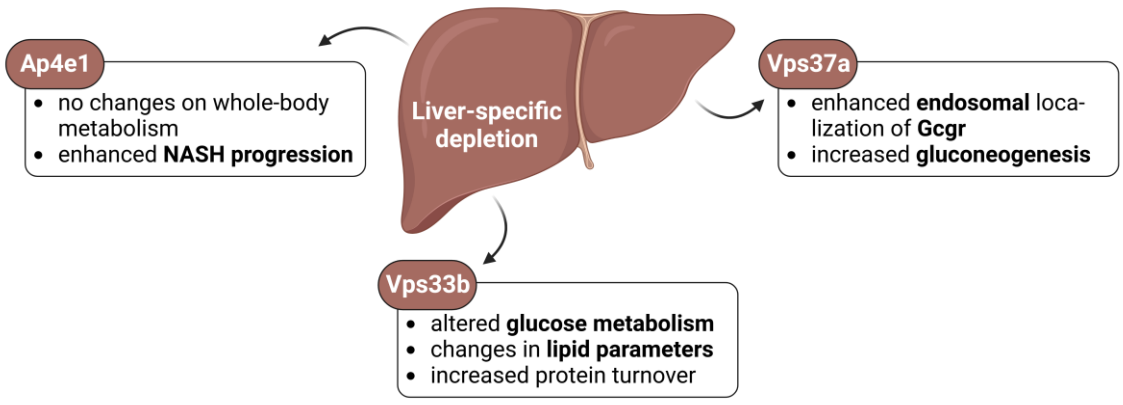

Figure 25 – Summary of the main observations of Ap4e1-, Vps33b-, or Vps37a-ablation in livers of mice.

4 MATERIALS AND METHODS

4.1 MATERIALS

Reagent or resource	Source	Identifier
Antibodies		
Vps37a 1:1000 (WB)	Atlas Antibodies	Cat# HPA024705
Ap4e1 1:500 (WB)	BD Transduction Labs	Cat# 612019
Gcgr 1:500 (IF)	Abcam	Cat# ab75240
Fk2-ubiquitin 1:250 (IF)	Enzo	Cat# ENZ-ABS840-0100
Ldlr 1:200 (IF)	Sigma Aldrich	Cat# SAB3500286
Ccdc93 1:200 (IF)	Proteintech	Cat# 16810445
Alexa 555 goat anti-rabbit	Thermo Fisher Scientific	Cat# A-21429
Alexa 647 goat anti-rabbit	Thermo Fisher Scientific	Cat# A-21244
Alexa 555 goat anti-rat	Thermo Fisher Scientific	Cat# A-21434
Alexa 647 goat anti-rat	Thermo Fisher Scientific	Cat# A-21247
Alexa 555 goat anti-chicken	Thermo Fisher Scientific	Cat# A-21437
Alexa 488 phalloidin	Thermo Fisher Scientific	Cat# A12379
Goat anti-rabbit HRP	Sigma Aldrich	Cat# A6154
Rabbit anti-mouse HRP	Thermo Fisher Scientific	Cat# 61-6520
p-AMPKα 1:1,000 (WB)	Cell Signaling s	Cat# 2535
AMPKα 1:1,000 (WB)	Cell Signaling	Cat# 2603
p-Creb 1:1,000 (WB)	Cell Signaling	Cat# 9198
Creb 1:1,000 (WB)	Cell Signaling	Cat# 9197

Vps33b 1:1,000 (WB)	Proteintech	Cat# 12195-AP
CAMKII-α 1:1,000 (WB)	Cell Signaling	Cat# 50049
p-CAMKII-α/β 1:1,000 (WB)	Novus biologicals	Cat# NB300184
Akt 1:1,000 (WB)	Cell Signaling	Cat# 9272
p-Akt 1:1,000 (WB)	Cell Signaling	Cat# 4060
Lamp1 1:1,000 (WB)	Cell Signaling	Cat# 3243S
Asgr1 1:1,000 (WB), 1:200 (IF)	Atlas Antibodies	Cat# HPA011954
Vps37b 1:1,000 (WB)	Sigma Aldrich	Cat# HPA038217
Vps37c 1:1,00 (WB)	Abcam	Cat# ab151753
Vps28 1:1,000 (WB)	Abcam	Cat# ab167172
Tsg101 1:1,000 (WB)	Abcam	Cat# ab30871
p-p70 S6K 1:1,000 (WB)	Cell Signaling	Cat# 9234S
p70 S6K 1:1,000 (WB)	Cell Signaling	Cat# 34475S
p-rpS6 1:1,000 (WB)	Cell Signaling	Cat# 4856
p-PKA substrate 1:1,000 (WB)	Cell Signaling	Cat# 5054S
E-Cadherin 1:5,000 (WB)	Proteintech	Cat# 20874-1-AP
Vinculin 1:10,000 (WB)	Abcam	Cat# ab129002
VCP 1:10,000 (WB)	Abcam	Cat# ab11433

Bacterial and virus strains		
AAV8-LP1-Cremut	Jimena et al., 2021	N/A
AAV8-LP1-CreWT	Jimena et al., 2021	N/A
AAV8-LP1-GFPmut	Bühler et al., 2021	N/A
AAV8-LP1-mVps37a	Sekar et al., 2022	N/A
Biological samples		
Cryopreserved primary human hepatocytes	Lonza	N/A
Chemicals, peptides, and recombinant proteins		
Amersham ECL Prime	Cytiva	Cat# RPN2232
Collagenase	Sigma Aldrich	Cat# C5138-1G
cOmplete EDTA-free Protease Inhibitor Cocktail	Roche	Cat# 11836170001
Cy-5-Glucagon	Sekar et al., 2022	N/A
DAPI	Life Technologies	Cat# D3571
dexamethasone	Sigma Aldrich	Cat# D4902
Glucagon	Millipore	Cat# 05-23-2700
Huminsulin®Normal 100	Lilly	Cat# HI0210
Interferin	Polyplus	Cat# 40950
LysoTracker™	Thermo Fisher Scientific	Cat# L7528
MOWIOL 4-88 reagent	Merck Millipore	Cat# 475904
penicillin-streptomycin	Sigma Aldrich	Cat# P4333
Phosphostop-phosphatase inhibitor tablets	Roche	Cat# 4906845001
Rat tail Collagen I	Sigma Aldrich	Cat# 11179179001
Sera Plus (Special Processed FBS)	PAN-Biotech	Cat# P30-3702
Sodium pyruvate	Sigma Aldrich	Cat# P2580
TRIzol	Life Technologies	Cat# 15596018
William’s Medium E	PAN-Biotech	Cat# P04-29500

Critical commercial assays		
ALT activity assay kit	Sigma Aldrich	Cat# MAK052
Amplex Red Cholesterol Assay Kit	Thermo Fisher Scientific	Cat# A12216
AST activity assay kit	Sigma Aldrich	Cat# MAK055
ATP assay kit	Sigma Aldrich	Cat# MAK190
Bio-Rad Protein Assay Kit II	Bio-Rad	Cat# 5000002
Glycogen kit	Sigma Aldrich	Cat# MAK016
Insulin Elisa kit	CrystalChem	Cat# 90080
L-Amino acid kit	Sigma Aldrich	Cat# MAK002
QuantiTect Reverse Transcription Kit	Qiagen	Cat# 205311
Triglyceride assay kit	Abcam	Cat# ab65336
Experimental models: Organisms/strains		
BKS(D)-Leprdb/JOrlRj (heterozygous)	Janvier	N/A
BKS(D)-Leprdb/JOrlRj (homozygous)	Janvier	N/A
C57BL/6N	Janvier	N/A
C57BL/6N-Ap4e1$^{tm1c(KOMP)Wtsi}$/H	EUCOMM	EM:09035
Oligonucleotides		
Non-targeting control	Dharmacon	Cat# D-001810-10
Primer sequence for qRT-PCR	N/A	**Table 2**
siRNA luciferase: sense 5′-cuuAcGcuGAGuAcuucGAdTsdT-3′, antisense 5′-UCGAAGuACUcAGCGuAAGdTsdT-3′.	Sekar et al., 2022; Seitz et al., 2019 (Axolabs)	N/A
siRNA targeting Vps33b in LNP: sense 5'-cccuuuGGAucGAauuGcAdTsdT-3' antisense 5'-UGcAAUUCGAUCcAAAGGGdTsdT-3'	This study (Axolabs)	N/A

siRNA targeting Vps37a in LNP: sense 5´-cguAcAGAuuAGAauGAcAdTsdT-3' antisense 5´-UGUcAUUCuAAUCUGuACGdTsdT-3'	Sekar et al., 2022 (Axolabs)	N/A
Tsg101 siRNA	Dharmacon	Cat# L-049922-01
Ubap1 siRNA	Dharmacon	Cat# L-047375-01
Vps28 siRNA	Dharmacon	Cat# L-045159-01
Vps33b siRNA	Dharmacon	Cat# L-057494-01
Vps37b siRNA	Dharmacon	Cat# L-057449-01
Vps37c siRNA	Dharmacon	Cat# L-063041-01
Recombinant DNA		
Plasmid: pdsAAV2-LP1-Cremut	Jimena et al., 2022	N/A
Plasmid: pdsAAV2-LP1-CreWT	Jimena et al., 2022	N/A
Plasmid: pdsAAV2-LP1-GFPmut	Bühler et al., 2021	N/A
Plasmid: pdsAAV2-LP1-mVps37a	Sekar et al., 2022	N/A
Software		
Graphpad Prism 9	GraphPad Software	https://www.graphpad.com
ImageJ (Fiji)	ImageJ, v. 1.54b	https://imagej.net/software/fiji/
Perseus v1.6.15.0	Tyanova et al., 2016	https://maxquant.net/perseus/
Other		
Power SYBR Green PCR Master Mix	Thermo Fisher Scientific	Cat# 4367659
MicroAmp® Optical 384-well Reaction Plate	Applied Biosystems	N/A
MicroAmp® Optical Adhesive Film	Applied Biosystems	N/A
Nitrocellulose Membrane	Amersham	N/A
Novex™ Tris-Glycine Mini Gel	Invitrogen	N/A
Parafilm	Pechinery Inc.	N/A

Gloves (Safe Skin Purple Nitrile)	Kimberly Clark	N/A
Glucometer Test strips Accu Check Inform II	Roche	N/A
Embedding cassette	Carl Roth	N/A
NORM-JECT-F Luer Solo 1 ml Syringe	B. Braun Melsungen AG	Cat# NJ-9166017
Microvette CB 300 LH	Sarstedt AG & Co. KG	Cat# 16.443
60x Immersion oil ne = 1.518	Olympus	Cat# IMMOIL-F30CC
40x Immersion oil ne = 1.406	Olympus	Cat# SIL300CS-30CC
Bond-Breaker TCEP Solution	Thermo Fisher Scientific	Cat# 77720
SuperSignal West Pico PLUS Chemiluminescent Substrate	Thermo Fisher Scientific	Cat# 34580
SuperSignal West Femto Maximum Sensitivity Substrate	Thermo Fisher Scientific	Cat# 34096
High Fat Diet 60%	Research Diets, Inc.	Cat# D12492i
Methionine-choline deficient diet (MCD)	Research Diets, Inc.	Cat# A06071302
LFD	Research Diets, Inc.	Cat# A06071314
Fructose-palmitate rich diet (FPC)	Research Diets, Inc.	Cat# D17020104i
Standard chow diet	Altromin	Cat# 1314
Serological pipettes (5, 10, 25, 50 ml)	Grainer Bio-One	N/A
Trans-Blot Turbo RTA Midi 0.2 µm Nitrocellulose Transfer Kit	Bio-Rad	Cat# 1704271
Insulin Syringe Volume: 0.3 mm (30G) x 8 mm. Micro-Fine permanently attached needle	BD (Fisher)	Cat# 324826
Sterican needles 0.4 mm (27G) x 20 mm	B. Braun Melsungen AG	Cat# 4657705
Safe-Lock Tubes (0.5, 1.5, 2.0, 5.0 ml)	Eppendorf	N/A
CombiTips Advanced (0.1, 0.5, 2.5, 5, 10 ml)	Eppendorf	N/A
Micro tube 1.1 ml Z-Gel	Sarstedt AG & Co. KG	Cat# 41.1378.005

Sterile filter (0.22 µM)	Sartorius	N/A
Conical Centrifugal Tubes (15, 50 ml)	Falcon	N/A
Novex WedgeWell 8–16% Tris-Glycine Mini Gels	Thermo Fisher Scientific	Cat# XP08165BOX
Instruments		
Analytical scales	Sartorius	N/A
Bioruptor Sonication device	Diagenode	N/A
ChemiDoc Imaging System	Bio Rad	N/A
Eppendorf Concentrator Plus (Vacuum dryer)	Eppendorf	N/A
Freezer, -20°C	Liebherr	N/A
Freezer, -80°C	Thermo Fisher Scientific	N/A
Fridge, 4°C	Liebherr	N/A
Glucometer Accu-Check Performa	Roche	N/A
Heat Block (Thermostat Plus), ThermoMixer	Eppendorf	N/A
Microplate Shaker	VWR International	N/A
Multipipette E3	Eppendorf	N/A
NanoDrop 2000 spectrophotometer	Thermo Fisher Scientific	N/A
pH-meter	VWR International	N/A
Pipettes (10, 20, 100, 200, 1000 µl)	Eppendorf	N/A
QuantStudio 6/7 Flex-Real-Time PCR System	Applied Biosystems	N/A
Table Centrifuge	Thermo Fisher Scientific	N/A
Table Centrifuge 5702 R	Eppendorf	N/A
Trans-Blot Turbo Blotting System	Bio Rad	N/A
Varioskan LUX multimode microplate reader	Thermo Fisher Scientific	N/A
Vortex Genie-2	Scientific Industries Inc.	N/A
Water bath	Neolab	N/A

4.2 METHODS

4.2.1 ANIMALS

All animal experiments were approved by local authorities and conducted in accordance with the institutional animal welfare officer (Government of upper Bavaria (ROB): ROB-55.2-2532.Vet_02-17-49; ROB-55.2-2532.Vet_02-21-66; ROB-55.2-2532.Vet_03-15-40). Standard mouse house conditions were applied with 12 h dark-light cycle at 22 °C. Mice were fed *ad libitum* with regular rodent chow diet unless indicated otherwise. For Ap4e1 liver KO experiments, Ap4e1$^{fl/fl}$ (C57BL/6N-Ap4e1$^{tm1c(KOMP)Wtsi}$/H) mice were bred in house. Vps33b KD and Vps37a OE experiments were performed in C57BL/6N wildtype mice obtained from Janvier Laboratories. All animal experiments were carried out in male mice with littermates as controls. Instead of sample size predetermination, group sizes were based on recently published work with similar readouts. Mice were randomly assigned to groups based on initial bodyweight.

Upon experiment termination, mice were 6 h fasted and sacrificed by cervical dislocation and decapitated. Blood serum was collected, and tissues were dissected, snap-frozen in liquid nitrogen, and stored at -70 to -80 °C.

4.2.2 *IN VIVO* INJECTIONS AND MOUSE DIETS

Knockout (KO) of Ap4e1 in livers of Ap4e1$^{fl/fl}$ mice was achieved by injection with rAAV8-LP1-Cre^{WT} for liver-specific expression of Cre-recombinase (2x10^{11} GC/mouse). As control, rAAV8-LP1-Cre^{mut} was injected, coding for a non-functional version of Cre. Both constructs were used previously (Jimena et al., 2022). AAV packaging was performed by Vigene Biosciences. Chow-fed Ap4e1$^{fl/fl}$ mice were injected AAVs at 10 weeks of age. Mice were maintained on chow diet for 6 weeks and then subjected to 60 % HFD feeding for 14 weeks before sacrifice and organ withdrawal. Mice that were fed MCD diet were injected AAVs at 10 weeks and fed either MCD (methionine-choline deficient diet) or control LFD (low-fat diet) starting from 13 weeks of age for 5 weeks until sacrifice. For FPC (fructose-palmitate-cholesterol rich diet) feeding (Xiaobo Wang et al., 2016), FPC diet was started at 5 weeks of age and mice were injected AAVs at 9 weeks of age. FPC was continued for another 12 weeks until sacrifice. Mice in FPC group received drinking water supplemented with 42 g/L glucose (55 %) and fructose (45 %, w/v) (Loft et al., 2021).

Liver Vps33b KDs were performed by injection of 1 mg/kg siRNA-containing LNP via tailvein injection, as described previously (Seitz et al., 2019; Sekar et al., 2022; Zeigerer et al., 2012, 2015). Injections were repeated once per week.

Construct generation and injections for the overexpression of Vps37a in livers was performed exactly as detailed in Sekar et al., 2022.

4.2.3 TOLERANCE TESTS *IN VIVO* AND FASTING-REFEEDING

For glucose and insulin tolerance tests, mice were fasted for 6 h during the light cycle and 2 g/kg bodyweight glucose or 1 IU/kg insulin were injected intraperitoneally (i.p.). For pyruvate tolerance tests, mice were fasted 16 h mainly during the dark cycle and injected i.p. with 2 g/kg sodium pyruvate. Blood glucose levels were measured before i.p. injection (0 min) and at 15, 30, 45, 60, 90, and 120 min.

Alterations in fasting-refeeding were assessed by fasting mice over night for 16 hours to measure fasting blood glucose. Then, mice were given food for 2 hours and blood glucose was measured again. Food intake and body weight alterations were measured.

4.2.4 BLOOD PARAMETER ANALYSIS

For the determination of serum cholesterol, ALP, AST, and AST levels, full blood was collected into gel-coated microcentrifugation tubes during organ withdrawal and centrifuged at 4 °C and 10,000 g for 5 min. Cholesterol species were measured as free cholesterol and separately as cholesterol content from HDL and LDL particles. To measure the latter two, commercially available kits (Beckmann Coulter OSR6187 & OSR6183) were used. Here, distinct detergents allow for the sequential release and enzymatic removal of cholesterol either from within non-HDL or non-LDL particles. Cholesterol released in a subsequent step originates then from the remaining HDL or LDL particles, respectively. Finally, using the cholesterol esterase/oxidase system coupled with a fluorochrome-generating peroxidase, the cholesterol released from either HDL or LDL particles was detected photometrically. Serum parameters were assessed using the Beckman Coulter AU480 Chemistry Analyzer.

To determine plasma levels of AST and ALT in chow-, LFD-, MCD- and FPC-fed mice, plasma was collected from living animals through the tailvein into heparin-coated tubes. Plasma was obtained by centrifugation at 2000 g, 4 °C, 5 min. Parameters were measured using corresponding commercial activity assays (Sigma Aldrich).

For plasma insulin levels during ipGTT, blood plasma was collected right before and 15 min after glucose administration as described above. Plasma insulin was measured using a commercial enzyme-linked immunosorbent assay (ELISA) kit (Crystal Chem).

4.2.5 TISSUE METABOLITE MEASUREMENTS

Liver ATP, L-amino acid, and glycogen content was determined using corresponding commercially available assay kits from Sigma Aldrich on snap-frozen tissue pieces. Liver triglycerides were measured using commercial kits from abcam. Assays were performed according to manufacturer instructions.

4.2.6 HEPATOCYTE ISOLATION AND SIRNA TRANSFECTION

Primary hepatocytes were isolated from 8-12-weeks old male C57BL/6N mice by collagenase perfusion (Zellmer et al., 2010). After anesthesia by i.p. injection of ketamine/xylazine, the liver was perfused through the *vena cava* with EGTA-buffer for 5-10 min, followed by collagenase buffer perfusion for 10-15 min. Once digestion was visible, the liver was removed, hepatocytes were gently washed out in suspension buffer, and filtered through a 100 nm pore mesh. Cells were washed twice by centrifuging 5 min at 50 g (4 °C) and resuspended in suspension buffer.

Primary hepatocytes were seeded in collagen-coated 24-well plates at 200,000 cells/well in William's Medium E with 10 % fetal calf serum (FCS), 5 % penicillin-streptomycin and 100 nM dexamethasone in a 37 °C incubator with 5 % CO_2. After 1 h of attachment, cells were washed once with room temperature PBS and incubated with siRNA-containing OptiMEM/William's E Medium mixture with 1.2 µl/well interferin. siRNA was used at 60 nM (Vps33b) or 40 nM (Vps37b, Vps37c, Vps28, Tsg101, Ubap1). After 5-6 h, primary hepatocytes were covered with a second layer of Rat Tail Collagen I and cells were maintained with medium changes after 1 and 3 days (William's Medium E, 10 % FCS, 5 % P/S, no dexamethasone) (Zeigerer et al., 2017).

Where indicated, primary hepatocytes of 9 weeks old mice after 3 weeks LNP-induced Vps33b liver KD were isolated as described above and cultured on collagen-coated plates, without any additional siRNA transfection and without second collagen layer. Human cryopreserved primary hepatocytes were obtained from Lonza Group Ltd. and cultured as described for murine cells.

Primary murine and human hepatocytes in sandwich culture were, where specified, treated with bovine serum albumin (BSA)-conjugated 100 µM palmitate and 500 µM oleate for 3 days after seeding to induce steatosis *in vitro* (Sekar et al., 2022).

4.2.7 PRIMARY HEPATOCYTE STIMULATIONS

All assays were performed 3 days after RNAi. To measure cholesterol secretion *in vitro*, medium was changed to serum- and dexamethasone-free William's Medium E and

supernatant was collected after 5 hours. Cholesterol was measured using an Amplex Red Cholesterol Assay Kit (Invitrogen) and cholesterol amounts were normalized to protein content, measured by DC Protein Assay Kit (Bio-Rad).

Insulin stimulations were performed by treating hepatocytes with 100 nM insulin for 10 min after 2 hours serum-starvation in William's Medium E. Cells were lysed in RIPA and subjected to immunoblotting for detection of Akt phosphorylation, as detailed below.

To detect Ampk activation, hepatocytes were treated with 200 µM AICAR for 1 hour in serum-free William's Medium E. Cells were lysed in RIPA and subjected to immunoblotting.

Glucagon stimulations were performed using 100 nM glucagon. For immunoblotting of p-Creb, hepatocytes were treated for 15 min after 2 h serum-starvation. For gene expression analysis, cells were treated with glucagon for 5 h without prior starvation.

4.2.8 IMMUNOBLOTTING AND QUANTIFICATION

For the detection of protein levels in primary hepatocytes and snap-frozen liver pieces, proteins were isolated using modified RIPA (25 mM Tris-HCl (pH 7.6), 150 mM NaCl, 1 % NP-40, 0.5 % SDC, 0.1 % SDS, 0.5 mM EDTA) or stronger lysis buffer (25 mM Tris-HCl (pH 7.6), 150 mM NaCl. 1 % NP-40, 1 % SDS, 0.1 % Triton X-100, 0.5 mM EDTA, 5 mM $MgCl_2$, 1 mM $CaCl_2$) for the isolation of Creb and Ampk protein, supplemented with PhosStop and cOmplete protease inhibitor. Tissue was minced on ice using pistols. Proteins were extracted by centrifugation at 10,000 g for 5 min at 4 °C and protein concentration was determined using DC Protein Assay Kit. Protein lysates were complemented with Laemmlli buffer and 20-40 µg protein were subjected to SDS-Page on 8-16 % or 4-12 % Tris-Glycine gels. Separated proteins were blotted to nitrocellulose membranes (i.e. western blotting) by semi-dry transfer and detected by chemiluminescence with horseradish peroxidase (HRP)-conjugated secondary antibodies (1:10,000 dilution). Primary antibody staining was performed at 4 °C overnight after 1 h blocking in 5 % milk in 0.1 % tween-supplemented tris-buffered saline (TBST) at room temperature. Secondary antibodies were added for 1 h at room temperature after 3x7 min TBST washing. Western blot images presented in this work are representative of repeated experiments.

4.2.9 QRT-PCR USING SYBR GREEN

Human or mouse tissue was lysed in TriZol using a bead homogenizer and RNA was isolated by phenol-chloroform extraction. Human mRNA expression levels were measured in tissues

obtained from cohorts of patients with NAFLD and NASH and obesity and T2D published previously (Koliaki et al., 2015; Sekar et al., 2022). RNA purity and amount was assessed by NanoDrop and 1 µg RNA were subjected to cDNA generation using QuantiTect RT Kit (Qiagen). mRNA expression levels were determined in a 10 µl reaction containing 5 µl SYBR Green, 200 nM primers (**Table 2**). Cycling conditions using QuantStudio 6 or 7 were set to 50 °C (2 min), 95 °C (10 min) and 40 cycles of 95 °C (15 s) and 60 °C (1 min). Gene expression was quantified using $2^{-\Delta\Delta Ct}$ and presented relative to the corresponding average control.

Table 2 – qPCR primers used in this study.
Human transcripts are indicated by "*h*", murine transcripts by "*m*". Primer sequences for transcript names marked with an asterisk were obtained from Harward Primer Bank (Xiaowei Wang & Seed, 2003). All others were generated using NCBI primer-BLAST (Ye et al., 2012).

Transcript name	Forward primer (5'-3')	Reverse primer (5'-3')
h_AP4E1	ATAGTGGAGAAGACGCTGACGG	TCTTCTTCGTGCTTGGAGGTG
m_Ap4e1	TCATCCAAGCACGAAGAAGAGAAA	GCATCGTATCCAAGCATCTCACA
m_Ap4m1	GTTTCTTAAAGCGCCAGCCTC	GGAAATCATGGCGGTTCTGG
m_Ap4b1	CTGTGCTAGGCTCCCACATC	CACGGGACAGTTTCCACAGA
m_Ap4s1	AGGCAAAGACGCTCATCCC	CTAGGCACTGAGTTTGCGCT
m_Vps33b	TTGTCCATCACTGAGAATGGTTT	TCCGCAGGTTGGAGAAGGTTAG
*m_Pik3r1**	ACACCACGGTTTGGACTATGG	GGCTACAGTAGTGGGCTTGG
*m_Acacb**	CGCTCACCAACAGTAAGGTGG	GCTTGGCAGGGAGTTCCTC
*m_Mapk3**	TCCGCCATGAGAATGTTATAGGC	GGTGGTGTTGATAAGCAGATTGG
*m_Mapk9**	CAGACTGTACCCTCAAGATCCT	ATGCACCCGACAGACCAGA
m_Foxo1	TTCAATTCGCCACAATCTGTCC	GGGTGATTTTCCGCTCTTGC
m_Insr	ATGAGAGGTGCAGTGTGGCT	AGTCACAGGGCCAACGATGT
m_Fasn	CTTCCGAGATTCCATCCTACGC	TGGCAGTCAGGCTCACAAACG
*m_Apoc3**	TACAGGGCTACATGGAACAAGC	CAGGGATCTGAAGTGATTGTCC
*m_Abcb11**	TCTGACTCAGTGATTCTTCGCA	CCCATAAACATCAGCCAGTTGT
*m_Apoh**	TGCCATGTTGCTATTGCAGGA	GGCTTGCAGGAGTAGACAATCT
h_VPS37A	ACTCACACTCCAGTATAGCCGA	TGAGGAAACTGTGGAGGAAGCA
h_RPLP0	TGCTGATGGGCAAGAACACC	CGGATATGAGGCAGCAGTTTCTC
h_TBP	ACGCCAGCTTCGGAGAGTTC	CAAACCGCTTGGGATTATATTCG

h_GAPDH	TGGCAAATTCCATGGCACCG	ATCTCGCTCCTGGAAGATGGTG
m_G6pc	TCGGAGACTGGTTCAACCTC	AGGTGACAGGGAACTGCTTTAT
m_Pck1	ATGTGTGGGCGATGACATT	AACCCGTTTTCTGGGTTGAT
m_Gcgr	ATTGGCGATGACCTCAGTGTGA	GCAATAGTTGGCTATGATGCCG
m_Tsg101	GCAGCCACAGGCATATTGGA	AATGATGGCAGTTCCAGGGAG
m_Vps28	TTTGCCGTGGTGSSGSCGATG	CAGGCTGCAGTGTACTCATTGG
m_Vps37b	GAGGACACTGAGAACATGGCAGA	CAGCTTCCGCTTGCTCTGGT
m_Vps37c	GAGGTGCCGTTGGAAACGTT	GGCGCTTTGGAGGGACATCT
m_Ubap1	AGAGGTGCCAACACTGACATCC	GTTGGGCACTTGTGACACTGAG
m_Gapdh	CACTGAGCATCTCCCTCACA	GTGGGTGCAGCGAACTTTAT
m_Rplp0	AGATTCGGGATATGCTGTTGGC	TCGGGTCCTAGACCAGTGTTC
m_Hprt	TGTATACCTAATCATTATGCCG	GACATCTCGAGCAAGTCTTT

4.2.10 Immunofluorescence and confocal microscopy

Primary hepatocytes in collagen sandwich on collagen coated glass coverslips were stained for Ldlr and Ccdc93 three days after Vps33b RNAi. Hepatocytes were washed once with cold PBS and fixed in 4 % PFA for 30 min at room temperature. Cells were permeabilized with 0.1 % Triton X-100 in PBS and blocked for 2 h in 10 % horse serum at room temperature. Primary antibodies were added in 5 % horse serum overnight at room temperature while shaking and washed the whole day by repeated replacement with TNT buffer (10 mM Tris-HCl (pH 8.0), 300 mM NaCl, 0.1 % tween). Secondary antibody (1:1,000) and phalloidin staining (1:700) was performed overnight, gently shaking at 4 °C. Cells were washed again with TNT for 8-16 hours and incubated with 4,6-diamidino-2-phenylindole (DAPI) for 5 min, before mounting on glass slides with MOWIOL 4-88 (0.1 g/ml).

To label Ldlr surface levels, primary hepatocytes were 2 h serum-starved and washed with cold phosphate-buffered saline (PBS) three days after RNAi. Diluted in cold William's Medium E without FCS, fluorescently labeled DiI-LDL was given to the cells in the dark on ice for 2 h. Cells were fixed on ice for 30 min in 4 % PFA and washed twice in cold PBS. DAPI nuclear staining and mounting was performed as described above. Surface labeling of Gcgr in steatotic primary hepatocytes using Cy5-Gcg was performed even-handedly with 200 nM of Cy5-Gcg (Sekar et al., 2022).

For Asgr1 stainings of livers sections, whole livers of Vps33b KD and control mice were fixed by paraformaldehyde (PFA) perfusion. Therefore, mice were anesthetized by i.p. injection of ketamine/xylazine mice after 3 weeks of repeated LNP injections. The abdominal walls and chest cavity were opened to expose liver and heart, respectively. By inserting a needle into the right ventricle, the liver was flushed with PBS for 5 min, followed by 7-10 min perfusion with 4 % PFA in PBS until the liver became obviously fixed (i.e. hard). The right ventricle was cut to allow excess liquid drainage. The liver was removed and dissected, stored in PFA overnight, and transferred to 30 % sucrose in PBS for 72 h. Liver pieces were embedded in optimal cutting temperature (OCT) oil and sectioned to 6 µm thick slices using a Cryostat. Slides were treated with 0.1 % glycine in PBS for 5 min and permeabilized with 0.1 % Triton X-100 in PBS for 10 min. Blocking was performed at room temperature for 15 min with 3 % BSA in PBS and primary antibodies were added at room temperature in 3 % BSA for 2 h. After washing 3 times 5 min with 0.1 % Triton X-100, secondary antibodies were added at room temperature in 3 % BSA for 45 min. Slides were washed again and coverslips were mounted with MOWIOL 4-88 (0.1 g/ml) onto the slide.

LysoTracker lysosomal labeling was performed with primary hepatocytes in monolayer (no second layer of collagen). Cells were either isolated from control and Vps33b KD mice after 3 weeks of LNP injection, or from wildtype mice. In case of the latter, Vps33b KD was achieved by RNAi. Cells from *in vivo* KD were stained one day after seeding, cells with *in vitro* KD 48 h after RNAi. Staining was performed by treating cells with 500 nM LysoTracker for 30 min at 37 °C, 5 % CO_2 in William's Medium E without FCS. Cells were washed with cold PBS and fixed in 4 % PFA 15 min on ice, followed by 15 min at room temperature. Nuclei were stained with DAPI and coverslips were mounted as described above.

4.2.11 Confocal microscopy and analysis

Immunofluorescently labeled samples were imaged with a laser-scanning confocal microscope (Olympus FluoView 1200; Olympus Corporation), equipped with an Olympus UPlanSAPO 60x 1.35 and 40x 1.25 solid immersion oil lens objective. Step size for z-stack acquisition was 600 nm. Quantifications of mean intensity were performed in Fiji (ImageJ v1.54b) with maximum intensity projected z-stacks (Schindelin et al., 2012). Mean intensity of primary-antibody omitted samples was subtracted as background.

Ccdc93 particle analysis was performed on maximum intensity projected z-stacks using Fiji. Background was subtracted with a rolling ball radius of 50 pixels and threshold was set manually, adjusting for variable intensities of individual particles. Particle count, total area, and average size were analyzed per individual cell.

Images presented in this work are representative images of at least 4 images per condition with minimum 30 cells.

4.2.12 HISTOLOGY

Histological examination of liver tissue was performed by the Helmholtz Munich Pathology Core Facility Snap-frozen liver pieces of chow-fed Control- and KO-inducing AAV-injected Ap4e1$^{fl/fl}$ mice were fixed in 4 % formalin, paraffin embedded, and cut into 3 µm slices. Liver pieces of FPC-fed mice and their respective chow-fed control mice were fixed in Histofix directly without freezing. Tissue slices were stained under standardized conditions for haematoxylin and eosin (H&E) and Sirius red on a Discovery XT automated stainer (Ventana Medical Systems). Liver sections were automatically analyzed with an Axio Scan.Z1 digital slide scanner (ZEISS) at 20x magnification. Image evaluation was conducted by Definiens Developer XD2 (Definiens) (Feuchtinger et al., 2015). Lipid- and Sirius red-positive area was digitally determined and presented relative to total analyzed tissue area. Inflammatory foci were manually counted per defined tissue area (Loft et al., 2021).

4.2.13 PROTEOMICS

For proteomics analysis, snap-frozen liver pieces of 6 h starved mice with LNP injections for 3 weeks were dounce-homogenized in 2 % SDC/150 mM Tris-HCl buffer (pH 8.5) and boiled at 99 °C, 1000 rpm, for 10 min. Tissue was further dissociated by sonication for 15 min at 4 °C using Bioruptor at high intensity with on/off intervals of 30 s and protein concentration was determined by DC Protein Assay Kit (Bio-Rad). 25 µg protein were reduced and alkylated in 100 µl of 2 % SDC buffer with 40 mM chloroacetamide (CAA) and 10 mM tris(2-carboxyethyl)phosphine (TCEP) for 10 min at 45 °C with 1000 rpm. Proteins were digested over night at 37 °C and 1000 rpm with 0.5 µg/µl of LysC and Trypsin. Samples were acidified by adding 1:1 of 2 % trifluoroacetic acid (TFA)/isopropanol, resulting in 1 % TFA/isopropanol final concentration. Protein mixtures were transferred to stop-and-go-extraction tips (stage tips) filled with SDB-RPS (polystyrene-divinylbenzene, reversed phase sulfonate). Before loading the tips with protein, tips were washed with acetonitrile (ACN), activated with 1 % TFA/30 % methanol, and washed again with 0.2 % TFA at 1000 g for 7 min. Samples were loaded onto the stage tips by centrifugation at 1000 g until all liquid disappeared from the tip. Loaded samples were washed with 1 % TFA/ethyl aceteate, 1 % TFA/isopropanol, and 0.2 % TFA at 1000 g for 5 min each time. Protein was eluted with (v/v) 80 % ACN, 15 % ddH_2O, 5 % ammonia solution (25 %) and dried using a SpeedVac concentrator for 45 min at 45 °C. Protein was

dissolved in buffer composed of 2 % ACN and 0.1 TFA and concentration measured using NanoDrop.

MS runs were performed by the group of Dr. Natalie Krahmer, HMGU. 2 µg peptides were loaded on a 1.9 µm C18 ReproSil particle-packed 50 cm column with 75 µm inner diameter at 60 °C for MS analysis. Using a two buffer system with 0.1 % formic acid (1) and 80 % ACN in 0.1 formic acid (2), peptides were separated by reversed-phase chromatography on a 120 min gradient (95 min: 5-30 % buffer (1); 5 min: 30-60 % buffer (2)) at a flow rate of 300 nl on an EASY-nLC 1200 system (Thermo Fisher Scientific). MS data was obtained with a data-dependent top-15 method and 20 ms maximum injection time, 300-1650 Th scan range, and $3x10^6$ automatic gain control target. The target value for higher-energy collisional dissociation fragmentation sequencing was set to $1x10^5$ and the scan range window to 1.4 Th. Resolution for survey scans and higher-energy dissociation spectra was 60,000 and 15,000, respectively, with 28 ms maximum injection time and underfill ratio of 20 or 40 %. The dynamic exclusion was set to 30 s.

MS data was processed in MaxQuant v.1.5.6.4 and proteins and peptides were identified by reverse target-decoy approach using Andromeda peptide search against mouse UniProt FASTA database. Quantification was performed in MaxQuant, bioinformatic analysis in Perseus v1.6.15.0 (Tyanova et al., 2016) with annotations from UniProt, GO, and KEGG. Annotated proteins were filtered for 70 % valid values in six biological replicates for both conditions (control and Vps33b KD). Significantly up- or downregulated proteins were determined by student's t-test ($P < 0.05$) or permutation-based FDR ($P < 0.05$). Hierarchical clustering of z-scored protein expression was performed in Perseus.

Data was further analyzed using STRING network analysis (Szklarczyk et al., 2021). Proteins downregulated significantly by t-test ($P < 0.05$) were subjected to full STRING network analysis, including physical and functional associations of medium confidence 0.400. MCL clustering was performed with an inflation parameter of 3. Top 4 biggest clusters were selected for further analysis.

5 APPENDIX

5.1 ABBREVIATIONS

AAV	Adeno Associated Virus
ACN	acetonitrile
AGP	asiaglycoprotein
AICAR	5-Aminoimidazole-4-carboxamide ribonucleotide
Alb	albumin
Alfp	α-fetoprotein
ALP	alkaline phosphatase
ALT	alanine aminotransferase
AMP	adenosine monophosphate
AMPA	α-amino-3-hydroxy-5-methyl-4-isoxazolepropionic acid
Ampk	AMP-activated kinase
AOC	area of the curve
Ap-4	adaptor protein 4 subunit ε
Ap4e1	adaptor protein 4 subunit ε
$Ap4e1^{fl/fl}$	Ap4e1 floxed mice (homozygous)
APP	amyloid precursor protein
ARC	arthrogryposis-renal dysfunction-cholestasis
AST	aspartate aminotransferase
ATG9A	autophagy-related protein 9A
ATP	adenosine triphosphate
BMI	Body Mass Index
BSA	bovine serum albumin
CaMKII	Ca^{2+}/calmodulin-dependent protein kinase II
CaMKKII	Ca^{2+}/calmodulin-dependent protein kinase kinase II
Ccdc93	coiled-coil domain-containing 93
CHEVI	class C homologs in endosome-vesicle interaction
CORVET	class C core vacuole/endosome tethering
Cre	causes recombination
Ctrl	control
CVD	cardiovascular disease
DAPI	4,6-diamidino-2-phenylindole
DNL	*de novo* lipogenesis
EEA1	early endosomal antigen 1
EGF	endosomal growth factor
EGFR	endosomal growth factor receptor
ELISA	enzyme-linked immunosorbent assay
ESCRT	endosomal sorting complex required for transport
FCS	fetal calf serum
FDR	false discovery rate
FHF	FTS-Hook-FHIP
FPC	fructose, palmitate and cholesterol
GAN	Gubra Amylin NASH
Gcgr	Glucagon receptor
GDP	guanosine diphosphate
GPCR	G protein coupled receptor
GTP	guanosine triphosphate
GTT	glucose tolerance test
HCC	hepatocellular carcinoma
HDL	High-density lipoprotein
HE	haematoxylin-eosin
HFD	High Fat Diet
HGP	hepatic glucose production

HIV	human immunodeficiency virus
HMGU	Helmholtz Centre Munich
HOPS	homotypic fusion and vacuole protein sorting
HSC	hepatic stellate cells
HSP	hereditary spastic paraplegia
ILV	intraluminal vesicles
IMPC	International Mouse Phenotyping Consortium
InsR	insulin receptor
ip	intraperitoneal
IR	insulin resistance
ITT	insulin tolerance test
KD	knockdown
KO	knockout
LC-MS	liquid chromatography mass spectrometry
Ldlr	LDL receptor
Ldlrap1	Ldlr associated protein 1
LKB1	Liver kinase B1
LNP	lipid nanoparticles
MCD	methionine-choline deficient
MCL	Markov clustering
mTORC1	mammalian target of rapamycin 1
mut	mutated
MVB	multivesicular bodies
NAFLD	non-alcoholic fatty liver disease
NASH	non-alcoholic steatohepatitis
NEFA	non-esterified fatty acid
NSF	N-ethylmaleimide-sensitive fusion protein
OE	overexpression
p70 S6K	phosphorylation of p70 S6 kinase
PGC1A	peroxisome proliferator-activated receptor gamma coactivator 1-α
PI3P	phosphatidylinositol 3-phosphate
PIP	phosphatidylinositol phosphate
PKA	protein kinase A
PKCε	protein kinase C-ε
PM	plasma membrane
PNS	post nuclear supernatant
PTT	pyruvate tolerance test
rAAV	recombinant AAV
Rab	ras-related in brain
ROB	government of upper Bavaria (Regierung Oberbayern)
rpS6	S6 ribosomal protein
SDB-RPS	polystyrene-divinylbenzene, reversed phase sulfonate
SEM	standard error of the mean
SNARE	soluble NSF attachment receptor
SPG	progressive spastic paraplegia
Stage tips	stop-and-go-extraction tips
T1D	type 1 diabetes
T2D	type 2 diabetes
TARP	transmembrane AMPA receptor regulatory protein
TBST	tween-supplemented tris-buffered saline
TCEP	tris(2-carboxyethyl)phosphine
TFA	trifluoroacetic acid
TFAM	mitochondrial transcription factor A
TG	triglyceride
TGN	*trans*-Golgi network
Tsg101	tumor susceptibility gene 101

Ubap1	Ubiquitin-associated protein 1
Vps28	vacuolar protein sorting 28
Vps33b	vacuolar protein sorting 33b
Vps37a	vacuolar protein sorting 37a
Vps37b	vacuolar protein sorting 37b
Vps37c	vacuolar protein sorting 37c
WAT	white adipose tissue
WT	wild-type

5.2 LISTS OF TABLES AND FIGURES

5.2.1 TABLES

5.2.2 FIGURES

5.3 LIST OF REFERENCES

Abdel-Misih, S. R. Z., & Bloomston, M. (2010). Liver Anatomy. *Surgical Clinics of North America*, *90*(4), 643–653. https://doi.org/10.1016/j.suc.2010.04.017

Abou Jamra, R., Philippe, O., Raas-Rothschild, A., Eck, S. H., Graf, E., Buchert, R., Borck, G., Ekici, A., Brockschmidt, F. F., Nöthen, M. M., Munnich, A., Strom, T. M., Reis, A., & Colleaux, L. (2011). Adaptor protein complex 4 deficiency causes severe autosomal-recessive intellectual disability, progressive spastic paraplegia, shy character, and short stature. *American Journal of Human Genetics*, *88*(6), 788–795. https://doi.org/10.1016/J.AJHG.2011.04.019

Aguilar, R. C., Boehm, M., Gorshkova, I., Crouch, R. J., Tomita, K., Saito, T., Ohno, H., & Bonifacino, J. S. (2001). Signal-binding Specificity of the μ4 Subunit of the Adaptor Protein Complex AP-4. *Journal of Biological Chemistry*, *276*, 13145–13152. https://doi.org/10.1074/jbc.M010591200

Anderson, R. G. W., Goldstein, J. L., & Brown, M. S. (1977). A mutation that impairs the ability of lipoprotein receptors to localise in coated pits on the cell surface of human fibroblasts. *Nature*, *270*(5639), 695–699. https://doi.org/10.1038/270695a0

Angulo, P., Kleiner, D. E., Dam-Larsen, S., Adams, L. A., Bjornsson, E. S., Charatcharoenwitthaya, P., Mills, P. R., Keach, J. C., Lafferty, H. D., Stahler, A., Haflidadottir, S., & Bendtsen, F. (2015). Liver Fibrosis, but No Other Histologic Features, Is Associated With Long-term Outcomes of Patients With Nonalcoholic Fatty Liver Disease. *Gastroenterology*, *149*(2), 389-397.e10. https://doi.org/10.1053/J.GASTRO.2015.04.043

Atkinson, M. A., Eisenbarth, G. S., & Michels, A. W. (2014). Type 1 diabetes. *Lancet*, *383*(9911), 69–82. https://doi.org/10.1016/S0140-6736(13)60591-7

Babst, M., Wendland, B., Estepa, E. J., & Emr, S. D. (1998). The Vps4p AAA ATPase regulates membrane association of a Vps protein complex required for normal endosome function. *The EMBO Journal*, *17*(11), 2982–2993. https://doi.org/10.1093/EMBOJ/17.11.2982

Bache, K. G., Stuffers, S., Malerød, L., Slagsvold, T., Raiborg, C., Lechardeur, D., Wälchli, S., Lukacs, G. L., Brech, A., & Stenmark, H. (2006). The ESCRT-III subunit hVps24 is required for degradation but not silencing of the epidermal growth factor receptor. *Molecular Biology of the Cell*, *17*(6), 2513–2523. https://doi.org/10.1091/MBC.E05-10-0915/ASSET/IMAGES/LARGE/ZMK0060676560008.JPEG

Baker, R. W., Jeffrey, P. D., Zick, M., Phillips, B. P., Wickner, W. T., & Hughson, F. M. (2015). A direct role for the Sec1/Munc18-family protein Vps33 as a template for SNARE assembly. *Science*, *349*(6252), 1111–1114. https://doi.org/10.1126/science.aac7906

Bartuzi, P., Billadeau, D. D., Favier, R., Rong, S., Dekker, D., Fedoseienko, A., Fieten, H., Wijers, M., Levels, J. H., Huijkman, N., Kloosterhuis, N., Van Der Molen, H., Brufau, G., Groen, A. K., Elliott, A. M., Kuivenhoven, J. A., Plecko, B., Grangl, G., McGaughran, J., … Van De Sluis, B. (2016). CCC- and WASH-mediated endosomal sorting of LDLR is required for normal clearance of circulating LDL. *Nature Communications*, *7*(1), 1–11. https://doi.org/10.1038/ncomms10961

Behne, R., Teinert, J., Wimmer, M., D'Amore, A., Davies, A. K., Scarrott, J. M., Eberhardt, K., Brechmann, B., Chen, I. P. F., Buttermore, E. D., Barrett, L., Dwyer, S., Chen, T., Hirst, J., Wiesener, A., Segal, D., Martinuzzi, A., Duarte, S. T., Bennett, J. T., … Ebrahimi-Fakhari, D. (2020). Adaptor protein complex 4 deficiency: A paradigm of childhood-onset hereditary spastic paraplegia caused by defective protein trafficking. *Human Molecular Genetics*, *29*(2), 320–334. https://doi.org/10.1093/hmg/ddz310

Bem, D., Smith, H., Banushi, B., Burden, J. J., White, I. J., Hanley, J., Jeremiah, N., Rieux-Laucat, F., Bettels, R., Ariceta, G., Mumford, A. D., Thomas, S. G., Watson, S. P., & Gissen, P. (2015). VPS33B regulates protein sorting into and maturation of a-granule progenitor organelles in mouse megakaryocytes. *Blood*, *126*(2), 133–143. https://doi.org/10.1182/blood-2014-12-614677

Berghöfer, A., Pischon, T., Reinhold, T., Apovian, C. M., Sharma, A. M., & Willich, S. N. (2008). Obesity prevalence from a European perspective: A systematic review. *BMC Public Health*, *8*(1), 1–10. https://doi.org/10.1186/1471-2458-8-200/TABLES/2

Blüher, M. (2019). Obesity: global epidemiology and pathogenesis. *Nature Reviews Endocrinology*, *15*(5), 288–298. https://doi.org/10.1038/s41574-019-0176-8

Boehm, M., & Bonifacino, J. S. (2001). Adaptins: The Final Recount. *Molecular Biology of the Cell*, *12*(10), 2907. https://doi.org/10.1091/MBC.12.10.2907

Boll, W., Ohno, H., Songyang, Z., Rapoport, I., Cantley, L. C., Bonifacino, J. S., & Kirchhausen, T. (1996). Sequence requirements for the recognition of tyrosine-based endocytic signals by clathrin AP-2 complexes. *EMBO Journal*, *15*(21), 5789–5795. https://doi.org/10.1002/J.1460-2075.1996.TB00965.X

Bomholt, A. B., Johansen, C. D., Christensen, J. B., Kjeldsen, S. A. S., Galsgaard, K. D., Winther-Sørensen, M., Serizawa, R., Hornum, M., Porrini, E., Pedersen, J., Ørskov, C., Gluud, L. L., Sørensen, C. M., Holst, J. J., Albrechtsen, R., & Wewer Albrechtsen, N. J. (2022). Evaluation of commercially available glucagon receptor antibodies and glucagon receptor expression. *Communications Biology*, *5*(1), 1–13. https://doi.org/10.1038/s42003-022-04242-7

Bonifacino, J. S. (2014). Adaptor proteins involved in polarized sorting. *Journal of Cell Biology*,

204(1), 7–17. https://doi.org/10.1083/jcb.201310021

Bonifacino, J. S., & Glick, B. S. (2004). The Mechanisms of Vesicle Budding and Fusion. *Cell*, *116*(2), 153–166. https://doi.org/10.1016/S0092-8674(03)01079-1

Bonifacino, J. S., & Traub, L. M. (2003). Signals for sorting of transmembrane proteins to endosomes and lysosomes. *Annual Review of Biochemistry*, *72*, 395–447. https://doi.org/10.1146/annurev.biochem.72.121801.161800

Brodsky, F. M., Chen, C.-Y., Knuehl, C., Towler, M. C., & Wakeham, D. E. (2001). Biological Basket Weaving: Formation and Function of Clathrin-Coated Vesicles. *Annual Review of Cell and Developmental Biology*, *17*, 517–568. https://doi.org/10.1146/annurev.cellbio.17.1.517

Brown, M. S., & Goldstein, J. L. (1976). Analysis of a mutant strain of human fibroblasts with a defect in the internalization of receptor-bound low density lipoprotein. *Cell*, *9*(4), 663–674. https://doi.org/10.1016/0092-8674(76)90130-6

Brunet, S., Sardon, T., Zimmerman, T., Wittmann, T., Pepperkok, R., Karsenti, E., & Vernos, I. (2004). Characterization of the TPX2 Domains Involved in Microtubule Nucleation and Spindle Assembly in Xenopus nucleation around chromatin and functions in a network of other molecules , some of which also are regulated by. *Mol Biol Cell*, *15*(December), 5318–5328. https://doi.org/10.1091/mbc.E04

Bühler, L., Maida, A., Vogl, E. S., Georgiadi, A., Takacs, A., Kluth, O., Schürmann, A., Feuchtinger, A., von Toerne, C., Tsokanos, F. F., Klepac, K., Wolff, G., Sakurai, M., Üstünel, B. E., Nawroth, P., & Herzig, S. (2021). Lipocalin 13 enhances insulin secretion but is dispensable for systemic metabolic control. *Life Science Alliance*, *4*(4). https://doi.org/10.26508/LSA.202000898

Burgos, P. V., Mardones, G. A., Rojas, A. L., daSilva, L. L. P., Prabhu, Y., Hurley, J. H., & Bonifacino, J. S. (2010). Sorting of the Alzheimer's Disease Amyloid Precursor Protein Mediated by the AP-4 Complex. *Developmental Cell*, *18*(3), 425–436. https://doi.org/10.1016/j.devcel.2010.01.015

Buttgereit, F., & Brand, M. D. (1995). A hierarchy of ATP-consuming processes in mammalian cells. *Biochemical Journal*, *312*(1), 163–167. https://doi.org/10.1042/bj3120163

Cajulao, J. M. B., Hernandez, E., von Zastrow, M. E., & Sanchez, E. L. (2022). Glucagon receptor-mediated regulation of gluconeogenic gene transcription is endocytosis-dependent in primary hepatocytes. *Molecular Biology of the Cell*, *33*(10). https://doi.org/10.1091/MBC.E21-09-0430/ASSET/IMAGES/LARGE/MBC-33-AR90-G006.JPEG

Calebiro, D., Nikolaev, V. O., Gagliani, M. C., De Filippis, T., Dees, C., Tacchetti, C., Persani, L., & Lohse, M. J. (2009). Persistent cAMP-Signals Triggered by Internalized G-Protein–Coupled Receptors. *PLoS Biology*, *7*(8). https://doi.org/10.1371/JOURNAL.PBIO.1000172

Carroll, B., & Dunlop, E. A. (2017). The lysosome: A crucial hub for AMPK and mTORC1 signalling. *Biochemical Journal*, *474*(9), 1453–1466. https://doi.org/10.1042/BCJ20160780

Chen, W. J., Goldstein, J. L., & Brown, M. S. (1990). NPXY, a sequence often found in cytoplasmic tails, is required for coated pit-mediated internalization of the low density lipoprotein receptor. *Journal of Biological Chemistry*, *265*(6), 3116–3123. https://doi.org/10.1016/S0021-9258(19)39742-X

Collins, B. M., McCoy, A. J., Kent, H. M., Evans, P. R., & Owen, D. J. (2002). Molecular Architecture and Functional Model of the Endocytic AP2 Complex. *Cell*, *109*(4), 523–535. https://doi.org/10.1016/S0092-8674(02)00735-3

Cullinane, A. R., Straatman-Iwanowska, A., Zaucker, A., Wakabayashi, Y., Bruce, C. K., Luo, G., Rahman, F., Gürakan, F., Utine, E., Zkan, T. B., Denecke, J., Vukovic, J., Di Rocco, M., Mandel, H., Cangul, H., Matthews, R. P., Thomas, S. G., Rappoport, J. Z., Arias, I. M., … Gissen, P. (2010). Mutations in VIPAR cause an arthrogryposis, renal dysfunction and cholestasis syndrome phenotype with defects in epithelial polarization. *Nature Genetics*, *42*(4), 303–312. https://doi.org/10.1038/ng.538

Czaja, M. J. (2016). Function of Autophagy in Nonalcoholic Fatty Liver Disease. *Digestive Diseases and Sciences*, *61*(5), 1304–1313. https://doi.org/10.1007/S10620-015-4025-X/FIGURES/1

Day, C. P., & James, O. F. W. (1998). Steatohepatitis: A tale of two “Hits”? *Gastroenterology*, *114*(4 I), 842–845. https://doi.org/10.1016/S0016-5085(98)70599-2

De Aguiar Vallim, T. Q., Tarling, E. J., & Edwards, P. A. (2013). Pleiotropic roles of bile acids in metabolism. *Cell Metabolism*, *17*(5), 657–669. https://doi.org/10.1016/J.CMET.2013.03.013

De Pace, R., Skirzewski, M., Damme, M., Mattera, R., Mercurio, J., Foster, A. M., Cuitino, L., Jarnik, M., Hoffmann, V., Morris, H. D., Han, T. U., Mancini, G. M. S., Buonanno, A., & Bonifacino, J. S. (2018). Altered distribution of ATG9A and accumulation of axonal aggregates in neurons from a mouse model of AP-4 deficiency syndrome. *PLoS Genetics*, *14*(4), 1–30. https://doi.org/10.1371/journal.pgen.1007363

Dell’Angelica, E. C., Klumperman, J., Stoorvogel, W., & Bonifacino, J. S. (1998). Association of the AP-3 Adaptor Complex with Clathrin. *Science*, *280*(5362), 431–434.

https://doi.org/10.1126/SCIENCE.280.5362.431

Dell'Angelica, E. C., Mullins, C., & Bonifacino, J. S. (1999). AP-4, a novel protein complex related to clathrin adaptors. *Journal of Biological Chemistry*, *274*(11), 7278–7285. https://doi.org/10.1074/jbc.274.11.7278

Demir, S., Nawroth, P. P., Herzig, S., & Ekim Üstünel, B. (2021). Emerging Targets in Type 2 Diabetes and Diabetic Complications. *Advanced Science*, *8*(18). https://doi.org/10.1002/ADVS.202100275

Dickinson, M. E., Flenniken, A. M., Ji, X., Teboul, L., Wong, M. D., White, J. K., Meehan, T. F., Weninger, W. J., Westerberg, H., Adissu, H., Baker, C. N., Bower, L., Brown, J. M., Brianna Caddle, L., Chiani, F., Clary, D., Cleak, J., Daly, M. J., Denegre, J. M., … Murakami, A. (2016). High-throughput discovery of novel developmental phenotypes. *Nature*, *537*(7621), 508–514. https://doi.org/10.1038/nature19356

Drake, J. C., Alway, S. E., Hollander, J. M., & Williamson, D. L. (2010). AICAR treatment for 14 days normalizes obesity-induced dysregulation of TORC1 signaling and translational capacity in fasted skeletal muscle. *American Journal of Physiology - Regulatory Integrative and Comparative Physiology*, *299*(6). https://doi.org/10.1152/ajpregu.00337.2010

Dukes, J. D., Richardson, J. D., Simmons, R., & Whitley, P. (2008). A dominant-negative ESCRT-III protein perturbs cytokinesis and trafficking to lysosomes. *Biochemical Journal*, *411*(2), 233–239. https://doi.org/10.1042/BJ20071296

Duman, J. G., & Forte, J. G. (2003). What is the role of SNARE proteins in membrane fusion? *Am J Physiol Cell Physiol*, *285*(2), C237–C249. https://doi.org/10.1152/ajpcell.00091.2003.-Soluble

Ebrahimi-Fakhari, D., Alecu, J. E., Ziegler, M., Geisel, G., Jordan, C., D'Amore, A., Yeh, R. C., Akula, S. K., Saffari, A., Prabhu, S. P., Sahin, M., Yang, E., Bulk, S., Depierreux, F., Habibzadeh, P., Iyer, A. S., Kaminska, M., Kim, S., King, S. D., … Van Ravenswaaij-Arts, C. M. A. (2021). Systematic Analysis of Brain MRI Findings in Adaptor Protein Complex 4–Associated Hereditary Spastic Paraplegia. *Neurology*, *97*(19), e1942–e1954. https://doi.org/10.1212/WNL.0000000000012836

Ebrahimi-Fakhari, D., Cheng, C., Dies, K., Diplock, A., Pier, D. B., Ryan, C. S., Lanpher, B. C., Hirst, J., Chung, W. K., Sahin, M., Rosser, E., Darras, B., & Bennett, J. T. (2018). Clinical and genetic characterization of AP4B1-associated SPG47. *American Journal of Medical Genetics*, *176*(2), 311–318. https://doi.org/10.1002/AJMG.A.38561

Ebrahimi-Fakhari, D., Teinert, J., Behne, R., Wimmer, M., D'Amore, A., Eberhardt, K., Brechmann, B., Ziegler, M., Jensen, D. M., Nagabhyrava, P., Geisel, G., Carmody, E.,

Shamshad, U., Dies, K. A., Yuskaitis, C. J., Salussolia, C. L., Ebrahimi-Fakhari, D., Pearson, T. S., Saffari, A., … Sahin, M. (2020). Defining the clinical, molecular and imaging spectrum of adaptor protein complex 4-associated hereditary spastic paraplegia. *Brain*, *143*(10), 2929–2944. https://doi.org/10.1093/BRAIN/AWZ307

Ekstedt, M., Nasr, P., & Kechagias, S. (2017). Natural History of NAFLD/NASH. *Curr Hepatology Rep*, *16*, 391–397. https://doi.org/10.1007/s11901-017-0378-2

Elia, N., Sougrat, R., Spurlin, T. A., Hurley, J. H., & Lippincott-Schwartz, J. (2011). Dynamics of endosomal sorting complex required for transport (ESCRT) machinery during cytokinesis and its role in abscission. *Proceedings of the National Academy of Sciences of the United States of America*, *108*(12), 4846–4851. https://doi.org/10.1073/PNAS.1102714108/-/DCSUPPLEMENTAL/PNAS.201102714SI.PDF

Færch, K., Vistisen, D., Pacini, G., Torekov, S. S., Johansen, N. B., Witte, D. R., Jonsson, A., Pedersen, O., Hansen, T., Lauritzen, T., Jørgensen, M. E., Ahrén, B., & Holst, J. J. (2016). Insulin Resistance Is Accompanied by Increased Fasting Glucagon and Delayed Glucagon Suppression in Individuals With Normal and Impaired Glucose Regulation. *Diabetes*, *65*(11), 3473–3481. https://doi.org/10.2337/DB16-0240

Fedoseienko, A., Wijers, M., Wolters, J. C., Dekker, D., Smit, M., Huijkman, N., Kloosterhuis, N., Klug, H., Schepers, A., Van Dijk, K. W., Levels, J. H. M., Billadeau, D. D., Hofker, M. H., Van Deursen, J., Westerterp, M., Burstein, E., Kuivenhoven, J. A., & Van De Sluis, B. (2018). The COMMD family regulates plasma LDL levels and attenuates atherosclerosis through stabilizing the CCC complex in endosomal LDLR traffcking. *Circulation Research*, *122*(12), 1648–1660. https://doi.org/10.1161/CIRCRESAHA.117.312004

Ferrandon, S., Feinstein, T. N., Castro, M., Wang, B., Bouley, R., Potts, J. T., Gardella, T. J., & Vilardaga, J. P. (2009). Sustained cyclic AMP production by parathyroid hormone receptor endocytosis. *Nature Chemical Biology*, *5*(10), 734–742. https://doi.org/10.1038/nchembio.206

Feuchtinger, A., Stiehler, T., Jütting, U., Marjanovic, G., Luber, B., Langer, R., & Walch, A. (2015). Image analysis of immunohistochemistry is superior to visual scoring as shown for patient outcome of esophageal adenocarcinoma. *Histochemistry and Cell Biology*, *143*(1), 1–9. https://doi.org/10.1007/S00418-014-1258-2/METRICS

Forbes, J. M., & Cooper, M. E. (2013). Mechanisms of diabetic complications. *Physiological Reviews*, *93*(1), 137–188. https://doi.org/10.1152/physrev.00045.2011

French, A. P., Mills, S., Swarup, R., Bennett, M. J., & Pridmore, T. P. (2008). Colocalization of fluorescent markers in confocal microscope images of plant cells. *Nature Protocols*, *3*(4),

619–628. https://doi.org/10.1038/nprot.2008.31

Friedman, S. L., Neuschwander-Tetri, B. A., Rinella, M., & Sanyal, A. J. (2018). Mechanisms of NAFLD development and therapeutic strategies. *Nature Medicine*, *24*(7), 908–922. https://doi.org/10.1038/s41591-018-0104-9

Frizzell, R. T., Hendrick, G. K., Biggers, D. W., Lacy, D. B., Donahue, D. P., Green, D. R., Carr, R. K., Williams, P. E., Stevenson, R. W., & Cherrington, A. D. (1988). Role of Gluconeogenesis in Sustaining Glucose Production During Hypoglycemia Caused by Continuous Insulin Infusion in Conscious Dogs. *Diabetes*, *37*(6), 749–759. https://doi.org/10.2337/DIAB.37.6.749

Fry, J., & Finley, W. (2005). The prevalence and costs of obesity in the EU. *Proceedings of the Nutrition Society*, *64*(3), 359–362. https://doi.org/10.1079/pns2005443

Fu, K., Wang, C., Gao, Y., Fan, S., Zhang, H., Sun, J., Jiang, Y., Liu, C., Guan, L., Liu, J., Huang, M., & Bi, H. (2019). Metabolomics and lipidomics reveal the effect of hepatic Vps33b deficiency on bile acids and lipids metabolism. *Frontiers in Pharmacology*, *10*(MAR), 276. https://doi.org/10.3389/fphar.2019.00276

Gallage, S., Avila, J. E. B., Ramadori, P., Focaccia, E., Rahbari, M., Ali, A., Malek, N. P., Anstee, Q. M., & Heikenwalder, M. (2022). A researcher's guide to preclinical mouse NASH models. *Nature Metabolism*, *4*(12), 1632–1649. https://doi.org/10.1038/s42255-022-00700-y

Galmes, R., ten Brink, C., Oorschot, V., Veenendaal, T., Jonker, C., van der Sluijs, P., & Klumperman, J. (2015). Vps33B is required for delivery of endocytosed cargo to lysosomes. *Traffic*, *16*(12), 1288–1305. https://doi.org/10.1111/tra.12334

Gao, G. P., Alvira, M. R., Wang, L., Calcedo, R., Johnston, J., & Wilson, J. M. (2002). Novel adeno-associated viruses from rhesus monkeys as vectors for human gene therapy. *Proceedings of the National Academy of Sciences of the United States of America*, *99*(18), 11854. https://doi.org/10.1073/PNAS.182412299

Garcia, D., Hellberg, K., Chaix, A., Wallace, M., Herzig, S., Badur, M. G., Lin, T., Shokhirev, M. N., Pinto, A. F. M., Ross, D. S., Saghatelian, A., Panda, S., Dow, L. E., Metallo, C. M., & Shaw, R. J. (2019). Genetic Liver-Specific AMPK Activation Protects against Diet-Induced Obesity and NAFLD. *Cell Reports*, *26*(1), 192-208.e6. https://doi.org/10.1016/j.celrep.2018.12.036

Garcia, D., & Shaw, R. J. (2017). AMPK: Mechanisms of Cellular Energy Sensing and Restoration of Metabolic Balance. *Molecular Cell*, *66*(6), 789–800. https://doi.org/10.1016/j.molcel.2017.05.032

Garrus, J. E., Von Schwedler, U. K., Pornillos, O. W., Morham, S. G., Zavitz, K. H., Wang, H. E., Wettstein, D. A., Stray, K. M., Côté, M., Rich, R. L., Myszka, D. G., & Sundquist, W. I. (2001). Tsg101 and the vacuolar protein sorting pathway are essential for HIV-1 budding. *Cell*, *107*(1), 55–65. https://doi.org/10.1016/S0092-8674(01)00506-2

Gebhardt, R. (1992). Metabolic zonation of the liver: Regulation and implications for liver function. *Pharmacology and Therapeutics*, *53*(3), 275–354. https://doi.org/10.1016/0163-7258(92)90055-5

Ghislat, G., Patrons, M., Rizzutos, R., & Knecht, E. (2012). Withdrawal of essential amino acids increases autophagy by a pathway involving Ca2+/calmodulin-dependent kinase kinase-β (CaMKK-β). *The Journal of Biological Chemistry*, *287*(46), 38625–38636. https://doi.org/10.1074/JBC.M112.365767

Gilleron, J., Gerdes, J. M., & Zeigerer, A. (2019). Metabolic regulation through the endosomal system. *Traffic*, *20*(8), 552–570. https://doi.org/10.1111/tra.12670

Gilleron, J., Querbes, W., Zeigerer, A., Borodovsky, A., Marsico, G., Schubert, U., Manygoats, K., Seifert, S., Andree, C., Stöter, M., Epstein-Barash, H., Zhang, L., Koteliansky, V., Fitzgerald, K., Fava, E., Bickle, M., Kalaidzidis, Y., Akinc, A., Maier, M., & Zerial, M. (2013). Image-based analysis of lipid nanoparticle-mediated siRNA delivery, intracellular trafficking and endosomal escape. *Nature Biotechnology*, *31*(7), 638–646. https://doi.org/10.1038/nbt.2612

Gilleron, J., & Zeigerer, A. (2022). Endosomal trafficking in metabolic homeostasis and diseases. *Nature Reviews Endocrinology*, 1–18. https://doi.org/10.1038/s41574-022-00737-9

Gillooly, D. J., Morrow, I. C., Lindsay, M., Gould, R., Bryant, N. J., Gaullier, J. M., Parton, R. G., & Stenmark, H. (2000). Localization of phosphatidylinositol 3-phosphate in yeast and mammalian cells. *The EMBO Journal*, *19*(17), 4577–4588. https://doi.org/10.1093/EMBOJ/19.17.4577

Gissen, P., Johnson, C. A., Morgan, N. V., Stapelbroek, J. M., Forshew, T., Cooper, W. N., McKiernan, P. J., Klomp, L. W. J., Morris, A. A. M., Wraith, J. E., McClean, P., Lynch, S. A., Thompson, R. J., Lo, B., Quarrell, O. W., Di Rocco, M., Trembath, R. C., Mandel, H., Wali, S., … Maher, E. R. (2004). Mutations in VPS33B, encoding a regulator of SNARE-dependent membrane fusion, cause arthrogryposis-renal dysfunction-cholestasis (ARC) syndrome. *Nature Genetics*, *36*(4), 400–404. https://doi.org/10.1038/ng1325

Gissen, P., Tee, L., Johnson, C. A., Genin, E., Caliebe, A., Chitayat, D., Clericuzio, C., Denecke, J., Rocco, M., Fischler, B., FitzPatrick, D., García-Cazorla, A., Guyot, D., Jacquemont, S., Koletzko, S., Leheup, B., Mandel, H., Sanseverino, M. T. V., Houwen,

R. H. J., … Maher, E. R. (2006). Clinical and molecular genetic features of ARC syndrome. *Human Genetics*, *120*(3), 396–409. https://doi.org/10.1007/s00439-006-0232-z

Gleason, C. E., Lu, D., Witters, L. A., Newgard, C. B., & Birnbaum, M. J. (2007). The role of AMPK and mTOR in nutrient sensing in pancreatic β-cells. *Journal of Biological Chemistry*, *282*(14), 10341–10351. https://doi.org/10.1074/jbc.M610631200

Goldstein, J. L., DeBose-Boyd, R. A., & Brown, M. S. (2006). Protein sensors for membrane sterols. *Cell*, *124*(1), 35–46. https://doi.org/10.1016/j.cell.2005.12.022

Guidotti, J. E., Brégerie, O., Robert, A., Debey, P., Brechot, C., & Desdouets, C. (2003). Liver cell polyploidization: A pivotal role for binuclear hepatocytes. *Journal of Biological Chemistry*, *278*(21), 19095–19101. https://doi.org/10.1074/jbc.M300982200

Habegger, K. M., Heppner, K. M., Geary, N., Bartness, T. J., DiMarchi, R., & Tschöp, M. H. (2010). The metabolic actions of glucagon revisited. *Nature Reviews Endocrinology*, *6*(12), 689–697. https://doi.org/10.1038/nrendo.2010.187

Haeusler, R. A., McGraw, T. E., & Accili, D. (2018). Metabolic Signalling: Biochemical and cellular properties of insulin receptor signalling. *Nature Reviews Molecular Cell Biology*, *19*(1), 31–44. https://doi.org/10.1038/nrm.2017.89

Hanley, J., Dhar, D. K., Mazzacuva, F., Fiadeiro, R., Burden, J. J., Lyne, A. M., Smith, H., Straatman-Iwanowska, A., Banushi, B., Virasami, A., Mills, K., Lemaigre, F. P., Knisely, A. S., Howe, S., Sebire, N., Waddington, S. N., Paulusma, C. C., Clayton, P., & Gissen, P. (2017). Vps33b is crucial for structural and functional hepatocyte polarity. *Journal of Hepatology*, *66*(5), 1001–1011. https://doi.org/10.1016/j.jhep.2017.01.001

Harris, R. L., van den Berg, C. W., & Bowen, D. J. (2012). ASGR1 and ASGR2 , the Genes that Encode the Asialoglycoprotein Receptor (Ashwell Receptor), Are Expressed in Peripheral Blood Monocytes and Show Interindividual Differences in Transcript Profile . *Molecular Biology International*, *2012*, 1–10. https://doi.org/10.1155/2012/283974

Hawley, S. A., Pan, D. A., Mustard, K. J., Ross, L., Bain, J., Edelman, A. M., Frenguelli, B. G., & Hardie, D. G. (2005). Calmodulin-dependent protein kinase kinase-beta is an alternative upstream kinase for AMP-activated protein kinase. *Cell Metabolism*, *2*(1), 9–19. https://doi.org/10.1016/J.CMET.2005.05.009

Hawley, S. A., Ross, F. A., Gowans, G. J., Tibarewal, P., Leslie, N. R., & Hardie, D. G. (2014). Phosphorylation by Akt within the ST loop of AMPK-α1 down-regulates its activation in tumour cells. *The Biochemical Journal*, *459*(2), 275–287. https://doi.org/10.1042/BJ20131344

He, G., Gupta, S., Yi, M., Michaely, P., Hobbs, H. H., & Cohen, J. C. (2002). ARH Is a Modular Adaptor Protein That Interacts with the LDL Receptor, Clathrin, and AP-2. *Journal of Biological Chemistry*, *277*(46), 44044–44049. https://doi.org/10.1074/JBC.M208539200

Hebbard, L., & George, J. (2011). Animal models of nonalcoholic fatty liver disease. *Nature Reviews Gastroenterology and Hepatology*, *8*(1), 34–44. https://doi.org/10.1038/nrgastro.2010.191

Heilbronn, L. K., Seng, K. G., Turner, N., Campbell, L. V., & Chisholm, D. J. (2007). Markers of Mitochondrial Biogenesis and Metabolism Are Lower in Overweight and Obese Insulin-Resistant Subjects. *The Journal of Clinical Endocrinology & Metabolism*, *92*(4), 1467–1473. https://doi.org/10.1210/JC.2006-2210

Henne, W. M., Buchkovich, N. J., & Emr, S. D. (2011). The ESCRT Pathway. *Developmental Cell*, *21*(1), 77–91. https://doi.org/10.1016/j.devcel.2011.05.015

Herzig, S., Long, F., Jhala, U. S., Hedrick, S., Quinn, R., Bauer, A., Rudolph, D., Schutz, G., Yoon, C., Puigserver, P., Spiegelman, B., & Montminy, M. (2001). CREB regulates hepatic gluconeogenesis through the coactivator PGC-1. *Nature*, *413*(6852), 179–183. https://doi.org/10.1038/35093131

Higgins, K., Moore, B. A., Berberovic, Z., Adissu, H. A., Eskandarian, M., Flenniken, A. M., Shao, A., Imai, D. M., Clary, D., Lanoue, L., Newbigging, S., Nutter, L. M. J., Adams, D. J., Bosch, F., Braun, R. E., Brown, S. D. M., Dickinson, M. E., Dobbie, M., Flicek, P., … Moshiri, A. (2022). Analysis of genome-wide knockout mouse database identifies candidate ciliopathy genes. *Scientific Reports*, *12*(1), 1–17. https://doi.org/10.1038/s41598-022-19710-7

Hirst, J., Barlow, L., Francisco, G. C., Sahlender, D. A., Seaman, M. N. J., Dacks, J. B., & Robinson, M. S. (2011). The Fifth Adaptor Protein Complex. *PLoS Biology*, *9*(10). https://doi.org/10.1371/JOURNAL.PBIO.1001170

Hirst, J., Bright, N. A., Rous, B., & Robinson, M. S. (1999). Characterization of a fourth adaptor-related protein complex. *Molecular Biology of the Cell*, *10*(8), 2787–2802. https://doi.org/10.1091/mbc.10.8.2787

Hirst, J., Irving, C., & Borner, G. H. H. (2013). Adaptor Protein Complexes AP-4 and AP-5: New Players in Endosomal Trafficking and Progressive Spastic Paraplegia. *Traffic*, *14*(2), 153–164. https://doi.org/10.1111/tra.12028

Hong Feng, G., Lih, C.-J., & Cohen, S. N. (2000). TSG101 Protein Steady-State Level Is Regulated Posttranslationally by an Evolutionarily Conserved COOH-Terminal Sequence. *Cancer Research*, *60*, 1736–1741. http://aacrjournals.org/cancerres/article-pdf/60/6/1736/2483209/ch060001736.pdf

Houde, V. P., Ritorto, M. S., Gourlay, R., Varghese, J., Davies, P., Shpiro, N., Sakamoto, K., & Alessi, D. R. (2014). Investigation of LKB1 Ser431 phosphorylation and Cys433 farnesylation using mouse knockin analysis reveals an unexpected role of prenylation in regulating AMPK activity. *Biochemical Journal*, *458*(1), 41–56. https://doi.org/10.1042/BJ20131324

Hummel, K. P., Dickie, M. M., & Coleman, D. L. (1966). Diabetes, a new mutation in the mouse. *Science*, *153*(3740), 1127–1128. https://doi.org/10.1126/science.153.3740.1127

Hunter, M. R., Hesketh, G. G., Benedyk, T. H., Gingras, A. C., & Graham, S. C. (2018). Proteomic and Biochemical Comparison of the Cellular Interaction Partners of Human VPS33A and VPS33B. *Journal of Molecular Biology*, *430*(14), 2153–2163. https://doi.org/10.1016/j.jmb.2018.05.019

Hurley, J. H. (2010). The ESCRT complexes. *Critical Reviews in Biochemistry and Molecular Biology*, *45*(6), 463–487. https://doi.org/10.3109/10409238.2010.502516

Hurley, R. L., Anderson, K. A., Franzone, J. M., Kemp, B. E., Means, A. R., & Witters, L. A. (2005). The Ca2+/calmodulin-dependent protein kinase kinases are AMP-activated protein kinase kinases. *Journal of Biological Chemistry*, *280*(32), 29060–29066. https://doi.org/10.1074/jbc.M503824200

Huttlin, E. L., Bruckner, R. J., Paulo, J. A., Cannon, J. R., Ting, L., Baltier, K., Colby, G., Gebreab, F., Gygi, M. P., Parzen, H., Szpyt, J., Tam, S., Zarraga, G., Pontano-Vaites, L., Swarup, S., White, A. E., Schweppe, D. K., Rad, R., Erickson, B. K., … Wade Harper, J. (2017). Architecture of the human interactome defines protein communities and disease networks. *Nature*, *545*(7655), 505–509. https://doi.org/10.1038/nature22366

Ioannou, G. N. (2016). The Role of Cholesterol in the Pathogenesis of NASH. *Trends in Endocrinology & Metabolism*, *27*(2), 84–95. https://doi.org/10.1016/J.TEM.2015.11.008

Irannejad, R., Tomshine, J. C., Tomshine, J. R., Chevalier, M., Mahoney, J. P., Steyaert, J., Rasmussen, S. G. F., Sunahara, R. K., El-Samad, H., Huang, B., & Von Zastrow, M. (2013). Conformational biosensors reveal GPCR signalling from endosomes. *Nature*, *495*(7442), 534–538. https://doi.org/10.1038/nature12000

Ivankovic, D., Drew, J., Lesept, F., White, I. J., López Doménech, G., Tooze, S. A., & Kittler, J. T. (2020). Axonal autophagosome maturation defect through failure of ATG9A sorting underpins pathology in AP-4 deficiency syndrome. *Autophagy*, *16*(3), 391–407. https://doi.org/10.1080/15548627.2019.1615302

James, P. T. (2004). Obesity: The worldwide epidemic. *Clinics in Dermatology*, *22*(4), 276–280. https://doi.org/10.1016/J.CLINDERMATOL.2004.01.010

Janah, L., Kjeldsen, S., Galsgaard, K. D., Winther-Sørensen, M., Stojanovska, E., Pedersen, J., Knop, F. K., Holst, J. J., & Albrechtsen, N. J. W. (2019). Glucagon Receptor Signaling and Glucagon Resistance. *International Journal of Molecular Sciences 2019, Vol. 20, Page 3314*, *20*(13), 3314. https://doi.org/10.3390/IJMS20133314

Janssen, F., Bardoutsos, A., & Vidra, N. (2020). Obesity Prevalence in the Long-Term Future in 18 European Countries and in the USA. *Obes Facts*, *13*, 514–527. https://doi.org/10.1159/000511023

Jimena, A., Nunez, A., Dittner, C., Becker, J., Loft, A., Mhamane, A., Maida, A., Georgiadi, A., Tsokanos, P., Klepac, K., Molocea, E., Merahbi, R., Motzler, K., Geppert, J., Karikari, R. A., Szendrödi, J., Feuchtinger, A., Hofmann, S., Melchior, F., & Herzig, S. (2022). Fasting-sensitive SUMO-switch on Prox1 controls hepatic cholesterol metabolism. *BioRxiv*, 2022.08.17.504229. https://doi.org/10.1101/2022.08.17.504229

Kellendonk, C., Opherk, C., Anlag, K., Schütz, G., & Tronche, F. (2000). Hepatocyte-specific expression of Cre recombinase. *Genesis*, *26*(2), 151–153. https://doi.org/10.1002/(SICI)1526-968X(200002)26:2<151::AID-GENE17>3.0.CO;2-E

Kelly, T., Yang, W., Chen, C. S., Reynolds, K., & He, J. (2008). Global burden of obesity in 2005 and projections to 2030. *International Journal of Obesity*, *32*(9), 1431–1437. https://doi.org/10.1038/ijo.2008.102

Kim, J., Kwon, H., Kalsoom, F., Sajjad, M. A., Lee, H. W., Lim, J. H., Jung, J., Chwae, Y. J., Park, S., Shin, H. J., & Kim, K. (2022). Ca2+/Calmodulin-Dependent Protein Kinase II Inhibits Hepatitis B Virus Replication from cccDNA via AMPK Activation and AKT/mTOR Suppression. *Microorganisms*, *10*(3), 498. https://doi.org/10.3390/MICROORGANISMS10030498/S1

Koliaki, C., Szendroedi, J., Kaul, K., Jelenik, T., Nowotny, P., Jankowiak, F., Herder, C., Carstensen, M., Krausch, M., Knoefel, W. T., Schlensak, M., & Roden, M. (2015). Adaptation of Hepatic Mitochondrial Function in Humans with Non-Alcoholic Fatty Liver Is Lost in Steatohepatitis. *Cell Metabolism*, *21*(5), 739–746. https://doi.org/10.1016/j.cmet.2015.04.004

Kolmus, K., Erdenebat, P., Szymanska, E., Stewig, B., Goryca, K., Derezinska-Wołek, E., Szumera-Ciećkiewicz, A., Brewinska-Olchowik, M., Piwocka, K., Prochorec-Sobieszek, M., Mikula, M., & Czynska, M. M. (2021). Concurrent depletion of Vps37 proteins evokes ESCRT-I destabilization and profound cellular stress responses. *Journal of Cell Science*, *134*(1). https://doi.org/10.1242/JCS.250951/237108

Koshland, D. E. (2002). The Seven Pillars of Life. *Science*, *295*(5563), 2215–2216. https://doi.org/10.1126/SCIENCE.1068489

Krahmer, N., Najafi, B., Schueder, F., Quagliarini, F., Steger, M., Seitz, S., Kasper, R., Salinas, F., Cox, J., Uhlenhaut, N. H., Walther, T. C., Jungmann, R., Zeigerer, A., Borner, G. H. H., & Mann, M. (2018). Organellar Proteomics and Phospho-Proteomics Reveal Subcellular Reorganization in Diet-Induced Hepatic Steatosis. *Developmental Cell*, *47*(2), 205-221.e7. https://doi.org/10.1016/j.devcel.2018.09.017

Krämer, L., & Ungermann, C. (2011). HOPS drives vacuole fusion by binding the vacuolar SNARE complex and the Vam7 PX domain via two distinct sites. *Molecular Biology of the Cell*, *22*. https://doi.org/10.1091/mbc.E11-02-0104

Krebs, E. G., Graves, D. J., & Fischer, E. H. (1959). Factors Affecting the Activity of Muscle Phosphorylase b Kinase. *Journal of Biological Chemistry*, *234*(11), 2867–2873. https://doi.org/10.1016/S0021-9258(18)69685-1

Levkowitz, G., Waterman, H., Ettenberg, S. A., Katz, M., Tsygankov, A. Y., Alroy, I., Lavi, S., Iwai, K., Reiss, Y., Ciechanover, A., Lipkowitz, S., & Yarden, Y. (1999). Ubiquitin ligase activity and tyrosine phosphorylation underlie suppression of growth factor signaling by c-Cbl/Sli-1. *Molecular Cell*, *4*(6), 1029–1040. https://doi.org/10.1016/S1097-2765(00)80231-2

Li, L., Liu, D. W., Yan, H. Y., Wang, Z. Y., Zhao, S. H., & Wang, B. (2016). Obesity is an independent risk factor for non-alcoholic fatty liver disease: evidence from a meta-analysis of 21 cohort studies. *Obesity Reviews*, *17*(6), 510–519. https://doi.org/10.1111/OBR.12407

Liu, J., Zhang, Y., Tian, Y., Huang, W., Tong, N., & Fu, X. (2022). Integrative biology of extracellular vesicles in diabetes mellitus and diabetic complications. *Theranostics*, *3*, 1342–1372. https://doi.org/10.7150/thno.65778

Loft, A., Alfaro, A. J., Schmidt, S. F., Pedersen, F. B., Terkelsen, M. K., Puglia, M., Chow, K. K., Feuchtinger, A., Troullinaki, M., Maida, A., Wolff, G., Sakurai, M., Berutti, R., Ekim Üstünel, B., Nawroth, P., Ravnskjaer, K., Diaz, M. B., Blagoev, B., & Herzig, S. (2021). Liver-fibrosis-activated transcriptional networks govern hepatocyte reprogramming and intra-hepatic communication. *Cell Metabolism*, *33*(8), 1685-1700.e9. https://doi.org/10.1016/j.cmet.2021.06.005

Majumder, P., Edmison, D., Rodger, C., Patel, S., Reid, E., & Gowrishankar, S. (2022). AP-4 regulates neuronal lysosome composition, function, and transport via regulating export of critical lysosome receptor proteins at the trans-Golgi network. *Molecular Biology of the Cell*, *33*(12). https://doi.org/10.1091/MBC.E21-09-0473/ASSET/IMAGES/LARGE/MBC-33-AR102-G006.JPEG

Malaguarnera, M., Di Rosa, M., Nicoletti, F., & Malaguarnera, L. (2009). Molecular

mechanisms involved in NAFLD progression. *Journal of Molecular Medicine*, *87*(7), 679–695. https://doi.org/10.1007/S00109-009-0464-1/FIGURES/3

Malerød, L., Stuffers, S., Brech, A., & Stenmark, H. (2007). Vps22/EAP30 in ESCRT-II mediates endosomal sorting of growth factor and chemokine receptors destined for lysosomal degradation. *Traffic*, *8*(11), 1617–1629. https://doi.org/10.1111/J.1600-0854.2007.00630.X

Mantovani, A., Byrne, C. D., Bonora, E., & Targher, G. (2018). Nonalcoholic fatty liver disease and risk of incident type 2 diabetes: A meta-analysis. *Diabetes Care*, *41*(2), 372–382. https://doi.org/10.2337/dc17-1902

Margall-Ducos, G., Celton-Morizur, S., Couton, D., Brégerie, O., & Desdouets, C. (2007). Liver tetraploidization is controlled by a new process of incomplete cytokinesis. *Journal of Cell Science*, *120*(20), 3633–3639. https://doi.org/10.1242/JCS.016907

Matsuda, S., Miura, E., Matsuda, K., Kakegawa, W., Kohda, K., Watanabe, M., & Yuzaki, M. (2008). Accumulation of AMPA Receptors in Autophagosomes in Neuronal Axons Lacking Adaptor Protein AP-4. *Neuron*, *57*(5), 730–745. https://doi.org/10.1016/j.neuron.2008.02.012

Mattera, R., Park, S. Y., De Pace, R., Guardia, C. M., & Bonifacino, J. S. (2017). AP-4 mediates export of ATG9A from the trans-Golgi network to promote autophagosome formation. *Proceedings of the National Academy of Sciences of the United States of America*, *114*(50), E10697–E10706. https://doi.org/10.1073/pnas.1717327114

McNew, J. A., Parlatl, F., Fukuda, R., Johnston, R. J., Paz, K., Paumet, F., Söllner, T. H., & Rothman, J. E. (2000). Compartmental specificity of cellular membrane fusion encoded in SNARE proteins. *Nature*, *407*(6801), 153–159. https://doi.org/10.1038/35025000

Menon, S., Dibble, C. C., Talbott, G., Hoxhaj, G., Valvezan, A. J., Takahashi, H., Cantley, L. C., & Manning, B. D. (2014). Spatial Control of the TSC Complex Integrates Insulin and Nutrient Regulation of mTORC1 at the Lysosome. *Cell*, *156*(4), 771–785. https://doi.org/10.1016/J.CELL.2013.11.049

Miaczynska, M., Pelkmans, L., & Zerial, M. (2004). Not just a sink: Endosomes in control of signal transduction. *Current Opinion in Cell Biology*, *16*(4), 400–406. https://doi.org/10.1016/j.ceb.2004.06.005

Mishra, S. K., Watkins, S. C., & Traub, L. M. (2002). The autosomal recessive hypercholesterolemia (ARH) protein interfaces directly with the clathrin-coat machinery. *Proceedings of the National Academy of Sciences of the United States of America*, *99*(25), 16099–16104. https://doi.org/10.1073/PNAS.252630799

Morrison, K. R., Smiles, W. J., Ling, N. X. Y., Hoque, A., Shea, G., Ngoei, K. R. W., Yu, D., Murray-Segal, L., Scott, J. W., Galic, S., Kemp, B. E., Petersen, J., & Oakhill, J. S. (2022). An AMPKα2-specific phospho-switch controls lysosomal targeting for activation. *Cell Reports*, *38*(7), 110365. https://doi.org/10.1016/J.CELREP.2022.110365

Mota, M., Banini, B. A., Cazanave, S. C., & Sanyal, A. J. (2016). Molecular Mechanisms of Lipotoxicity and Glucotoxicity in Nonalcoholic Fatty Liver Disease. *Metabolism*, *65*(8), 1049. https://doi.org/10.1016/J.METABOL.2016.02.014

Mridha, A. R., Wree, A., Robertson, A. A. B., Yeh, M. M., Johnson, C. D., Van Rooyen, D. M., Haczeyni, F., Teoh, N. C. H., Savard, C., Ioannou, G. N., Masters, S. L., Schroder, K., Cooper, M. A., Feldstein, A. E., & Farrell, G. C. (2017). NLRP3 inflammasome blockade reduces liver inflammation and fibrosis in experimental NASH in mice. *Journal of Hepatology*, *66*(5), 1037–1046. https://doi.org/10.1016/j.jhep.2017.01.022

Müller, T. D., Finan, B., Clemmensen, C., Di Marchi, R. D., & Tschöp, M. H. (2017). The new biology and pharmacology of glucagon. In *Physiological Reviews* (Vol. 97, Issue 2). https://doi.org/10.1152/physrev.00025.2016

Müller, T. D., Klingenspor, M., & Tschöp, M. H. (2021). Revisiting energy expenditure: how to correct mouse metabolic rate for body mass. *Nature Metabolism*, *3*(9), 1134–1136. https://doi.org/10.1038/s42255-021-00451-2

Murray, D. H., Jahnel, M., Lauer, J., Avellaneda, M. J., Brouilly, N., Cezanne, A., Morales-Navarrete, H., Perini, E. D., Ferguson, C., Lupas, A. N., Kalaidzidis, Y., Parton, R. G., Grill, S. W., & Zerial, M. (2016). An endosomal tether undergoes an entropic collapse to bring vesicles together. *Nature*, *537*(7618), 107–111. https://doi.org/10.1038/nature19326

Müsch, A. (2004). Microtubule organization and function in epithelial cells. *Traffic*, *5*(1), 1–9. https://doi.org/10.1111/J.1600-0854.2003.00149.X

Nakatsu, F., & Ohno, H. (2003). Adaptor protein complexes as the key regulators of protein sorting in the post-Golgi network. *Cell Structure and Function*, *28*(5), 419–429. https://doi.org/10.1247/csf.28.419

Nalbach, K., Schifferer, M., Lichtenthaler, S., Elazar, Z., & Behrends, C. (2022). Spatial Proteomics Reveals Disturbances in Trafficking and Interactions Along the Secretory Pathway Upon Loss of Neuropathy-Associated TECPR2. *Preprint at SSRN*. https://doi.org/10.2139/SSRN.4054841

Neuschwander-Tetri, B. A. (2010). Hepatic lipotoxicity and the pathogenesis of nonalcoholic steatohepatitis: the central role of nontriglyceride fatty acid metabolites. *Hepatology*, *52*(2), 774–788. https://doi.org/10.1002/HEP.23719

O'Leary, J. G., Landaverde, C., Jennings, L., Goldstein, R. M., & Davis, G. L. (2011). Patients With NASH and Cryptogenic Cirrhosis Are Less Likely Than Those With Hepatitis C to Receive Liver Transplants. *Clinical Gastroenterology and Hepatology*, *9*(8), 700-704.e1. https://doi.org/10.1016/J.CGH.2011.04.007

Oakhill, J. S., Chen, Z. P., Scott, J. W., Steel, R., Castelli, L. A., Linga, N., Macaulay, S. L., & Kemp, B. E. (2010). β-Subunit myristoylation is the gatekeeper for initiating metabolic stress sensing by AMP-activated protein kinase (AMPK). *Proceedings of the National Academy of Sciences of the United States of America*, *107*(45), 19237–19241. https://doi.org/10.1073/PNAS.1009705107/SUPPL_FILE/PNAS.1009705107_SI.PDF

Ogurtsova, K., da Rocha Fernandes, J. D., Huang, Y., Linnenkamp, U., Guariguata, L., Cho, N. H., Cavan, D., Shaw, J. E., & Makaroff, L. E. (2017). IDF Diabetes Atlas: Global estimates for the prevalence of diabetes for 2015 and 2040. *Diabetes Research and Clinical Practice*, *128*, 40–50. https://doi.org/10.1016/J.DIABRES.2017.03.024

Ohno, H., Aguilar, R. C., Yeh, D., Taura, D., Saito, T., & Bonifacino, J. S. (1998). The medium subunits of adaptor complexes recognize distinct but overlapping sets of tyrosine-based sorting signals. *Journal of Biological Chemistry*, *273*(40), 25915–25921. https://doi.org/10.1074/jbc.273.40.25915

Ohya, T., Miaczynska, M., Coskun, Ü., Lommer, B., Runge, A., Drechsel, D., Kalaidzidis, Y., & Zerial, M. (2009). Reconstitution of Rab- and SNARE-dependent membrane fusion by synthetic endosomes. *Nature*, *459*(7250), 1091–1097. https://doi.org/10.1038/nature08107

Oughtred, R., Rust, J., Chang, C., Breitkreutz, B. J., Stark, C., Willems, A., Boucher, L., Leung, G., Kolas, N., Zhang, F., Dolma, S., Coulombe-Huntington, J., Chatr-aryamontri, A., Dolinski, K., & Tyers, M. (2021). The BioGRID database: A comprehensive biomedical resource of curated protein, genetic, and chemical interactions. *Protein Science*, *30*(1), 187–200. https://doi.org/10.1002/PRO.3978

Oz, H. S., Im, H. J., Chen, T. S., De Villiers, W. J. S., & McClain, C. J. (2006). Glutathione-enhancing agents protect against steatohepatitis in a dietary model. *Journal of Biochemical and Molecular Toxicology*, *20*(1), 39–47. https://doi.org/10.1002/JBT.20109

Pais, R., Barritt, A. S., Calmus, Y., Scatton, O., Runge, T., Lebray, P., Poynard, T., Ratziu, V., & Conti, F. (2016). NAFLD and liver transplantation: Current burden and expected challenges. *Journal of Hepatology*, *65*(6), 1245–1257. https://doi.org/10.1016/J.JHEP.2016.07.033

Paolo, G. Di, & Camilli, P. De. (2006). Phosphoinositides in cell regulation and membrane dynamics. *Nature*, *443*, 651–657. https://doi.org/10.1038/nature05185

Park, S. Y., & Guo, X. (2014). Adaptor protein complexes and intracellular transport. *Bioscience Reports*, *34*(4), 381–390. https://doi.org/10.1042/BSR20140069

Paumet, F., Rahimian, V., & Rothman, J. E. (2004). The specificity of SNARE-dependent fusion is encoded in the SNARE motif. *Proceedings of the National Academy of Sciences*, *101*(10), 3376–3380. https://doi.org/10.1073/PNAS.0400271101

Perry, R. J., Camporez, J. P. G., Kursawe, R., Titchenell, P. M., Zhang, D., Perry, C. J., Jurczak, M. J., Abudukadier, A., Han, M. S., Zhang, X. M., Ruan, H. Bin, Yang, X., Caprio, S., Kaech, S. M., Sul, H. S., Birnbaum, M. J., Davis, R. J., Cline, G. W., Petersen, K. F., & Shulman, G. I. (2015). Hepatic Acetyl CoA Links Adipose Tissue Inflammation to Hepatic Insulin Resistance and Type 2 Diabetes. *Cell*, *160*(4), 745–758. https://doi.org/10.1016/J.CELL.2015.01.012

Perry, R. J., Zhang, D., Guerra, M. T., Brill, A. L., Goedeke, L., Nasiri, A. R., Rabin-Court, A., Wang, Y., Peng, L., Dufour, S., Zhang, Y., Zhang, X. M., Butrico, G. M., Toussaint, K., Nozaki, Y., Cline, G. W., Petersen, K. F., Nathanson, M. H., Ehrlich, B. E., & Shulman, G. I. (2020). Glucagon stimulates gluconeogenesis by INSP3R1-mediated hepatic lipolysis. *Nature*, *579*(7798), 279–283. https://doi.org/10.1038/s41586-020-2074-6

Petersen, M. C., Madiraju, A. K., Gassaway, B. M., Marcel, M., Nasiri, A. R., Butrico, G., Marcucci, M. J., Zhang, D., Abulizi, A., Zhang, X. M., Philbrick, W., Hubbard, S. R., Jurczak, M. J., Samuel, V. T., Rinehart, J., & Shulman, G. I. (2016). Insulin receptor Thr1160 phosphorylation mediates lipid-induced hepatic insulin resistance. *The Journal of Clinical Investigation*, *126*(11), 4361–4371. https://doi.org/10.1172/JCI86013

Petersen, M. C., & Shulman, G. I. (2018). Mechanisms of insulin action and insulin resistance. *Physiological Reviews*, *98*(4), 2133–2223. https://doi.org/10.1152/physrev.00063.2017

Petersen, M. C., Vatner, D. F., & Shulman, G. I. (2017). Regulation of hepatic glucose metabolism in health and disease. *Nature Reviews Endocrinology*, *13*(10), 572–587. https://doi.org/10.1038/nrendo.2017.80

Pezze, P. D., Ruf, S., Sonntag, A. G., Langelaar-Makkinje, M., Hall, P., Heberle, A. M., Navas, P. R., Van Eunen, K., Tölle, R. C., Schwarz, J. J., Wiese, H., Warscheid, B., Deitersen, J., Stork, B., Fäßler, E., Schäuble, S., Hahn, U., Horvatovich, P., Shanley, D. P., & Thedieck, K. (2016). A systems study reveals concurrent activation of AMPK and mTOR by amino acids. *Nature Communications*, *7*. https://doi.org/10.1038/ncomms13254

Phillips-Krawczak, C. A., Singla, A., Starokadomskyy, P., Deng, Z., Osborne, D. G., Li, H., Dick, C. J., Gomez, T. S., Koenecke, M., Zhang, J. S., Dai, H., Sifuentes-Dominguez, L. F., Geng, L. N., Kaufmann, S. H., Hein, M. Y., Wallis, M., McGaughran, J., Gecz, J., Van De Sluis, B., … Burstein, E. (2015). COMMD1 is linked to the WASH complex and

regulates endosomal trafficking of the copper transporter ATP7A. *Molecular Biology of the Cell*, *26*(1), 91–103. https://doi.org/10.1091/MBC.E14-06-1073/ASSET/IMAGES/LARGE/91FIG7.JPEG

Pineda, E., Sanchez-Romero, L. M., Brown, M., Jaccard, A., Jewell, J., Galea, G., Webber, L., & Breda, J. (2018). Forecasting Future Trends in Obesity across Europe: The Value of Improving Surveillance. *Obes Facts*, *11*, 360–371. https://doi.org/10.1159/000492115

Pouwels, S., Sakran, N., Graham, Y., Leal, A., Pintar, T., Yang, W., Kassir, R., Singhal, R., Mahawar, K., & Ramnarain, D. (2022). Non-alcoholic fatty liver disease (NAFLD): a review of pathophysiology, clinical management and effects of weight loss. *BMC Endocrine Disorders*, *22*(1). https://doi.org/10.1186/S12902-022-00980-1

Pruniau, V. P. E. G., Louagie, E., Brouwers, B., Declercq, J., & Creemers, J. W. M. (2013). The AlfpCre mouse revisited: Evidence for liver steatosis related to growth hormone deficiency. *Hepatology*, *58*(6), 2209–2210. https://doi.org/10.1002/hep.26483

Pullen, N., & Thomas, G. (1997). The modular phosphorylation and activation of p70s6k. *FEBS Letters*, *410*(1), 78–82. https://doi.org/10.1016/S0014-5793(97)00323-2

Raiborg, C., Bremnes, B., Mehlum, A., Gillooly, D. J., D'Arrigo, A., Stang, E., & Stenmark, H. (2001). FYVE and coiled-coil domains determine the specific localisation of Hrs to early endosomes. *Journal of Cell Science*, *114*(12), 2255–2263. https://doi.org/10.1242/JCS.114.12.2255

Raney, M. A., & Turcotte, L. P. (2008). Evidence for the involvement of CaMKII and AMPK in Ca2+- dependent signaling pathways regulating FA uptake and oxidation in contracting rodent muscle. *Journal of Applied Physiology*, *104*(5), 1366–1373. https://doi.org/10.1152/JAPPLPHYSIOL.01282.2007/ASSET/IMAGES/LARGE/ZDG0050878890006.JPEG

Raskin, P., & Unger, R. H. (1978). Hyperglucagonemia and Its Suppression. *The New England Journal of Medicine*, *299*(9), 433–436. https://doi.org/10.1056/NEJM197808312990901

Richter, M. L., Deligiannis, I. K., Yin, K., Danese, A., Lleshi, E., Coupland, P., Vallejos, C. A., Matchett, K. P., Henderson, N. C., Colome-Tatche, M., & Martinez-Jimenez, C. P. (2021). Single-nucleus RNA-seq2 reveals functional crosstalk between liver zonation and ploidy. *Nature Communications*, *12*(1), 1–16. https://doi.org/10.1038/s41467-021-24543-5

Roden, M., & Shulman, G. I. (2019). The integrative biology of type 2 diabetes. *Nature*, *576*(7785), 51–60. https://doi.org/10.1038/s41586-019-1797-8

Rogerson, C., & Gissen, P. (2016). The CHEVI tethering complex: facilitating special deliveries. *Journal of Pathology*, *240*(3), 249–252. https://doi.org/10.1002/path.4785

Rozman, J., Rathkolb, B., Oestereicher, M. A., Schütt, C., Ravindranath, A. C., Leuchtenberger, S., Sharma, S., Kistler, M., Willershäuser, M., Brommage, R., Meehan, T. F., Mason, J., Haselimashhadi, H., Aguilar-Pimentel, A., Becker, L., Treise, I., Moreth, K., Garrett, L., Hölter, S. M., … De Angelis, M. H. (2018). Identification of genetic elements in metabolism by high-throughput mouse phenotyping. *Nature Communications*, *9*(1), 1–16. https://doi.org/10.1038/s41467-017-01995-2

Sánchez-Lozada, L. G., Mu, W., Roncal, C., Sautin, Y. Y., Abdelmalek, M., Reungjui, S., Le, M., Nakagawa, T., Lan, H. Y., Yu, X., & Johnson, R. J. (2010). Comparison of free fructose and glucose to sucrose in the ability to cause fatty liver. *European Journal of Nutrition*, *49*(1), 1–9. https://doi.org/10.1007/S00394-009-0042-X

Schindelin, J., Arganda-Carreras, I., Frise, E., Kaynig, V., Longair, M., Pietzsch, T., Preibisch, S., Rueden, C., Saalfeld, S., Schmid, B., Tinevez, J. Y., White, D. J., Hartenstein, V., Eliceiri, K., Tomancak, P., & Cardona, A. (2012). Fiji: an open-source platform for biological-image analysis. *Nature Methods*, *9*(7), 676–682. https://doi.org/10.1038/nmeth.2019

Schmidt, O., & Teis, D. (2012). The ESCRT machinery. *Current Biology*, *22*(4), R116–R120. https://doi.org/10.1016/j.cub.2012.01.028

Schulze, R. J., Schott, M. B., Casey, C. A., Tuma, P. L., & McNiven, M. A. (2019). The cell biology of the hepatocyte: A membrane trafficking machine. *Journal of Cell Biology*, *218*(7), 2096–2112. https://doi.org/10.1083/jcb.201903090

Schwenk, F., Baron, U., & Rajewsky, K. (1995). A cre-transgenic mouse strain for the ubiquitous deletion of loxP-flanked gene segments including deletion in germ cells. *Nucleic Acids Research*, *23*(24), 5080–5081. https://doi.org/10.1093/nar/23.24.5080

Segev, N. (2001). Ypt/Rab GTPases: Regulators of Protein Trafficking. *Critical Reviews in Biochemistry and Molecular Biology*, *100*(p.re11). https://doi.org/10.1126/STKE.2001.100.RE11

Seifert, R., & Wenzel-Seifert, K. (2002). Constitutive activity of G-proteins-coupled receptors: Cause of disease and common property of wild-type receptors. *Naunyn-Schmiedeberg's Archives of Pharmacology*, *366*(5), 381–416. https://doi.org/10.1007/S00210-002-0588-0/METRICS

Seitz, S., Kwon, Y., Hartleben, G., Jülg, J., Sekar, R., Krahmer, N., Najafi, B., Loft, A., Gancheva, S., Stemmer, K., Feuchtinger, A., Hrabe de Angelis, M., Müller, T. D., Mann, M., Blüher, M., Roden, M., Berriel Diaz, M., Behrends, C., Gilleron, J., … Zeigerer, A. (2019). Hepatic Rab24 controls blood glucose homeostasis via improving mitochondrial plasticity. *Nature Metabolism*, *1*(10), 1009–1026. https://doi.org/10.1038/s42255-019-

0124-x

Sekar, R., Motzler, K., Kwon, Y., Novikoff, A., Jülg, J., Najafi, B., Wang, S., Warnke, A. L., Seitz, S., Hass, D., Gancheva, S., Kahl, S., Yang, B., Finan, B., Schwarz, K., Okun, J. G., Roden, M., Blüher, M., Müller, T. D., … Zeigerer, A. (2022). Vps37a regulates hepatic glucose production by controlling glucagon receptor localization to endosomes. *Cell Metabolism*, *34*(11), 1824-1842.e9. https://doi.org/10.1016/j.cmet.2022.09.022

Shenoy, S. K., Barak, L. S., Xiao, K., Ahn, S., Berthouze, M., Shukla, A. K., Luttrell, L. M., & Lefkowitz, R. J. (2007). Ubiquitination of β-arrestin links seven-transmembrane receptor endocytosis and ERK activation. *Journal of Biological Chemistry*, *282*(40), 29549–29562. https://doi.org/10.1074/jbc.M700852200

Shenoy, S. K., McDonald, P. H., Kohout, T. A., & Lefkowitz, R. J. (2001). Regulation of receptor fate by ubiquitination of activated β2-adrenergic receptor and β-arrestin. *Science*, *294*(5545), 1307–1313. https://doi.org/10.1126/science.1063866

Shih, W., Gallusser, A., & Kirchhausen, T. (1995). A clathrin-binding site in the hinge of the β2 chain of mammalian AP-2 complexes. *Journal of Biological Chemistry*, *270*(52), 31083–31090. https://doi.org/10.1074/jbc.270.52.31083

Simmen, T., Höning, S., Icking, A., Tikkanen, R., & Hunziker, W. (2002). AP-4 binds basolateral signals and participates in basolateral sorting in epithelial MDCK cells. *Nature Cell Biology*, *4*(2), 154–159. https://doi.org/10.1038/ncb745

Simonsen, A., Lippé, R., Christoforidis, S., Gaullier, J. M., Brech, A., Callaghan, J., Toh, B. H., Murphy, C., Zerial, M., & Stenmark, H. (1998). EEA1 links PI(3)K function to Rab5 regulation of endosome fusion. *Nature*, *394*(6692), 494–498. https://doi.org/10.1038/28879

Spang, A. (2016). Membrane tethering complexes in the endosomal system. *Frontiers in Cell and Developmental Biology*, *4*, 1–7. https://doi.org/10.3389/fcell.2016.00035

Stuffers, S., Brech, A., & Stenmark, H. (2009). ESCRT proteins in physiology and disease. *Experimental Cell Research*, *315*(9), 1619–1626. https://doi.org/10.1016/j.yexcr.2008.10.013

Südhof, T. C., & Rothman, J. E. (2009). Membrane Fusion: Grappling with SNARE and SM Proteins. *Science*, *323*(5913), 474–477. https://doi.org/10.1126/SCIENCE.1161748

Sutkeviciute, I., & Vilardaga, J. P. (2020). Structural insights into emergent signaling modes of G protein-coupled receptors. *The Journal of Biological Chemistry*, *295*(33), 11626–11642. https://doi.org/10.1074/JBC.REV120.009348

Szklarczyk, D., Gable, A. L., Nastou, K. C., Lyon, D., Kirsch, R., Pyysalo, S., Doncheva, N. T.,

Legeay, M., Fang, T., Bork, P., Jensen, L. J., & von Mering, C. (2021). The STRING database in 2021: Customizable protein-protein networks, and functional characterization of user-uploaded gene/measurement sets. *Nucleic Acids Research*, *49*(D1), D605–D612. https://doi.org/10.1093/nar/gkaa1074

Szymanska, E., Budick-Harmelin, N., & Miaczynska, M. (2018). Endosomal "sort" of signaling control: The role of ESCRT machinery in regulation of receptor-mediated signaling pathways. *Seminars in Cell and Developmental Biology*, *74*, 11–20. https://doi.org/10.1016/j.semcdb.2017.08.012

Tabák, A. G., Herder, C., Rathmann, W., Brunner, E. J., & Kivimäki, M. (2012). Prediabetes: A high-risk state for developingdiabetes. *Lancet*, *379*(9833), 2279. https://doi.org/10.1016/S0140-6736(12)60283-9

Toh, W. H., Tan, J. Z. A., Zulkefli, K. L., Houghton, F. J., & Gleeson, P. A. (2017). Amyloid precursor protein traffics from the Golgi directly to early endosomes in an Arl5b- and AP4-dependent pathway. *Traffic*, *18*(3), 159–175. https://doi.org/10.1111/tra.12465

Trefts, E., Gannon, M., & Wasserman, D. H. (2017). The liver. *Current Biology*, *27*(21), R1147–R1151. https://doi.org/10.1016/J.CUB.2017.09.019

Tyanova, S., Temu, T., Sinitcyn, P., Carlson, A., Hein, M. Y., Geiger, T., Mann, M., & Cox, J. (2016). The Perseus computational platform for comprehensive analysis of (prote)omics data. *Nature Methods*, *13*(9), 731–740. https://doi.org/10.1038/NMETH.3901

van der Beek, J., Jonker, C., van der Welle, R., Liv, N., & Klumperman, J. (2019). CORVET, CHEVI and HOPS – Multisubunit tethers of the endo-lysosomal system in health and disease. *Journal of Cell Science*, *132*(10). https://doi.org/10.1242/jcs.189134

Verkerk, A. J. M. H., Schot, R., Dumee, B., Schellekens, K., Swagemakers, S., Bertoli-Avella, A. M., Lequin, M. H., Dudink, J., Govaert, P., van Zwol, A. L., Hirst, J., Wessels, M. W., Catsman-Berrevoets, C., Verheijen, F. W., de Graaff, E., de Coo, I. F. M., Kros, J. M., Willemsen, R., Willems, P. J., … Mancini, G. M. S. (2009). Mutation in the AP4M1 Gene Provides a Model for Neuroaxonal Injury in Cerebral Palsy. *American Journal of Human Genetics*, *85*(1), 40–52. https://doi.org/10.1016/j.ajhg.2009.06.004

Wagner, R., Heni, M., Tabák, A. G., Machann, J., Schick, F., Randrianarisoa, E., Hrabě de Angelis, M., Birkenfeld, A. L., Stefan, N., Peter, A., Häring, H. U., & Fritsche, A. (2021). Pathophysiology-based subphenotyping of individuals at elevated risk for type 2 diabetes. *Nature Medicine*, *27*(1), 49–57. https://doi.org/10.1038/s41591-020-1116-9

Wang, C., Cheng, Y., Zhang, X., Li, N., Zhang, L., Wang, S., Tong, X., Xu, Y., Chen, G. qiang, Cheng, S., Fan, X., & Liu, J. (2018). Vacuolar Protein Sorting 33B Is a Tumor Suppressor in Hepatocarcinogenesis. *Hepatology*, *68*(6), 2239–2253.

https://doi.org/10.1002/hep.30077

Wang, J.-Q., Li, L.-L., Hu, A., Deng, G., Wei, J., Li, Y.-F., Liu, Y.-B., Lu, X.-Y., Qiu, Z.-P., Shi, X.-J., Zhao, X., Luo, J., & Song, B.-L. (2022). Inhibition of ASGR1 decreases lipid levels by promoting cholesterol excretion. *Nature*. https://doi.org/10.1038/s41586-022-05006-3

Wang, L., & Boyer, J. L. (2004). The Maintenance and Generation of Membrane Polarity in Hepatocytes. *Hepatology*, *39*(4), 892–899. https://doi.org/10.1002/hep.20039

Wang, Xiaobo, Zheng, Z., Caviglia, J. M., Corey, K. E., Herfel, T. M., Cai, B., Masia, R., Chung, R. T., Lefkowitch, J. H., Schwabe, R. F., & Tabas, I. (2016). Hepatocyte TAZ/WWTR1 Promotes Inflammation and Fibrosis in Nonalcoholic Steatohepatitis. *Cell Metabolism*, *24*(6), 848–862. https://doi.org/10.1016/j.cmet.2016.09.016

Wang, Xiaowei, & Seed, B. (2003). A PCR primer bank for quantitative gene expression analysis. *Nucleic Acids Research*, *31*(24). https://doi.org/10.1093/NAR/GNG154

Wang, Y. C., McPherson, K., Marsh, T., Gortmaker, S. L., & Brown, M. (2011). Health and economic burden of the projected obesity trends in the USA and the UK. *Lancet*, *378*(9793), 815–825. https://doi.org/10.1016/S0140-6736(11)60814-3

Weber, T., Zemelman, B. V., McNew, J. A., Westermann, B., Gmachl, M., Parlati, F., Söllner, T. H., & Rothman, J. E. (1998). SNAREpins: Minimal machinery for membrane fusion. *Cell*, *92*(6), 759–772. https://doi.org/10.1016/S0092-8674(00)81404-X

Wijers, M., Zanoni, P., Liv, N., Vos, D. Y., Jäckstein, M. Y., Smit, M., Wilbrink, S., Wolters, J. C., van der Veen, Y. T., Huijkman, N., Dekker, D., Kloosterhuis, N., van Dijk, T. H., Billadeau, D. D., Kuipers, F., Klumperman, J., von Eckardstein, A., Kuivenhoven, J. A., & van de Sluis, B. (2019). The hepatic WASH complex is required for efficient plasma LDL and HDL cholesterol clearance. *JCI Insight*, *4*(11). https://doi.org/10.1172/jci.insight.126462

Williams, C. D., Stengel, J., Asike, M. I., Torres, D. M., Shaw, J., Contreras, M., Landt, C. L., & Harrison, S. A. (2011). Prevalence of nonalcoholic fatty liver disease and nonalcoholic steatohepatitis among a largely middle-aged population utilizing ultrasound and liver biopsy: a prospective study. *Gastroenterology*, *140*(1), 124–131. https://doi.org/10.1053/J.GASTRO.2010.09.038

Woitok, M. M., Zoubek, M. E., Doleschel, D., Bartneck, M., Mohamed, M. R., Kießling, F., Lederle, W., Trautwein, C., & Cubero, F. J. (2020). Lipid-encapsulated siRNA for hepatocyte-directed treatment of advanced liver disease. *Cell Death and Disease*, *11*(5), 1–14. https://doi.org/10.1038/s41419-020-2571-4

Wollert, T., Wunder, C., Lippincott-Schwartz, J., & Hurley, J. H. (2009). Membrane scission by

the ESCRT-III complex. *Nature*, *458*(7235), 172–177. https://doi.org/10.1038/NATURE07836

Xiang, B., Zhang, G., Ye, S., Zhang, R., Huang, C., Liu, J., Tao, M., Ruan, C., Smyth, S. S., Whiteheart, S. W., & Li, Z. (2015). Characterization of a novel integrin binding protein, vps33b, which is important for platelet activation and in vivo thrombosis and hemostasis. *Circulation*, *132*(24), 2334–2344. https://doi.org/10.1161/CIRCULATIONAHA.115.018361

Xiang, H., Tao, Y., Jiang, Z., Huang, X., Wang, H., Cao, W., Li, J., Ding, R., Shen, M., Feng, R., Li, L., Guan, C., Liu, J., Ni, J., Chen, L., Wang, Z., Ye, Y., Zhong, Q., Liu, J., … Wu, X. (2022). Vps33B controls Treg cell suppressive function through inhibiting lysosomal nutrient sensing complex-mediated mTORC1 activation. *Cell Reports*, *39*(11), 110943. https://doi.org/10.1016/j.celrep.2022.110943

Yang, H., & Yang, L. (2016). Targeting cAMP/PKA pathway for glycemic control and type 2 diabetes therapy. *Journal of Molecular Endocrinology*, *57*(2), R93–R108. https://doi.org/10.1530/JME-15-0316

Yanovski, J. A. (2018). Trends in underweight and obesity — scale of the problem. *Nature Reviews Endocrinology*, *14*(1), 5–6. https://doi.org/10.1038/NRENDO.2017.157

Ye, J., Coulouris, G., Zaretskaya, I., Cutcutache, I., Rozen, S., & Madden, T. L. (2012). Primer-BLAST: a tool to design target-specific primers for polymerase chain reaction. *BMC Bioinformatics*, *13*, 134. https://doi.org/10.1186/1471-2105-13-134

Yki-Järvinen, H. (2014). Non-alcoholic fatty liver disease as a cause and a consequence of metabolic syndrome. *The Lancet Diabetes & Endocrinology*, *2*(11), 901–910. https://doi.org/10.1016/S2213-8587(14)70032-4

Younossi, Z. (2019). Non-alcoholic fatty liver disease – A global public health perspective. *Journal of Hepatology*, *70*(3), 531–544. https://doi.org/10.1016/J.JHEP.2018.10.033

Yu, I. M., & Hughson, F. M. (2010). Tethering factors as organizers of intracellular vesicular traffic. *Annual Review of Cell and Developmental Biology*, *26*, 137–156. https://doi.org/10.1146/ANNUREV.CELLBIO.042308.113327

Zeigerer, A., Bogorad, R. L., Sharma, K., Gilleron, J., Seifert, S., Sales, S., Berndt, N., Bulik, S., Marsico, G., D'Souza, R. C. J., Lakshmanaperumal, N., Meganathan, K., Natarajan, K., Sachinidis, A., Dahl, A., Holzhütter, H. G., Shevchenko, A., Mann, M., Koteliansky, V., & Zerial, M. (2015). Regulation of Liver Metabolism by the Endosomal GTPase Rab5. *Cell Reports*, *11*(6), 884–892. https://doi.org/10.1016/j.celrep.2015.04.018

Zeigerer, A., Gilleron, J., Bogorad, R. L., Marsico, G., Nonaka, H., Seifert, S., Epstein-Barash,

H., Kuchimanchi, S., Peng, C. G., Ruda, V. M., Conte-Zerial, P. Del, Hengstler, J. G., Kalaidzidis, Y., Koteliansky, V., & Zerial, M. (2012). Rab5 is necessary for the biogenesis of the endolysosomal system in vivo. *Nature*, *485*(7399), 465–470. https://doi.org/10.1038/nature11133

Zeigerer, A., Sekar, R., Kleinert, M., Nason, S., Habegger, K. M., & Müller, T. D. (2021). Glucagon's Metabolic Action in Health and Disease. *Comprehensive Physiology*, *11*(2), 1759. https://doi.org/10.1002/CPHY.C200013

Zeigerer, A., Wuttke, A., Marsico, G., Seifert, S., Kalaidzidis, Y., & Zerial, M. (2017). Functional properties of hepatocytes in vitro are correlated with cell polarity maintenance. *Experimental Cell Research*, *350*(1), 242–252. https://doi.org/10.1016/j.yexcr.2016.11.027

Zellmer, S., Schmidt-Heck, W., Godoy, P., Weng, H., Meyer, C., Lehmann, T., Sparna, T., Schormann, W., Hammad, S., Kreutz, C., Timmer, J., Von Weizsäcker, F., Thürmann, P. A., Merfort, I., Guthke, R., Dooley, S., Hengstler, J. G., & Gebhardt, R. (2010). Transcription factors ETF, E2F, and SP-1 are involved in cytokine-independent proliferation of murine hepatocytes. *Hepatology*, *52*(6), 2127–2136. https://doi.org/10.1002/HEP.23930

Zhang, C. S., Jiang, B., Li, M., Zhu, M., Peng, Y., Zhang, Y. L., Wu, Y. Q., Li, T. Y., Liang, Y., Lu, Z., Lian, G., Liu, Q., Guo, H., Yin, Z., Ye, Z., Han, J., Wu, J. W., Yin, H., Lin, S. Y., & Lin, S. C. (2014). The Lysosomal v-ATPase-Ragulator Complex Is a Common Activator for AMPK and mTORC1, Acting as a Switch between Catabolism and Anabolism. *Cell Metabolism*, *20*(3), 526–540. https://doi.org/10.1016/J.CMET.2014.06.014

Zhang, C. S., Li, M., Wang, Y., Li, X., Zong, Y., Long, S., Zhang, M., Feng, J. W., Wei, X., Liu, Y. H., Zhang, B., Wu, J., Zhang, C., Lian, W., Ma, T., Tian, X., Qu, Q., Yu, Y., Xiong, J., … Lin, S. C. (2022). The aldolase inhibitor aldometanib mimics glucose starvation to activate lysosomal AMPK. *Nature Metabolism*, *4*(10), 1369–1401. https://doi.org/10.1038/s42255-022-00640-7

Zhang, Y. L., Guo, H., Zhang, C. S., Lin, S. Y., Yin, Z., Peng, Y., Luo, H., Shi, Y., Lian, G., Zhang, C., Li, M., Ye, Z., Ye, J., Han, J., Li, P., Wu, J. W., & Lin, S. C. (2013). AMP as a Low-Energy Charge Signal Autonomously Initiates Assembly of AXIN-AMPK-LKB1 Complex for AMPK Activation. *Cell Metabolism*, *18*(4), 546–555. https://doi.org/10.1016/J.CMET.2013.09.005

Zhao, G. N., Zhang, P., Gong, J., Zhang, X. J., Wang, P. X., Yin, M., Jiang, Z., Shen, L. J., Ji, Y. X., Tong, J., Wang, Y., Wei, Q. F., Wang, Y., Zhu, X. Y., Zhang, X., Fang, J., Xie, Q., She, Z. G., Wang, Z., … Li, H. (2017). Tmbim1 is a multivesicular body regulator that

protects against non-alcoholic fatty liver disease in mice and monkeys by targeting the lysosomal degradation of Tlr4. *Nature Medicine*, *23*(6), 742–752. https://doi.org/10.1038/nm.4334

Zhou, Y., & Zhang, J. (2014). Arthrogryposis-renal dysfunction-cholestasis (ARC) syndrome: from molecular genetics to clinical features. *Italian Journal of Pediatrics*, *40*(77). https://doi.org/10.1186/s13052-014-0077-3

Zhu, M., Hao, S., Liu, T., Yang, L., Zheng, P., Zhang, L., & Ji, G. (2017). Lingguizhugan decoction improves non-alcoholic fatty liver disease by altering insulin resistance and lipid metabolism related genes: A whole trancriptome study by RNA-Seq. *Oncotarget*, *8*(47), 82621–82631. https://doi.org/10.18632/oncotarget.19734